



PROCEEDINGS
of the
Second International Conference
on the Ultrasonic Measurement and Imaging
of Tissue Elasticity[©]

Corpus Christi, Texas, U.S.A.
October 12-15, 2003

PROCEEDINGS

of the
Second International Conference
on the Ultrasonic Measurement and Imaging
of Tissue Elasticity

Corpus Christi, Texas, USA
October 12–15, 2003

Table of Contents

Foreword	3
Conference Evaluation and Questionnaire	5
Program.....	7
Conference-At-A-Glance	7
Program by Date and Time.....	8
Abstracts	21
Guest Lecture	21
Session A-1	22
Session A-2.....	22
Session B.....	23
Session C.....	30
Session D-1	36
Session E.....	42
SessionD-2	51
Session F	57
Session G	60
Session H	63
Session I.....	67
Session J	70
Session K.....	77
Session D-3	80
Session D-4	85
Session P	89
Author Index	97
Note Pages	98

FOREWORD

Dear Conference Delegate:

Welcome to the Second International Conference on the Ultrasonic Measurement and Imaging of Tissue Elasticity.

Last year was the inaugural year of this Conference. We expected a turnout of 35-40 delegates, but had 92. This year we are planning for 100 registrants from 16 countries, and we have accepted 72 scientific abstracts. We are heartened by the many delegates that are returning this year, as well as the many new ones. We feel that this attendance demonstrates the widespread surge of interest and excitement in the emerging field of imaging the elastic properties of tissue, and we hope that this Conference will be a catalyst for accelerated development of the field.

We have preserved the general format of the Conference this year. Based on your Conference Evaluation comments from last year, we have added two Sunday afternoon Tutorial/Panel Discussion sessions. We are indebted to Jonathan Rubin, MD, PhD from the University of Michigan, who has agreed to moderate these sessions. The first one will cover techniques for measuring tissue elastic properties *in vitro*, while the second will cover techniques for imaging tissue elastic attributes *in vivo*. There should be ample time for discussion at the end of each session.

This year we have added a small instrumentation exhibit which will open on Sunday evening at the Conference Reception and will continue to run through Tuesday afternoon. We are pleased that Hitachi Medical Corporation and Medison Corporation have chosen this Conference to introduce their new elasticity imaging instruments.

We have chosen Corpus Christi, Texas as the Conference venue this year because we felt that the city and the Omni Hotel provided an attractive, quiet location and a good value that should contribute to a successful conference. At the Conference dinner on Monday evening, Mr. Rick Stryker, Director of the Corpus Christi Museum of Science and History, has graciously volunteered to present a talk on the international scientific research and replication efforts of the Christopher Columbus Ships of Discovery. These replica ships have sailed over from Spain and are now housed here in the Museum.

We would like to thank the delegates, the reviewers and the session chairs for their continuing support of the Conference. Special thanks go again to our support staff at the Conference Secretariat office, Ms. Manette Price and Ms. Pam Clark, who have spent much time and effort in the many organizational aspects of the Conference, including the hotel, meals, website, correspondence and finances. Special thanks go also to Ms Karen Ophir who volunteered to design all the Conference artwork, publications and materials. Ms. Eva Maciejko from École Polytechnique in Montréal, Canada has kindly agreed to contribute her musical talents for your enjoyment during the Conference Dinner.

As it was from its inception, the Conference is held under the auspices of the University of Rochester Center for Biomedical Ultrasound and the Ultrasonics Laboratory at the University of Texas Medical School at Houston. However, all funding for the Conference is derived from registration fees alone. We hope that with your support we will be able to make this Conference an annual event.

Enjoy your Conference, and we look forward to seeing you at next year's Conference in England!

J. Ophir and K. Parker
Conference Organizers
October 12, 2003

Conference Evaluation and Questionnaire

SCORING:	Very Poor				Mid					Excellent
	1	2	3	4	5	6	7	8	9	10

OVERALL CONFERENCE:

Overall	1	2	3	4	5	6	7	8	9	10
Additional comments:										

SCIENTIFIC PROGRAM

Quality of the Presentations	1	2	3	4	5	6	7	8	9	10
Number of Presentations	1	2	3	4	5	6	7	8	9	10
Relevance of Presentations to the Conference's Theme	1	2	3	4	5	6	7	8	9	10
Time Allotted for Presentations	1	2	3	4	5	6	7	8	9	10
Time Allotted for Discussion	1	2	3	4	5	6	7	8	9	10
Poster Session	1	2	3	4	5	6	7	8	9	10
Guest Lecture – Subject	1	2	3	4	5	6	7	8	9	10
Tutorials and Panel Discussions	1	2	3	4	5	6	7	8	9	10
Equipment Exhibit	1	2	3	4	5	6	7	8	9	10
Student Participation	1	2	3	4	5	6	7	8	9	10
Additional comments:										

CONFERENCE MATERIALS:

Printed Proceedings Book	1	2	3	4	5	6	7	8	9	10
CD Proceedings	1	2	3	4	5	6	7	8	9	10
Other Registration Materials										
Additional comments:										

CONFERENCE FACILITIES

Room:	1	2	3	4	5	6	7	8	9	10
Temperature	1	2	3	4	5	6	7	8	9	10
Size: 10=Too Big; 5=just right; 1=Too Small	1	2	3	4	5	6	7	8	9	10
Seating	1	2	3	4	5	6	7	8	9	10
Registration Desk and Conference Office	1	2	3	4	5	6	7	8	9	10
Meals:	1	2	3	4	5	6	7	8	9	10
Conference Breakfasts and Lunches	1	2	3	4	5	6	7	8	9	10
Conference Dinner	1	2	3	4	5	6	7	8	9	10
Coffee Breaks	1	2	3	4	5	6	7	8	9	10
Audio-Visual Equipment	1	2	3	4	5	6	7	8	9	10
Additional comments:										

VENUE AND HOTEL

Venue – Corpus Christi and Environs	1	2	3	4	5	6	7	8	9	10
Area Attractions	1	2	3	4	5	6	7	8	9	10
Hotel:	1	2	3	4	5	6	7	8	9	10
Reservations	1	2	3	4	5	6	7	8	9	10
Transportation and Accessibility	1	2	3	4	5	6	7	8	9	10
Reception and Check – In	1	2	3	4	5	6	7	8	9	10
Accommodations	1	2	3	4	5	6	7	8	9	10
Facilities	1	2	3	4	5	6	7	8	9	10
Parking										
Additional comments:										

ADMINISTRATION

Website	1	2	3	4	5	6	7	8	9	10
Registration off-site	1	2	3	4	5	6	7	8	9	10
Registration on-site	1	2	3	4	5	6	7	8	9	10
Administrative staff	1	2	3	4	5	6	7	8	9	10
Correspondence	1	2	3	4	5	6	7	8	9	10
Additional comments:										

GENERAL INFORMATION

Should this conference be held Annually ?	Yes		No	
If Yes:				
I would plan to attend the next conference	Yes	Perhaps	No	
and present a paper(s) / poster(s)	Yes	Perhaps	No	
Other(s) from my lab would attend the next conference	Yes	Perhaps	No	
and he/she / they would present a paper(s) / poster(s)	Yes	Perhaps	No	
If No:				
At what interval should the Conference be held?	1 ½ years	2 years	3 years	
How did you learn of this conference? (Check all that apply)	<input type="checkbox"/> Email Announcement			
<input type="checkbox"/> Meetings Calendar in Journal of Ultrasound in Medicine and Biology	<input type="checkbox"/> Web Site		<input type="checkbox"/> Colleague	
<input type="checkbox"/> Other	<input type="checkbox"/> Returning Delegate			
Should this conference continue to have tutorials?	Yes		No	
Should this conference be held in other locations?	Yes		No	
Time of year for the conference	FALL	Winter	Spring	Summer
Duration of the conference	Shorter		OK as is	Longer
Tutorial suggestions:				
Location suggestions:				
Additional comments: (Improvements or Suggestions)				

Any comments are welcome at any time at <elasticity.conference@uth.tmc.edu>

CONFERENCE—AT—A—GLANCE

Second International Conference on the Ultrasonic Measurement and Imaging of Tissue Elasticity
Omni Bayfront Hotel – Corpus Christi, Texas, USA
October 12–15, 2003

Sunday, October 12

12:00P – 7:30P

12:00P – 5:00P	Registration Desk Open Conference Office Open	3 rd Floor Escalator Foyer Matagorda Room
2:30P – 3:45P	Session A-1: Bench-Top Methods for Measuring the Elastic Properties of Tissues (<i>In Vitro</i>) <i>Coffee Break</i>	Nueces Ballroom B Nueces Ballroom Foyer
3:45P – 4:15P	Session A-2: Methods for Imaging Elastic Attributes of Tissue	Nueces Ballroom B
4:15P – 5:30P	Opening Reception & Registration Desk Open	Bayview Room
5:30P – 7:30P	Session P: Posters Session X: Equipment Exhibit	Bayview Room Bayview Room

Monday, October 13

7:00A – 10:00P

7:00A – 5:30P	Registration Desk Open Conference Office Open	3 rd Floor Escalator Foyer Matagorda Room
Session P:	Posters	Nueces Ballroom Foyer
Session X:	Equipment Exhibit	Nueces Ballroom Foyer
7:00A – 7:55A	<i>Breakfast</i>	Glass Pavilion Restaurant Buffet
7:55A – 8:00A	Opening Remarks	Nueces Ballroom B
8:00A – 9:45A	Session B: Mechanical Measurement Techniques for Tissues	Nueces Ballroom B
9:45A – 10:15A	<i>Coffee Break</i>	Nueces Ballroom Foyer
10:15A – 11:45A	Session C: Mechanical Properties of Tissues	Nueces Ballroom B
11:45A – 1:15P	<i>Group Lunch</i>	Nueces Ballroom A
1:15P – 2:45P	Session D-1: Methods for Imaging Elastic Tissue Properties I	Nueces Ballroom B
2:45P – 3:15P	<i>Coffee Break</i>	Nueces Ballroom Foyer
3:15P – 5:30P	Session E: Clinical and Animal Applications and Results	Nueces Ballroom B
7:00P – 10:00P	Conference Dinner, Guest Speaker, Rick Stryker	Nueces Ballroom B

Tuesday, October 14

7:00A – 5:30P

7:00A – 5:30P	Registration Desk Open Conference Office Open	3 rd Floor Escalator Foyer Matagorda Room
Session P:	Posters	Nueces Ballroom Foyer
Session X:	Equipment Exhibit	Nueces Ballroom Foyer
7:00A – 8:00A	<i>Breakfast</i>	Glass Pavilion Restaurant Buffet
8:00A – 9:30A	Session D-2: Methods for Imaging Elastic Tissue Properties II	Nueces Ballroom B
9:30A – 10:00A	<i>Coffee Break</i>	Nueces Ballroom Foyer
10:00A – 10:45A	Session F: Biomechanical Tissue Modeling	Nueces Ballroom B
10:45A – 11:30A	Session G: Instrumentation and Phantoms	Nueces Ballroom B
11:30A – 1:30P	<i>Group Lunch</i>	Republic of Texas Bar & Grill
1:30P – 2:30P	Session H: Signal and Image Processing, and New Algorithms	Nueces Ballroom B
2:30P – 3:15P	Session I: Forward and Inverse Problems	Nueces Ballroom B
3:15P – 3:45P	<i>Coffee Break</i>	Nueces Ballroom Foyer
3:45P – 5:30P	Session J: Cardiovascular Elasticity	Nueces Ballroom B

Wednesday, October 15

7:00A – 1:00P

7:00A – 11:30A	Registration Desk Open Conference Office Open	3 rd Floor Escalator Foyer Matagorda Room
7:00A – 8:00A	<i>Breakfast</i>	Glass Pavilion Restaurant Buffet
8:00A – 8:45A	Session K: Complementary 3D and Multimodality Applications	Nueces Ballroom B
8:45A – 10:00A	Session D-3: Methods for Imaging Elastic Tissue Properties III	Nueces Ballroom B
10:00A – 10:30A	<i>Coffee Break</i>	Nueces Ballroom Foyer
10:30A – 11:30A	Session D-4: Methods for Imaging Elastic Tissue Properties IV	Nueces Ballroom B
11:30A – 1:00P	<i>Lunch</i>	Glass Pavilion Restaurant Buffet

PROGRAM

Second International Conference
on the Ultrasonic Measurement and Imaging
of Tissue Elasticity
Corpus Christi, Texas, USA
October 12–15, 2003

Sunday, October 12

12:00P – 7:30P

12:00P – 5:00P

Registration Desk Open
Conference Office Open

3rd Floor Escalator Foyer
Matagorda Room

Sunday

2:30P – 3:45P

**Session A-1: Bench-Top Methods for Measuring the Elastic Properties of
Tissues (*In Vitro*)**

Chair: JM Rubin, USA Co-Chair: T Krouskop, USA

Nueces Ballroom B

2:30P – 2:35P

INTRODUCTION.

*JM Rubin*¹.

¹University of Michigan, Ann Arbor, MI, USA.

2:35P – 2:45P

BENCH TOP TORSION TESTS FOR TESTING TISSUE VISCOELASTIC PROPERTIES.

*E Mazza*¹.

¹ETH Zürich, Swiss Federal Institute of Technology, Zürich, SWITZERLAND.

2:45P – 2:55P

TRANSIENT ELASTOGRAPHY FOR VISCOELASTIC MEASUREMENTS OF TISSUES.

*M Fink*¹.

¹Laboratoire Ondes et Acoustique, E.S.P.C.I., Paris, FRANCE.

2:55P – 3:05P

INDENTATION/NANO-INDENTATION AND VIBRATION TESTS IN SOFT TISSUES.

T Krouskop^{1,2}.

¹The University of Texas Medical School, Houston, Texas, USA; ²Baylor College of Medicine, Houston, Texas, USA.

3:05P – 3:15P

FREQUENCY-DEPENDENT CHARACTERIZATION OF THE VISCOELASTIC PROPERTIES OF SOFT TISSUES.

*MZ Kiss*¹.

¹The University of Wisconsin-Madison, Madison, WI, USA.

3:15P – 3:45P

GROUP DISCUSSION

3:45P – 4:15P

COFFEE BREAK

Nueces Ballroom Foyer

Sunday 4:15P – 5:30P
Session A-2: Methods for Imaging Elastic Attributes of Tissue
Chair: JM Rubin, USA Co-Chair: JC Bamber, UK Nueces Ballroom B

4:15P – 4:20P
INTRODUCTION.
*JM Rubin*¹.
¹University of Michigan, Ann Arbor, MI, USA.

4:20P – 4:30P
SONOELASTOGRAPHY IMAGING.
*L Taylor*¹.
¹University of Rochester, Rochester, NY, USA.

4:30P – 4:40P
ELASTOGRAPHY IMAGING.
*T Varghese*¹.
¹The University of Wisconsin-Madison, Madison, WI, USA.

4:40P – 4:50P
TRANSIENT ELASTOGRAPHY IMAGING.
*M Fink*¹.
¹Laboratoire Ondes et Acoustique, E.S.P.C.I., Paris, FRANCE.

4:50P – 5:00P
RADIATION PRESSURE VIBRO-ACOUSTOGRAPHY IMAGING.
*P Trompette*¹.
¹INSERM U556, Lyon, FRANCE.

5:00P – 5:30P
GROUP DISCUSSION

Sunday 5:30P – 7:30P
Opening Reception & Registration Desk Open
Session P: Posters Bayview Room
Session X: Equipment Exhibit Bayview Room
Bayview Room

Monday, October 13 7:00A – 10:00P

7:00A – 7:55A
BREAKFAST Glass Pavilion Restaurant Buffet

7:00A – 5:30P
Registration Desk Open 3rd Floor Escalator Foyer
Conference Office Open Matagorda Room
Session P: Posters Nueces Ballroom Foyer
Session X: Equipment Exhibit Nueces Ballroom Foyer

Monday 7:55A – 8:00A
OPENING REMARKS
J Ophir, KJ Parker Nueces Ballroom B

Monday 8:00A – 9:45A

Session B: Mechanical Measurement Techniques for Tissues

Chair: *M Fink, France*

Nueces Ballroom B

8:00A – 8:15A

02 MEASUREMENT OF VISCOELASTIC PROPERTIES OF SOFT BIOLOGICAL TISSUES WITH A DYNAMIC TORSION TEST.

E Mazza¹, D Valtorta¹.

¹ETH Zürich, Swiss Federal Institute of Technology, Zürich, SWITZERLAND.

8:15A – 8:30A

13 NONLINEAR INTERACTION OF SHEAR WAVES IN SOFT SOLIDS USING TRANSIENT ELASTOGRAPHY.

JL Gennisson¹, X Jacobs¹, S Catheline¹, M Tanter¹, C Barrière¹, D Royer¹, M Fink¹.

¹Laboratoire Ondes et Acoustique, E.S.P.C.I., Paris, FRANCE.

8:30A – 8:45A

14 VISCOELASTIC PROPERTIES OF SOFT SOLIDS USING TRANSIENT ELASTOGRAPHY.

S Catheline¹, JL Gennisson¹, G Delon¹, M Fink¹.

¹Laboratoire Ondes et Acoustique, E.S.P.C.I., Paris, FRANCE.

8:45A – 9:00A

54 VIBRATIONAL RESONANCE SPECTROSCOPY OF SOFT TISSUES.

GS Lin¹, LM Mobbs², BS Garra².

¹Advanced Imaging Associates, Fremont, California, USA; ²University of Vermont College of Medicine-Fletcher Allen Health Care, Burlington, VT, USA.

9:00A – 9:15A

63 RESONANCE FREQUENCY OF THE PLANTAR FASCIA.

YJ Chang¹, CL Wang¹, YW Shau¹, HM Chai¹.

¹National Taiwan University, Taipei, TAIWAN.

9:15A – 9:30A

67 AN OPTICAL VALIDATION FOR ULTRASOUND ELASTOMICROSCOPY.

Y Zheng¹, M Lu¹, Q Huang¹.

¹The Hong Kong Polytechnic University, HONG KONG.

9:30A – 9:45A

71 PARAMETER IDENTIFICATION OF TISSUE LUMPED MODELS BASED ON SEQUENCES OF ULTRASONIC STRAIN IMAGES.

E Turgay¹, S MacIntosh¹, R Rohling¹, S Salcudean¹.

¹University of British Columbia, Vancouver, British Columbia, CANADA.

9:45A – 10:15A

COFFEE BREAK

Nueces Ballroom Foyer

Monday 10:15A – 11:45A

Session C: Mechanical Properties of Tissues

Chair: *J Bamber, UK*

Nueces Ballroom B

10:15A – 10:30A

21 VISCOELASTIC CHARACTERIZATION OF *IN-VITRO* CANINE TISSUE.

MZ Kiss¹, T Varghese¹, U Techavipoo¹, M Hobson¹, TJ Hall¹, EL Madsen¹, J Jiang¹, JA Zagzebski¹, MA Kliewer¹.

¹The University of Wisconsin-Madison, Madison, WI, USA.

(Session C continues on next page)

10:30A – 10:45A

- 23 NONLINEAR SHEAR WAVES.
MF Hamilton¹, YA Ilinskii¹, GD Meegan¹, EA Zabolotskaya¹.
¹The University of Texas at Austin, Austin, Texas, USA.

10:45A – 11:00A

- 28 NONLINEAR PROPERTIES OF FIBROTIC TISSUES OBTAINED USING ULTRASOUND INDENTATION.
Y Zheng¹, Y Huang¹, S Leung², CYK Choi¹.
¹The Hong Kong Polytechnic University, HONG KONG; ²Prince of Wales Hospital, HONG KONG.

11:00A – 11:15A

- 35 MECHANICAL PROPERTY OF THE ACHILLES TENDON *IN VIVO*.
MC Lee¹, YW Shau¹, CL Wang², TY Hsiao².
¹National Taiwan University, Taipei, TAIWAN; ²National Taiwan University Hospital, Taipei, TAIWAN.

11:15A – 11:30A

- 61 A PRELIMINARY COMPARISON OF FREEHAND ELASTOGRAPHY AND REFLEX TRANSMISSION (ATTENUATION) IMAGING FOR VISUALIZING THERMALLY ABLATED TISSUE.
L Baker¹, A Kolen¹, J Bamber¹.
¹Institute of Cancer Research and Royal Marsden NHS Trust, Sutton, Surrey, UK.

11:30A – 11:45A

- 62 FREEHAND ELASTOGRAPHY OF THERMAL LESION ARRAYS IN EXCISED LIVER.
A Kolen¹, J Bamber¹.
¹Institute of Cancer Research and Royal Marsden NHS Trust, Sutton, Surrey, UK.

11:45A – 1:15P

GROUP LUNCH

Nueces Ballroom A

Monday 1:15P – 2:45P

Session D-1: Methods for Imaging Elastic Tissue Properties I

Chair: T Varghese, USA

Nueces Ballroom B

1:15P – 1:30P

- 04 ESTIMATION OF STRAIN TENSOR COMPONENTS FROM ANGULAR STRAIN IN ELASTOGRAPHY.
U Techavipoo¹, T Varghese¹, Q Chen¹, JA Zagzebski¹, EL Madsen¹.
¹University of Wisconsin-Madison, Madison, WI, USA.

1:30P – 1:45P

- 06 BRACHYTHERAPY SEEDS DETECTION USING VIBRO-ACOUSTOGRAPHY: A PILOT STUDY.
F Mitri¹, P Trompette¹, JY Chapelon¹.
¹INSERM U556, Lyon, FRANCE.

1:45P – 2:00P

- 16 THE FEASIBILITY OF USING ELASTOGRAPHY FOR IMAGING THE LOCAL STRAIN RATIOS IN HOMOGENEOUSLY POROUS MEDIA.
R Righetti^{1,2}, J Ophir^{1,2}, S Srinivasan^{1,2}, TA Krouskop^{1,3}.
¹The University of Texas Medical School, Houston, Texas, USA; ²University of Houston, Houston, Texas, USA; ³Baylor College of Medicine, Houston, Texas, USA.

(Session D-1 continues on next page)

2:00P – 2:15P

- 17 FEASIBILITY OF MODULUS IMAGING USING NANO-INDENTATION: COMPARISON OF MODULUS IMAGES WITH STRAIN ELASTOGRAMS USING PHANTOMS, PROSTATES, KIDNEYS AND CANCERS.

S Srinivasan^{1,2}, J Ophir^{1,2}, TA Krouskop^{1,3}, RE Price⁴.

¹The University of Texas Medical School, Houston, TX, USA; ²University of Houston, Houston, TX, USA; ³Baylor College of Medicine, Houston, TX, USA; ⁴The University of Texas M. D. Anderson Cancer Center, Houston, TX, USA.

2:15P – 2:30P

- 58 PALPATION IMAGING FOR BIOPSY GUIDANCE AND HAPTIC SENSOR-ACTUATOR APPLICATIONS IN MEDICINE.

W Khaled¹, S Reichling¹, OT Bruhns¹, GJ Monkman³, S Egersdrofer³, M Baumann⁴, H Boese⁴, H Freimuth⁵, A Tunayar⁵, A Lorenz⁶, A Pesavento⁶, K Kuehne², T Senge², U Scheipers¹, H Ermert¹.

¹Ruhr-University, Bochum, GERMANY; ²Urology University Hospital, Ruhr-University Bochum, Herne, GERMANY; ³Fachhochschule Regensburg, special field electrical engineering, GERMANY; ⁴Fraunhofer-Institut fuer Silicatforschung ISC, Wuerzburg, GERMANY; ⁵Institut fuer Mikrotechnik, Mainz GmbH, Mainz, GERMANY; ⁶LP-IT Innovative Technologies GmbH, Bochum, GERMANY.

2:30P – 2:45P

- 26 A STRAIN ESTIMATION METHOD USING REGULARIZED AUTOREGRESSIVE ANALYSIS.

Y Cui¹, E Brusseau¹, D Friboulet¹, D Vray¹.

¹CREATIS, Lyon, FRANCE.

2:45P – 3:15P

COFFEE BREAK

Nueces Ballroom Foyer

Monday**3:15P – 5:30P****Session E: Clinical and Animal Applications and Results**

Chair: B Garra, USA

Nueces Ballroom B

3:15P – 3:30P

- 33 SONOELASTIC DETECTION OF CANCER IN RADICAL PROSTATECTOMY SPECIMENS.

KJ Parker¹, BC Porter¹, LS Taylor¹, G Nadasdy², Z Wu¹, D Pasternack¹, PA di'Santagnes¹, P Nigwekar¹, RB Baggs¹, DJ Rubens¹.

¹University of Rochester, Rochester, NY, USA; ²Ohio State University Medical Center, Columbus OH, USA.

3:30P – 3:45P

- 27 SHEAR MODULUS IMAGING ON INTERSTITIAL ELECTROMAGNETIC WAVE COAGULATION TREATMENT OF HUMAN *IN VIVO* LIVER CARCINOMA.

C Sumi¹, M Kubota², G Wakabayashi³, M Tanabe³.

¹Sophia University, Tokyo, JAPAN; ²Yamachika Memorial Hospital, Kanagawa, JAPAN; ³Keio University Medical School, Tokyo, JAPAN.

3:45P – 4:00P

- 42 LESION SIZE RATIO FOR DIFFERENTIATING AMONG BREAST LESIONS.

TJ Hall¹, WE Svensson², P Von Behren³, Y Zhu⁴, J Malin³, C Spalding⁴, A Connors², D Chopra², C Lowery³.

¹University of Wisconsin-Madison, Madison, WI, USA; ²Charing Cross Hospital NHS Trust, London, UK; ³Siemens Medical Solutions Ultrasound Group, Issaquah, WA, USA; ⁴University of Kansas Medical Center, Kansas City, KS, USA.

(Session E continues on next page)

4:00P – 4:15P

46 OPTIMIZATION OF PRECOMPRESSION AND COMPRESSION FOR CLINICAL BREAST ELASTOGRAPHY.

BS Garra¹, E Jannicky¹, LM Mobbs¹, S Felker¹, L Weiss¹, S Srinivasan^{2,3}, J Ophir^{2,3}.

¹University of Vermont College of Medicine-Fletcher Allen Health Care, Burlington, VT, USA;

²The University of Texas Medical School, Houston, TX, USA; ³University of Houston, Houston, TX, USA.

4:15P – 4:30P

48 INITIAL DEMONSTRATION OF STAGING DEEP VENOUS THROMBOSIS USING ULTRASOUND ELASTICITY IMAGING.

JM Rubin¹, H Xie¹, K Kim¹, WF Weitzel¹, X Chen¹, M O'Donnell¹, SR Aglyamov², SY Emelianov², SK Wroblewski¹, DD Myers¹, TW Wakefield¹.

¹University of Michigan, Ann Arbor, MI, USA; ²University of Texas at Austin, Austin, TX, USA.

4:30P – 4:45P

51 ELASTOGRAPHIC CHARACTERISTICS OF BENIGN BREAST LESIONS THAT SONOGRAPHICALLY MAY MIMIC CANCER.

BS Garra¹, LM Mobbs¹, E Jannicky¹, S Felker¹, L Weiss¹, S Srinivasan^{2,3}, J Ophir^{2,3}.

¹University of Vermont College of Medicine-Fletcher Allen Health Care, Burlington, VT, USA;

²The University of Texas Medical School, Houston, TX, USA; ³University of Houston, Houston, TX, USA.

4:45P – 5:00P

53 VIBRATIONAL DOPPLER IMAGING IN DIFFERENTIATION OF BENIGN VERSUS MALIGNANT BREAST MASSES BY VDI:B-SCAN LESION AREA RATIO.

BS Garra¹, LM Mobbs¹, GS Lin².

¹University of Vermont College of Medicine-Fletcher Allen Health Care, Burlington, VT, USA;

²Advanced Imaging Associates, Fremont, California, USA.

5:00P – 5:15P

57 INTRAVASCULAR ULTRASOUND STRAIN IMAGING WITH ROTATING SINGLE ELEMENT TRANSDUCERS: INITIAL *IN VIVO* EXPERIMENTS.

C Perrey¹, W Bojara¹, S Holt¹, M Lindstaedt¹, H Ermert¹.

¹Ruhr University Bochum, GERMANY.

5:15P – 5:30P

69 MONITORING THE EFFECT OF ACUPUNCTURE NEEDLING ON HUMAN CONNECTIVE TISSUE *IN VIVO*.

HM Langevin¹, EE Konofagou², BS Garra¹.

¹University of Vermont, Burlington, VT, USA; ²Brigham and Women's Hospital – Harvard Medical School, Boston, MA, USA.

Monday 7:00P – 10:00P

Conference Dinner

Nueces Ballroom B

7:00P – 10:00P

00 THE APPLICATION OF HISTORICAL AND ARCHEOLOGICAL RESEARCH IN THE RE-CREATION OF THE SHIPS OF DISCOVERY. **See Abstract on Page 21**

Rick Stryker¹, Director.

¹Corpus Christi Museum of Science and History, Corpus Christi, Texas, USA.

Piano selections performed by Eva Maciejko, Montreal, CANADA.

Tuesday, October 14

7:00A – 5:30P

7:00A – 8:00A

BREAKFAST

Glass Pavilion Restaurant Buffet

7:00A – 5:30P

Registration Desk Open

Conference Office Open

Session P: Posters

Session X: Equipment Exhibit

3rd Floor Escalator Foyer

Matagorda Room

Nueces Ballroom Foyer

Nueces Ballroom Foyer

Tuesday

8:00A – 9:30A

Session D-2: Methods for Imaging Elastic Tissue Properties II

Chair: *H Ermert, Germany*

Nueces Ballroom B

8:00A – 8:15A

30 NONCONTACT ULTRASOUND INDENTATION USING WATER BEAM.

M Lu¹, Y Zheng¹.

¹The Hong Kong Polytechnic University, HONG KONG.

8:15A – 8:30A

31 ANISOTROPIC PROPERTIES OF BREAST CANCER - *IN VIVO* RESULTS UTILIZING A CUBIC MODEL.

R Sinkus¹, M Tanter², T Nisius³, C Kuhl⁴.

¹Philips Research, Hamburg, GERMANY; ²Laboratoire Ondes et Acoustique, E.S.P.C.I., Paris, FRANCE; ³RheinAhrCampus, Remagen, GERMANY; ⁴University Hospital, Bonn, GERMANY.

8:30A – 8:45A

08 PROSTATE ELASTOGRAPHY *IN VITRO*.

R Souchon¹, O Rouvière², A Gelet², J Ophir³, JY Chapelon¹.

¹INSERM U556, Lyon, FRANCE; ²Hopital Edouard Herriot, Lyon, FRANCE; ³The University of Texas Medical School, Houston, TX, USA.

8:45A – 9:00A

34 HIFU LESION FORMATION MONITORED BY “PASSIVE” ELASTOGRAPHY *IN VITRO*.

G Bouchoux¹, R Souchon¹, C Lafon¹, D Cathignol¹, JY Chapelon¹.

¹INSERM U556, Lyon, FRANCE.

9:00A – 9:15A

47 INTERFERENCE PATTERN APPROACHES TO MEASURE THE SHEAR MODULUS OF HOMOGENEOUS BIO-MATERIALS.

Z Wu¹, LS Taylor¹, DJ Rubens¹, KJ Parker¹.

¹University of Rochester, Rochester, NY, USA.

9:15A – 9:30A

50 A HIGH FREQUENCY (20 MHZ) ULTRASOUND BASED ELASTOGRAPHY SYSTEM FOR *IN VIVO* SKIN ELASTICITY IMAGING.

M Vogt¹, S Scharenberg², R Scharenberg², K Hoffmann¹, P Altmeyer¹, H Ermert¹.

¹Ruhr-University, Bochum, GERMANY; ²Taberna Pro Medicum GmbH, Lueneburg, GERMANY.

9:30A – 10:00A

COFFEE BREAK

Nueces Ballroom Foyer

Tuesday 10:00A – 10:45A
Session F: Biomechanical Tissue Modeling

Chair: *L Taylor, USA*

Nueces Ballroom B

10:00A – 10:15A

- 11 A GENERALIZED KELVIN-VOIGT VISCOELASTIC CONSTITUTIVE MODEL FOR SOFT TISSUE.
LS Taylor¹, DJ Rubens¹, KJ Parker¹.

¹University of Rochester, Rochester, NY, USA.

10:15A – 10:30A

- 15 FORWARD AND SENSITIVITY STUDIES RELATED TO TRANSIENT ELASTOGRAPHY.
E Park¹, AM Maniatty¹.

¹Rensselaer Polytechnic Institute, Troy, NY, USA.

10:30A – 10:45A

- 36 DYNAMIC RESPONSE OF THE PLANTAR SOFT TISSUES UNDER THE METATARSAL HEAD IN THE YOUNG AND ELDERLY.

TC Hsu¹, YW Shau², CL Wang³.

¹Chang Gung Memorial Hospital, Taoyuan TAIWAN; ²National Taiwan University, Taipei, TAIWAN;

³National Taiwan University Hospital, Taipei, TAIWAN.

Tuesday 10:45A – 11:30A
Session G: Instrumentation and Phantoms

Chair: *T Shiina, Japan*

Nueces Ballroom B

10:45A – 11:00A

- 37 BREAST AND PROSTATE CANCER DIAGNOSIS BY REAL-TIME TISSUE ELASTICITY IMAGING SYSTEM -A FEASIBILITY STUDY.

T Shiina¹, M Yamakawa¹, N Nitta¹, E Ueno¹, T Matsumura², S Tamano², R Shinomura², T Mitake².

¹University of Tsukuba, Tsukuba, JAPAN; ²Hitachi Medical Corporation, Kashiwa, JAPAN.

11:00A – 11:15A

- 38 AGAR/GELATIN LOW CONTRAST SPHERICAL LESION PHANTOMS FOR ASSESSING MR AND ULTRASOUND ELASTOGRAPHY PERFORMANCE.

E Madsen¹, G Frank¹, T Krouskop^{2,3}, M Hobson¹, H Shi¹, MM Dooley⁴, T Varghese¹, J Ophir².

¹University of Wisconsin-Madison, Madison, WI, USA; ²The University of Texas Medical School, Houston, Texas, USA; ³Baylor College of Medicine, Houston, Texas, USA; ⁴Dartmouth College, Hanover NH, USA.

11:15A – 11:30A

- 43 ELASTICITY RESEARCH PLATFORM.

WG Scott¹, RM Schmitt¹, RD Irving¹.

¹WinProbe Corporation, North Palm Beach, Florida, USA.

11:30A – 1:30P

GROUP LUNCH
REPUBLIC OF TEXAS BAR & GRILL
20th Floor Penthouse
270° Bay View, Walkout Terrace, & Telescope



Tuesday

1:30P – 2:30P

Session H:

Signal and Image Processing, and New Algorithms

Chair: T Hall, USA

Nueces Ballroom B

1:30P – 1:45P

40 ULTRASONIC TEMPERATURE IMAGING FOR GUIDING FOCUSED ULTRASOUND SURGERY: EFFECT OF ANGLE BETWEEN IMAGING BEAM AND THERAPY BEAM.

N Miller¹, K Bograchev¹, J Bamber¹.

¹Royal Marsden NHS Trust/Institute of Cancer Research, Sutton, Surrey, UK.

1:45P – 2:00P

41 THE STATISTICS OF MOTION TRACKING WITH LARGE DEFORMATIONS.

TJ Hall¹, LT Cook², Y Zhu².

¹University of Wisconsin-Madison, Madison, WI, USA; ²University of Kansas Medical Center, Kansas City, KS, USA.

2:00P – 2:15P

55 NOVEL MYOCARDIAL STRAIN IMAGING BASED ON 3-D DISPLACEMENT VECTOR MEASUREMENT.

N Nitta¹, Y Aoki¹, M Yamakawa¹, T Shiina¹.

¹University of Tsukuba, Tsukuba, JAPAN.

2:15P – 2:30P

60 SHEAR WAVE SPEED RECONSTRUCTION IN TRANSIENT ELASTOGRAPHY.

D Renzi¹, J McLaughlin¹.

¹Rensselaer Polytechnic Institute, Troy, NY, USA.

Tuesday

2:30P – 3:15P

Session I:

Forward and Inverse Problems

Chair: PE Barbone, USA

Nueces Ballroom B

2:30P – 2:45P

22 A VARIATIONAL FORMULATION LEADING TO DIRECT ELASTIC MODULUS RECONSTRUCTION.

PE Barbone¹.

¹Boston University, Boston, MA, USA.

2:45P – 3:00P

24 INTERIOR ELASTODYNAMICS INVERSE PROBLEMS: SHEAR WAVESPEED RECONSTRUCTION IN TRANSIENT ELASTOGRAPHY.

L Ji¹, J McLaughlin¹, D Renzi¹, J Yoon¹.

¹Rensselaer Polytechnic Institute, Troy, NY, USA.

3:00P – 3:15P

64 DIRECT RECONSTRUCTION OF ELASTIC MODULUS IMAGES FROM ULTRASOUND IMAGES.

A Oberai¹, N Gokhale¹, PE Barbone¹.

¹Boston University, Boston, MA, USA.

3:15P – 3:45P

COFFEE BREAK

Nueces Ballroom Foyer

Tuesday 3:45P – 5:30P
Session J: Cardiovascular Elasticity

Chair: G Cloutier, Canada

Nueces Ballroom B

3:45P – 4:00P

- 01 MYOCARDIAL REGIONAL ELASTIC PROPERTIES MAPPING BASED ON ECHOCARDIOGRAPHIC 3-D RECONSTRUCTION OF THE LEFT VENTRICLE.

SG Kolchanova¹, SS Ustuzganin¹, SY. Sokolov¹, ES Saveljeva¹, EV Marchenko², VV Chestukhin², BL Mironkov², FA Blyakhman¹.

¹Ural State University, Ekaterinburg, RUSSIA; ²Institute of Transplantology and Artificial Organs, Moscow, RUSSIA.

4:00P – 4:15P

- 05 CORRECTION FOR SIMULTANEOUS CATHETER ECCENTRICITY AND TILT ON STRAIN ESTIMATION IN INTRAVASCULAR ELASTOGRAPHY.

H Shi¹, T Varghese^{1,2}, G Gimelli³, JA Zagzebski¹, M Wolff³, EL Madsen¹.

¹Department of Medical Physics, University of Wisconsin-Madison, Madison, WI, USA.

4:15P – 4:30P

- 09 NON-INVASIVE VASCULAR ELASTOGRAPHY: THEORETICAL INVESTIGATION.

RL Maurice¹, J Ohayon², G Finet³, G Soulez⁴, G Cloutier¹.

¹University of Montreal Hospital - Research Center, Montreal, CANADA; ²Institut A. Bonniot, La Tronche, FRANCE; ³Cardiovascular Hospital, Claude Bernard University, Lyon, FRANCE; ⁴University of Montreal Hospital, Montreal, CANADA.

4:30P – 4:45P

- 32 IMAGING OF VULNERABLE PLAQUE IN CORONARY ARTERY BY PARAMETRIC IVUS AND ACOUSTIC MICROSCOPY.

Y Saijo¹, A Tanaka¹, H Sasaki¹, N Owada¹, Y Akino², M Tanaka¹.

¹Tohoku University, Sendai, JAPAN; ²Miyagi Social Insurance Hospital, Sendai, JAPAN.

4:45P – 5:00P

- 12 PERIPHERAL ARTERIAL STRAIN IMAGING USING EXTERNAL PRESSURE EQUALIZATION.

WF Weitzel¹, K Kim¹, JM Rubin¹, H Xie¹, X Chen¹, M O'Donnell¹.

¹University of Michigan, Ann Arbor, MI 48109, USA.

5:00P – 5:15P

- 20 IVUS MODULOGRAPHY OF VULNERABLE PLAQUES USING A PARAMETRIC FINITE ELEMENT MODEL: VALIDATION ON A PHANTOM AND HUMAN CORONARY ARTERY.

RA Baldewsing¹, JA Schaar^{1,2}, F Mastik¹, CWJ Oomens³, AFW van der Steen^{1,2}.

¹Erasmus Medical Center Rotterdam, Rotterdam, The NETHERLANDS; ²Interuniversity Cardiology Institute of the Netherlands (ICIN), Utrecht, The NETHERLANDS; ³Eindhoven University of Technology, Eindhoven, The NETHERLANDS.

5:15P – 5:30P

- 10 NON-INVASIVE ELASTICITY IMAGING IN SMALL VESSELS: EXPERIMENTS ON TISSUE-MIMICKING PHANTOMS.

RL Maurice¹, M Daronat¹, Z Qin¹, FS Foster², G Cloutier¹.

¹University of Montreal Hospital – Research center, Montreal, CANADA; ²Sunnybrook and Women's College Health Sciences Centre - University of Toronto, Toronto, CANADA.

7:00A – 8:00A

BREAKFAST

Glass Pavilion Restaurant Buffet

7:00A – 11:30A

Registration Desk Open

Conference Office Open

3rd Floor Escalator Foyer

Matagorda Room

Wednesday**8:00A – 8:45A****Session K: Complementary 3D and Multimodality Applications**Chair: *R Sinkus, Germany*

Nueces Ballroom B

8:00A – 8:15A

07 TISSUE REGION DELIMINATION THROUGH STATISTICALLY BASED PARAMETER CONSOLIDATION.

*EEW Van Houten¹, KP Mecke², JB Weaver³, KD Paulsen⁴.*¹University of Canterbury, Christchurch, NEW ZEALAND; ²Technische Universitat Darmstadt, Hessen, GERMANY; ³Dartmouth-Hitchcock Medical Center, Lebanon, NH, USA; ⁴Dartmouth College, Hanover, NH, USA.**8:15A – 8:30A**

70 SHEAR MODULUS ESTIMATION USING A PARALLELIZED PARTIAL VOLUME RECONSTRUCTION APPROACH.

*MM Doyley^{1,2}, EEW Van Houten³, JB Weaver^{1,2}, S Poplack^{1,2}, F Kennedy², KD Paulsen^{2,3}.*¹Dartmouth Medical School, Hanover, NH, USA; ²Dartmouth College, Hanover, NH, USA; ³Norris Cotton Cancer Center, Lebanon NH, USA.**8:30A – 8:45A**

45 NUMERICAL EVALUATION OF A 1.5D 3x3 BEAMFORMER ARRAY FOR REAL TIME CROSS-CORRELATION IMAGING (CCI).

*RM Schmitt¹, WG Scott¹, RD Irving¹.*¹WinProbe Corporation, North Palm Beach, Florida, USA.**Wednesday****8:45A – 10:00A****Session D-3: Methods for Imaging Elastic Tissue Properties III**Chair: *JL Katz, USA*

Nueces Ballroom B

8:45A – 9:00A56 SUPERSONIC SHEAR IMAGING: A NEW TECHNIQUE FOR TISSUE VISCOELASTICITY MAPPING. *IN VITRO AND IN VIVO RESULTS.**J Bercoff¹, M Muller¹, M Tanter¹, M Fink¹.*¹Laboratoire Ondes et Acoustique, E.S.P.C.I., Paris, FRANCE.**9:00A – 9:15A**

18 AN EXPERIMENTAL CHARACTERIZATION OF SPATIAL RESOLUTION IN ELASTOGRAPHY: ANALYSIS OF THE TRADEOFFS BETWEEN SPATIAL RESOLUTION AND CONTRAST-TO-NOISE RATIO.

*S Srinivasan^{1,2}, R Righetti^{1,2}, J Ophir^{1,2}.*¹The University of Texas Medical School, Houston, TX, USA; ²University of Houston, Houston, TX, USA.

(Session D-3 continues on next page)

9:15A – 9:30A

- 59 INTRAOPERATIVE APPLICATIONS OF ELASTICITY IMAGING USING VIBROGRAPHY.
B Brendel¹, S Siebers¹, M Scholz¹, C Welp¹, J Werner¹, A Lorenz², A Pesavento², H Ermert¹.
¹Ruhr-University, Bochum, GERMANY; ²LP-IT Innovative Technologies GmbH, Bochum, GERMANY.

9:30A – 9:45A

- 65 COMPARATIVE EVALUATION OF STRAIN AND RECONSTRUCTIVE ELASTOGRAPHY.
MM Doyley^{1,2}, S Srinivasan^{3,4}, A Mohns², J Ophir^{3,4}.
¹Dartmouth Medical School, Hanover, NH, USA; ²Dartmouth College, Hanover, NH, USA;
³The University of Texas Medical School, Houston, TX, USA; ⁴University of Houston, Houston, TX, USA.

9:45A – 10:00A

- 68 CONTINUED SCANNING ACOUSTIC MICROSCOPY AND ULTRASONIC WAVE PROPAGATION FOR IMAGING AND MEASUREMENTS OF CONNECTIVE TISSUE PROPERTIES.
JL Katz¹, Y Wang¹, HJ Hein², P Spencer¹, D Hazony⁴.
¹University of Missouri-Kansas City, Kansas City, Missouri, U.S.A.; ²Martin-Luther-University Halle-Saale Medical School, Halle/Saale, GERMANY; ⁴Case Western Reserve University, Cleveland, Ohio, USA.

10:00A – 10:30A

COFFEE BREAK

Nueces Ballroom Foyer

Wednesday 10:30A – 11:30A

Session D-4: Methods for Imaging Elastic Tissue Properties IV

Chair: Y Zheng, Hong Kong

Nueces Ballroom B

10:30A – 10:45A

- 03 PROGRESS IN THE ELASTOGRAPHIC IMAGING OF RADIOFREQUENCY ABLATED THERMAL LESIONS.
T Varghese¹, U Techavipoo¹, JA Zagzebski¹, Q Chen¹, W Liu¹, FT Lee Jr.¹.
¹University of Wisconsin-Madison, Madison, WI, USA.

10:45A – 11:00A

- 19 INFORMATION CONTENT IN TRANSIENT SONOELASTOGRAPHY.
J McLaughlin¹, JR Yoon¹.
¹Rensselaer Polytechnic Institute, Troy, NY, USA.

11:00A – 11:15A

- 29 ULTRASONIC MEASUREMENT OF INHOMOGENEOUS STRAINS IN ARTICULAR CARTILAGE INDUCED BY OSMOTIC LOADING.
Y Zheng¹, J Shi¹, L Qin², SG Patil¹.
¹The Hong Kong Polytechnic University, HONG KONG; ²The Chinese University of Hong Kong, HONG KONG.

11:15A – 11:30A

- 52 VIBRATIONAL DOPPLER IMAGING OF SOFT TISSUE MECHANICAL PROPERTIES.
GS Lin¹, LM Mobbs², BS Garra².
¹Advanced Imaging Associates, Fremont, California, USA; ²University of Vermont College of Medicine-Fletcher Allen Health Care, Burlington, VT, USA.

11:30A – 1:00P

LUNCH

Glass Pavilion Restaurant Buffet

Session P: Posters

- 25 DEVELOPMENT OF REAL-TIME TISSUE ELASTOGRAPHY.
T Oosaka¹, T Matsumura¹, N Murayama¹, T Mitake¹, E Ueno², Y Kim³, T Shiina².
¹Hitachi Medical Corporation, JAPAN; ²University of Tsukuba, JAPAN; ³University of Washington, USA.
- 39 X-RAY TOMOSYNTHESIS ELASTOGRAPHY: A FEASIBILITY STUDY.
MS Richards¹, PE Barbone¹, T Wu², DB Kopans², RH Moore².
¹Boston University, Boston, Mass, USA; ²Massachusetts General Hospital, Boston, Mass, USA.
- 44 CHARACTERIZATION OF THE MECHANICAL BEHAVIOR OF THE INCLUSION-MATRIX INTERFACE: THEORY AND SIMULATION OF BREAST LESION MODELS.
E Maciejko¹, M Bertrand¹, TA Krouskop².
¹École Polytechnique de Montréal, Montréal, Québec, CANADA; ²Baylor College of Medicine, Houston, TX, USA.
- 49 REALIZATION OF REALTIME TISSUE STIFFNESS ESTIMATION IN MEDICAL ULTRASOUND IMAGING SYSTEM.
M Jeong¹, S Kwon¹, J Park¹, G Cho¹.
¹Daejin University, Pocheon, Kyeonggi, KOREA.
- 66 PLANTAR TISSUES PROPERTIES OBTAINED USING ULTRASOUND INDENTATION FOR RHEUMATOID ARTHRITIS AND DIABETES MELLITUS PATIENTS.
Y Zheng¹, APC Choi¹, JMW Ho¹.
¹The Hong Kong Polytechnic University, HONG KONG.
- 72 A PROPOSAL FOR AN ACCURATE DATA COMPANDING TECHNIQUE BASED ON SEQUENTIAL DETECTION OF TIME DELAYS.
T Sato¹, Y Watanabe¹, S Goka¹, H Sekimoto¹.
¹Tokyo Metropolitan University, Tokyo, JAPAN.
- 73 AN ULTRASOUND PROPAGATION MODEL FOR CHARACTERIZING BIOMECHANICAL PROPERTIES OF OCULAR TISSUE.
J Liu¹, CJ Roberts¹.
¹The Ohio State University, Columbus OH, USA.
- 74 PRELIMINARY STUDIES ON NANOPARTICLE ELASTICITY CONTRAST.
J Liu¹, TJ Rosol¹.
¹The Ohio State University, Columbus OH, USA.

Session X: Equipment Exhibit

Hitachi Medical Corporation.
Kashiwa, JAPAN.

Medison Corporation.
Seoul, KOREA.

ABSTRACTS

Second International Conference on the Ultrasonic Measurement and Imaging of Tissue Elasticity

Corpus Christi, Texas, USA

October 12–15, 2003

Guest Lecture

00 **THE APPLICATION OF HISTORICAL AND ARCHAEOLOGICAL RESEARCH IN THE RE-CREATION OF THE SHIPS OF DISCOVERY.**

Rick Stryker¹, Director.

¹Corpus Christi Museum of Science and History, Corpus Christi, Texas, USA.

The **Niña**, **Pinta**, and **Santa María** are among the best known ships that ever sailed. Despite the fact that there are no pictures, plans, or contemporary descriptions of them, speculation about them is unceasing. In celebration of the Columbus Quincentenary, Spain recreated two sets of the ships after extensive archival and archaeological research. One set is in Huelva, Spain, the launching point of Columbus' first expedition, and the other set is in Corpus Christi – after having crossed the Atlantic in 1991.

The Corpus Christi Museum is home for the Columbus replicas as well as two of the most important shipwrecks in the western Hemisphere. The location, excavation and conservation of these two shipwrecks tell part of the story of how it was possible to recreate ships like those of Columbus. The first shipwreck is that of the Spanish treasure ships that wrecked on Padre Island in 1554. The second is the **La Belle**, La Salle's ship that wrecked in Matagorda Bay in 1686.



Since 1985, Mr. Stryker has been director of the Corpus Christi Museum of Science and History. Previously, he was assistant director of the Grand Rapids (Michigan) Public Museum. He has a master's degree in American History from the University of Delaware.

Session A-1: Bench-Top Methods for Measuring the Elastic Properties of Tissues (*In Vitro*)

Sunday, October 12 2:30P – 3:45P

There are several methods for measuring the some of the elastic constants of soft tissues *in vitro*. Some of the results may be technique-dependent. This tutorial/panel discussion will describe some of the methods used to make the measurements, and will discuss the underlying assumptions and their respective advantages/disadvantages.

INTRODUCTION *JM Rubin*

BENCH TOP TORSION TESTS FOR TESTING TISSUE VISCOELASTIC PROPERTIES *E Mazza*

TRANSIENT ELASTOGRAPHY FOR VISCOELASTIC MEASUREMENTS OF TISSUES. *M Fink*

INDENTATION/NANO-INDENTATION AND VIBRATION TESTS IN SOFT TISSUES. *T Krouskop*

FREQUENCY-DEPENDENT CHARACTERIZATION OF THE VISCOELASTIC PROPERTIES OF SOFT TISSUES. *MZ Kiss*

Session A-2: Methods for Imaging Elastic Attributes of Tissue

Sunday, October 12 4:15P – 5:30P

Several methods for imaging the elastic attributes of tissues *in vivo* have been described in the recent literature. This tutorial/panel discussion will concentrate on describing the various techniques, the assumption behind each one, and their intrinsic technical capabilities and limitations.

INTRODUCTION *JM Rubin*

SONOELASTOGRAPHY IMAGING. *L Taylor*

ELASTOGRAPHY IMAGING. *T Varghese*

TRANSIENT ELASTOGRAPHY IMAGING. *M Fink*

RADIATION PRESSURE VIBRO-ACOUSTOGRAPHY IMAGING. *P Trompette*

Session B: Mechanical Measurement Techniques for Tissues

Monday, October 13 8:00A – 9:45A

02 MEASUREMENT OF VISCOELASTIC PROPERTIES OF SOFT BIOLOGICAL TISSUES WITH A DYNAMIC TORSION TEST.

Edoardo Mazza¹, Davide Valtorta¹.

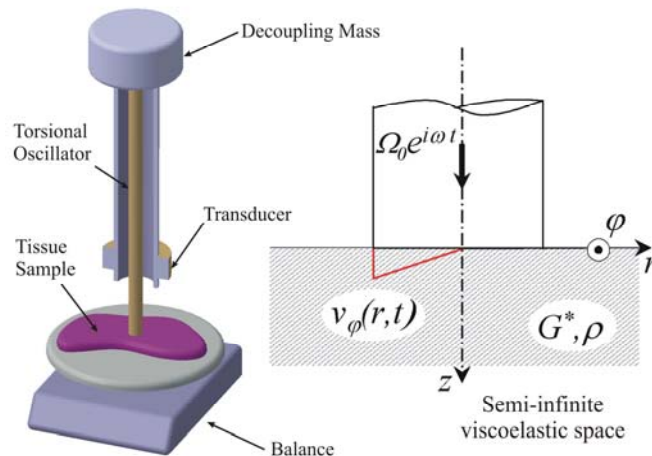
¹ETH Zürich, Swiss Federal Institute of Technology, 8062 Zürich, SWITZERLAND.

A novel technique for testing the mechanical properties of biological tissues is presented in this work. Soft tissues are characterized by means of a dynamic testing method, in which the tissue sample is made a part of a vibrating system. The experimental set-up is depicted in the figure: a rod of circular cross-section is excited at its torsional eigenfrequencies (from 1 kHz to 10 kHz) by an electromagnetic transducer (which represents the actuator as well as the sensor). Only the free end of the rod is laid against the soft tissue. The soft tissue sample lies on a balance, so that the contact force can be monitored.

The damping characteristics of the vibrating system and the resonance frequency are inferred from the control variables of a phase stabilization loop. Due to the contact with the soft tissue, changes occur in the dynamic properties of the torsional oscillator: the *Q-Factor* is reduced and the resonance frequency is shifted. From the differences between a calibration run (without soft tissue contact) and a measurement with soft tissue contact, the changes in the properties of the vibrating system are quantified. Based on an analytical model, the mechanical impedance of the material in contact is determined from these data and the complex shear modulus G^* is evaluated for each resonance frequency. The dependence of the complex shear modulus on contact force, vibration amplitude, frequency, and number of loading cycles can be studied with this experiment.

The mechanical properties of soft tissues are determined in the frequency range 1-10 kHz and compared with the results of quasi static experiments on the same tissue. Thanks to the high sensitivity of the sensor for vibration detection, the vibration amplitude can be kept very small, so that a linear viscoelastic material model can be used. The soft tissue is modeled as a semi-infinite, homogenous, isotropic medium; a boundary condition is applied in correspondence to the contact with the vibrating rod. The elastodynamic wave equation is solved for the specified torsional excitation. Depending on the soft tissue properties, shear waves (SH waves) propagate mainly in the radial direction or in the vertical direction, toward the tissue interior. From the analytical model, the mechanical impedance of the medium can be expressed as function of the material properties.

The experiment is designed to enable *in-vivo* measurements of material properties. In particular, the requirements for application during open surgery are satisfied: each component can be sterilized; performing the whole measurement requires only a few seconds, and; the experiment is non-destructive, since the amplitude of the vibration is small and the soft tissue is not damaged. Results obtained from *ex-vivo* measurements on bovine liver and kidney are presented, showing the frequency-dependent behavior of the complex shear modulus at high frequencies.



13 **NONLINEAR INTERACTION OF SHEAR WAVES IN SOFT SOLIDS USING TRANSIENT ELASTOGRAPHY.**

J.-L. Gennisson¹, X. Jacobs¹, S. Catheline¹, M. Tanter¹, C. Barrière¹, D. Royer¹, M. Fink¹.

¹Laboratoire Ondes et Acoustique, Université Paris VII, CNRS UMR 7587, ESPCI, 10 rue Vauquelin 75231 Paris cedex 05, FRANCE.

Transient elastography has shown its ability to map the elastic properties of soft tissues. Now, like other elastic imaging techniques (sonoelastography or magnetic resonance elastography), transient elastography is facing the following problem: in order to properly discriminate tumors, additional information such as nonlinearity is needed. While nonlinearity of longitudinal waves has long been studied in solids and fluids, almost no experimental work is found in the literature concerning shear waves in soft tissues. Thanks to the ultra-fast scanner, we present in this paper a nonlinear shear wave interaction experiment that illustrates theoretical results relating to nonlinear shear wave propagation, and quantifies the nonlinear behavior of a soft tissue phantom.

The ultra-fast scanner, developed in our laboratory, allows observing low frequency shear wave propagation in the body with a high frame rate (3000 Hz). Two low frequency plane shear waves ($\omega_1 = 100$ Hz, $\omega_2 = 140$ Hz) are generated by shaking transversally a rigid aluminum plate (11x17 cm) applied on one side of an Agar-gelatin phantom with a vibrator. In a typical experiment, 250 echographic images in the plane of shear wave polarization are recorded in memory. A displacement movie is obtained using crosscorrelation algorithm between successive speckle images. Thus it allows one to detect fast tissue motion induced by low frequency shear waves inside the medium. The transverse displacements field of the shear waves is measured in one dimension along the propagation axis (central axis of the rigid plate) on a distance of 40 mm which represents a few shear wavelengths. An accelerometer is set on the vibrator to control the excitation apparatus linearity.

The interaction between the two plane transverse waves with frequencies ω_1 and ω_2 is carefully studied. Harmonics and secondary waves are created during the propagation at frequencies: $3\omega_1$, $3\omega_2$, $\omega_1+2\omega_2$, $\omega_1-2\omega_2$, $\omega_2+2\omega_1$ and $\omega_2-2\omega_1$. The upper frequencies according to the theoretical prediction of the modified Burger's equation. Experiment with pure plane shear waves is compared to simulation of the modified Burger's equation including cubic nonlinearity and viscosity. Like in our previous papers, the nonlinear coefficient is quantified adjusting it as a simulation parameter in order to assure the best fit of harmonics evolution with propagation distance. The nonlinear coefficient deduced validates the order of magnitude of the Landau coefficients ($A \ll B, C$) found from other experiments (acousto-elasticity, finite-amplitude shear wave). The surprising difference found between these constants are thought to be closely related to the huge difference between the linear Lamé coefficients ($\lambda \gg \mu$).

In the last section, the feasibility of measuring the nonlinear elastic coefficient with non plane shear waves is discussed. In this case, the shear wave source is a rod and the ultrasonic signals are recorded with one single transducer. Due to diffraction effects, the harmonics and secondary waves are created at the same frequencies during the propagation but also at $2\omega_1$, $2\omega_2$, $\omega_2+\omega_1$ and $\omega_2-\omega_1$. A better understanding of these effects will lead us to determine nonlinearity coefficients of tissues *in vivo*.

By observing the transient propagation of a low frequency shear waves within soft tissues with ultrasound, one can reconstruct the local elastic properties. This method, known as transient elastography, is based on the hypothesis of a purely elastic medium. Here, we propose a more sophisticated method for studying of the viscoelastic properties of soft tissues.

The plane shear waves are generated for each frequency from 50 Hz to 500 Hz by a rigid plate (11x17 cm) in an Agar-gelatin phantom. With an ultrasonic array, 250 echographic images are recorded in memory during the shear wave propagation from a distance of 40 mm. The shear wave displacements field is estimated along the axis of propagation (the central axis of the rigid plate) using cross-correlation between successive ultrasonic signals stored in the memory. The velocity and attenuation are deduced from the spectral analysis of the phase delay and attenuation respectively.

The comparison of these experimental results to the prediction by the two simpler rheological models (the Voigt's model and the Maxwell's model) shows that the Maxwell's model is not relevant. This is confirmed by the inverse problem approach that will be described in this paper. Moreover some experimental results on beef muscle *in vitro* show the correct choice of the Voigt's model.

In the second part, tissue displacements are estimated along the ultrasonic beam of a single transducer with the shear elasticity probe. It is shown how one can measure the viscosity coefficient of the Voigt's model using a non-planar shear wave. In this case diffraction effects must be taken into account to avoid biased measurements. A numerical simulation based on Green's function in semi-infinite medium allows quantifying and correcting the diffraction effects. Finally, this simple and portable shear elasticity probe could be used as an ultrasonic rheometer for soft solids.

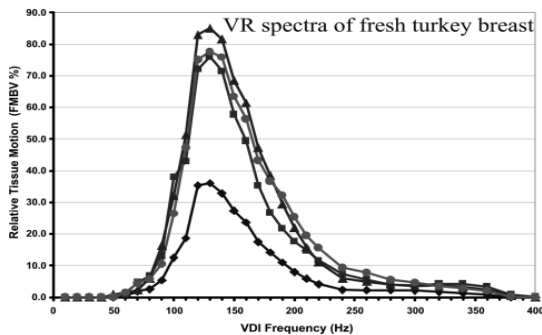
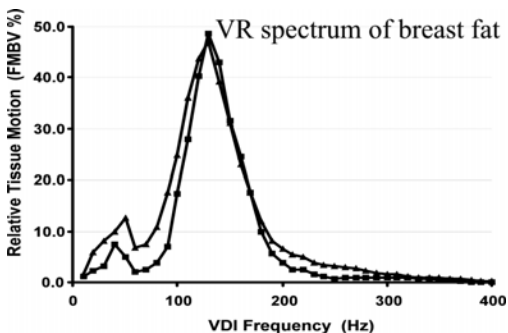
G. Sharat Lin¹, Louise M. Mobbs², Brian S. Garra².¹Advanced Imaging Associates, Fremont, California, USA; ²University of Vermont College of Medicine-Fletcher Allen Health Care, Burlington, VT, USA.

Objective: To evaluate vibrational resonance spectroscopy (VRS) as a new quantitative method for differentiation and characterization of soft tissues.

Methods: VRS utilizes an externally-applied vibration to induce tissue vibration responses over a range of audio excitation frequencies. By measuring the ultrasonic tissue Doppler amplitude at each vibrational frequency, a vibrational resonance (VR) spectrum is obtained. Sinusoidal waveforms were produced by an HP or Agilent 33120A functional generator and swept through a low audio range from 10 to 400 Hz in 10-Hz steps. After boosting by a 2-watt audio amplifier, the signals were used to drive an audio transducer attached through a vibration damping foam rubber pad to the side of an ultrasound transducer. Power Doppler imaging on a GE Diasonics Gateway scanner was used with custom software to measure the spatially-integrated Doppler echo amplitude within user-specified regions of interest. A flat linear array was operated at 6-MHz power Doppler, pulse repetition frequency at 500 Hz, and color gain at 10–15 dB below typical blood flow settings. Calibration of audio pathway frequency response was done with a sound level meter coupled to the audio transducer through a 2-cm acoustic standoff pad. The resulting calibration coefficients were used to correct all VR spectra to a flat frequency response. A variety of ultrasound phantoms (including several from Nuclear Associates and ATS); fresh and processed turkey breast; and muscle, fat, liver, and breasts of healthy human volunteers (after informed consent) were scanned with VRS.

Results: VRS produced spectra that were reproducible in shape, though not absolute amplitude, from one examination to another and from one transducer orientation to another. Phantoms yielded unique multi-peak VR spectra, reflecting their different compositions and the mechanical properties of any inclusion particles. Scanning one ATS phantom from each of four different accessible sides resulted in VR spectra of the same shape. *In vivo* scanning of human soft tissues exhibited a primary resonance peak at 120–130 Hz, each with unique peak shapes. Fatty tissues displayed the narrowest primary peaks with 53 ± 1.4 Hz FWHM (mean \pm SD full-width half-maximum). Organ parenchyma (liver, breast) demonstrated high-frequency broadening at 70 ± 2.5 Hz FWHM. Directional fibrous tissue (skeletal muscle) provided the broadest primary peaks at 93 ± 4.9 Hz FWHM. Early results with benign breast masses suggest a markedly altered VR spectrum. Fresh turkey breast consistently demonstrated a primary peak at 120–140 Hz with a width of 62 ± 11.4 Hz FWHM. Processed sliced turkey breast exhibited the same primary peak but with much greater variability in shape and more frequent high-frequency shoulders.

Conclusions: VRS provides reproducibly quantifiable spectral shape parameters that may be useful in differentiating complex elastic materials and different types of soft tissues – healthy and abnormal, *in vivo* and *in vitro*.



RESONANCE FREQUENCY OF THE PLANTAR FASCIA.

Yu-Jen Chang¹, Chung-Li Wang², Yio-Wha Shau³, Huei-Ming Chai⁴.

^{1,4}School and Graduate Institute of Physical Therapy, College of Medicine, National Taiwan University, Taipei, TAIWAN; ²Department of Orthopedic Surgery, National Taiwan University Hospital, College of Medicine, National Taiwan University, Taipei, TAIWAN; ³Institute of Applied Mechanics, National Taiwan University, Taipei, TAIWAN.

We measured the resonance frequency of the plantar fascia *in-vivo* using ultrasonography. Young volunteers stood on a specially designed platform, upon which ultrasound can insolate the planter fascia from beneath. An electronic vibrator was attached to the dorsal surface of the first metatarsophalangeal joint of the foot to be measured. The vibration speed of the plantar fascia was measured from the Doppler mode of ultrasonography in programmed frequency spectrum. The displacement of the plantar fascia was derived from the integral of the speed. Resonance frequency of the plantar fascia was defined as the frequency in which the plantar fascia showed the greatest displacement. The results showed that the resonance frequency of plantar fascia ranged between 26 and 32 Hz. The proposed technique is capable of determining the resonance frequency of the plantar fascia, which might be useful in investigating the mechanical properties of the plantar fascia *in-vivo*.

We have previously developed an ultrasound elastomicroscopy system for the assessment of soft tissues with fine structures. It includes a 50 MHz ultrasound system and a calibrated compression device using a load cell to measure compression in the specimen between a compressor and rigidly fixed specimen platform [1-3]. In this abstract, we introduced an optical validation method for this ultrasound elastomicroscopy system.

As shown in Figure 1, an ultrasound system and an optical system were set together to work simultaneously. The ultrasound transducer was located under the platform, which had a small hole at the center. Ultrasound propagated through a thin film covering the hole and into the soft sponge specimens on top of the specimen platform. A compressor was attached to the load cell and used to compress the specimen from the top. During a compression test on the specimen, the ultrasound signals were digitized at 500MHz and one lateral side of the specimen was monitored by an arthroscopy system. The displacements of the sponge tissues at different depths were estimated from the ultrasound echoes using a cross-correlation algorithm. Meanwhile, the displacements of the tissues were also measured using the recorded optical images of the side surface of the specimen. The displacements of the sponge tissues at similar depths as those selected in the ultrasound tracking were derived from the optical images using a 2-D cross-correlation algorithm.

Figure 2 shows a pair of typical results when a sponge specimen (approximately 2mm in thickness) was compressed by 10%. Results showed that the displacements measured by the two systems almost agreed with each other. As the deformation of the specimen increases, the difference of the measured displacements increases. This might be due to different deformation patterns of the sponge specimens in the middle portion and the surface region when the deformation was large. Efforts are being made to test specimens with uniform deformation pattern under large compression.

Acknowledgements: This project was partially supported by the Research Grant Council of Hong Kong (PolyU5199/02E, PolyU 5245/03E) and The Hong Kong Polytechnic University.

- References: [1] Zheng et al. *Med Biol Eng Comp* 38: 534-, 2001.
 [2] Zheng et al. *Phys Med Biol* 95: 3165-, 2002.
 [3] Zheng et al. *SPIE Med Imag: Ultrason Imag Sig Process Conf*: 398-, 2003.

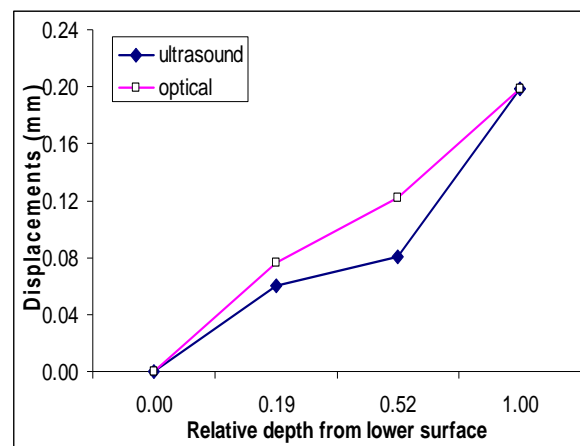
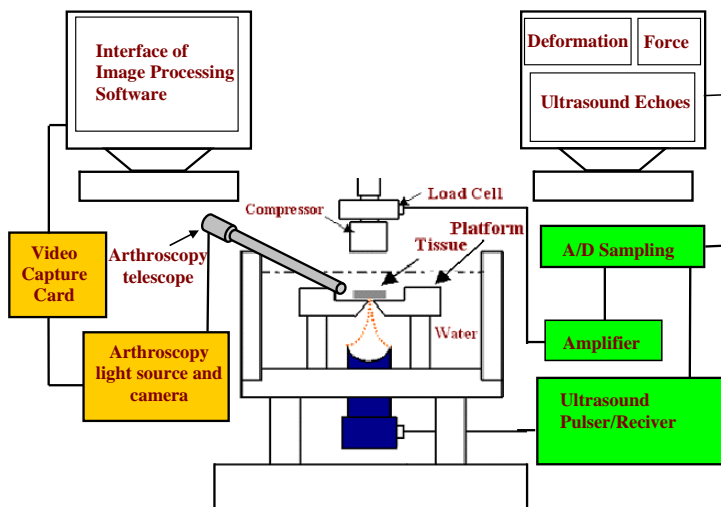


Figure 1. Schematic diagram of the optical validation system for the depth-dependent ultrasound indentation.

Figure 2. The displacements of tissues at different depths of a sponge specimen after 10% deformation was applied.

Emre Turgay¹, Scott MacIntosh¹, Robert Rohling¹, Septimiu Salcudean¹.

¹University of British Columbia, Vancouver, British Columbia, CANADA.

Introduction: A new method of imaging the viscoelastic properties of soft tissue with ultrasound is presented and partially validated in phantom studies. The key difference from standard elastography is the use of system identification techniques to estimate the parameters of a finite element model (FEM) of the tissue. To do this, the tissue boundary is excited mechanically by a computer-controlled vibrator. The resultant tissue motion is tracked in successive US images. The system identification method then computes the mechanical properties of the FEM that best fit the motion vectors.

Theory: A linear, lumped mass-spring-damper model:
$$M\ddot{X} + B\dot{X} + KX = f \quad (1)$$
 is assumed for the tissue, where X is a vector of element strains, f is the boundary traction, M , B and K are mass, viscosity and stiffness matrices dependent on the properties of tissue and on spatial boundary conditions.

In a first approach, (1) is re-written as:
$$\Theta \theta = U \quad (2)$$
 where θ is a vector of entries of M , B and K , and can be solved for by standard identification methods [Ljung L, System Identification, 1999]. U and θ depend on filtered measurements of X , X' and X'' and f . In a second approach, transfer functions between the lumped model elements in (1) are calculated using strain as inputs and outputs. Parametric results can then be extracted from the transfer function. For example, relative stiffness between elements is obtained via the transfer function magnitude at low frequency.

Methods: The apparatus shown in Figure 1 was constructed for validation studies. Preliminary work on estimating K and B is described here. Estimation of M is ongoing. B-mode images are captured using a 7 MHz linear array probe. A voice coil is used to create compressional waves. Phantoms with different stiffness and viscosity properties are created. The displacement information of each element is obtained by correlation-based speckle tracking.

Experimental Results: Figure 2 shows the stiffness plots of a three-layered phantom where the middle layer (agar) is stiffer than the top and bottom layers (gelatin). Both system identification methods capture the differences in stiffness. Viscosity and stiffness were estimated for phantoms made of polyurethane foam in water-glycerol solutions of different concentrations. An 80% increase in viscosity is observed when a 60% glycerol solution is compared to pure water, while stiffness changes are less than 5%.

Discussion: Unlike in prior work, a range of frequencies is used for stiffness estimation. This captures low-frequency tissue dynamics, not only statics, and might prove to be less sensitive to noise. The present approach can benefit from standard parameter identification techniques, such as regularization approaches that account for prior information, or coherence computation that indicates degree of linearity and usable frequency range. Simulations show that the method is consistent across different model sizes. These results are based on B-mode data. Improvements are expected by using RF data.

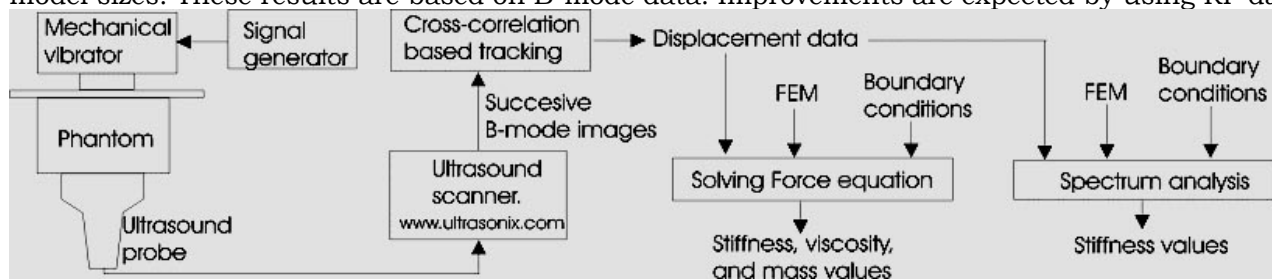


Figure 1: Experimental set-up.

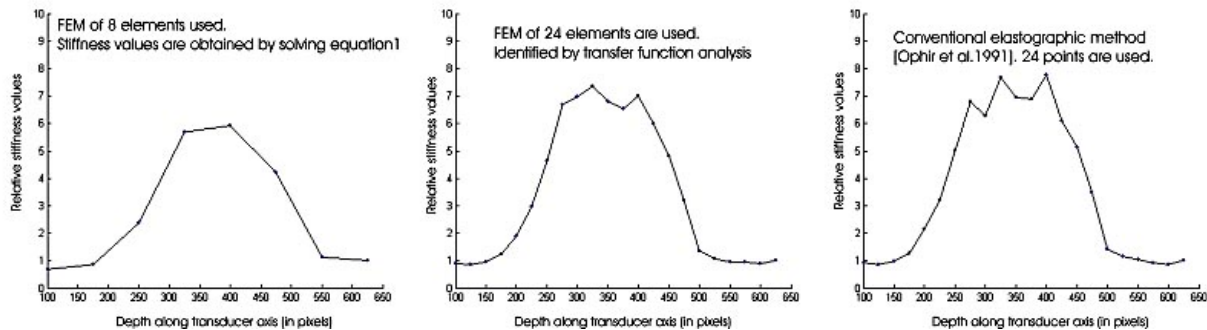


Figure 2: Identified stiffness of the gelatin-agar-gelatin phantom.

Session C: Mechanical Properties of Tissues

Monday, October 13 10:15A – 11:45A

21 **VISCOELASTIC CHARACTERIZATION OF *IN-VITRO* CANINE TISSUE.**

M.Z. Kiss¹, T. Varghese^{1,2}, U. Techavipoo¹, M. Hobson¹, T.J. Hall¹, E.L. Madsen¹, J. Jiang¹, J.A. Zagzebski¹, M.A. Kliewer³.

¹Department of Medical Physics, ²Department of Biomedical Engineering, ³Department of Radiology, The University of Wisconsin-Madison Madison, WI 53706, USA.

Mechanical properties of biological tissues are of interest for assessing the performance of elastographic methods that evaluate the stiffness characteristics of tissue. The mechanical properties of interest include the frequency dependent complex moduli, storage and loss moduli of tissues. Determination of the mechanical properties of biological tissues is often limited by proper geometry of the sample, as well as by the uniformity of the stress-strain relationship.

Measurements were performed on canine tissue specimens, including liver, muscle, and kidney over a load frequency range from 0.1 to 200 Hz. Tests were conducted using an EnduraTEC ELF 3200, a dynamic testing system for determining the mechanical properties of materials. Isotropic tissues were cut to cylindrical shape with a length less than one-third the diameter (20 mm), and were oriented in the system longitudinally. Anisotropic tissues were cut into blocks 10 mm on a side and 3–5 mm high, and tested on each principal axis. Stiffness changes of radio frequency ablated thermal lesions obtained at different temperatures were also evaluated. Experiments were conducted by uniaxially compressing tissue samples using plexiglass platens larger than the specimens and measuring the load response. Varying parameters such as pre-compression strain, total strain, and strain rate, provide a detailed picture of the viscoelastic properties of tissue.

The variation in the complex moduli over loading frequency for different tissue types will be presented and compared to theoretical results obtained using a Kelvin-Voigt model. Hysteresis curves that demonstrate the viscoelastic characteristics of tissue evaluated will also be presented.

*This work is supported in part by NIH grant T32CA09206, Wisconsin Alumni Research Foundation and start-up funds provided to Dr. Varghese by the Department of Medical Physics, Medical School and Graduate School at the University of Wisconsin-Madison.

23 **NONLINEAR SHEAR WAVES.**

Mark F. Hamilton¹, Yurii A. Ilinskii¹, G. Douglas Meegan¹, Evgenia A. Zabolotskaya¹.

¹Applied Research Laboratories, The University of Texas at Austin, Austin, Texas 78713-8029, USA.

Measurements reported by Catheline et al. [J. Acoust. Soc. Am. 112, 2404 (2002)] reveal that the elastic constants in Landau's expansion of the strain energy density differ by five to six orders of magnitude in a soft tissue phantom. The linear and nonlinear parameters associated with compressibility of tissue are four to six orders of magnitude greater than the elastic moduli connected with pure shear deformation. In situations like this it is very difficult to use Landau's formulation of the elastic energy for interpreting measurements of shear wave distortion. A concept proposed recently by the present authors (J. Acoust. Soc. Am., in review) permits the strain energy density to be expressed in such a way that the contributions due to compressibility and shear deformation are separated. With this approach, nonlinear longitudinal and shear waves in tissue can be considered separately, and for each process the elastic moduli are of the same order. The new expression for the strain energy density is explained by comparison with Landau's expansion, extended to fourth order. The coefficients in the latter are related through fourth order to those used in standard expansions of the equation of state for liquids.

The new expression for the elastic energy density is then applied to the analysis of shear waves. An evolution equation is derived in which the coefficient of nonlinearity is expressed explicitly through the material constants: the shear modulus μ , Landau's third-order elastic constant A , and a new fourth-order elastic constant D . The moduli μ , A , and D are of the same order, and for tissue-like media they are several orders less than the compressibility K and Landau's third-order elastic constants B and C , as well as the fourth-order elastic constants.

Finally, shear wave distortion and third-harmonic generation are investigated for linearly polarized waves, which possess only one displacement component. If μ and A are known, the solution for the third harmonic permits direct measurement of the modulus D .

Yongping Zheng¹, Yanping Huang¹, Singfai Leung², Charles Y.K. Choi¹.

¹The Hong Kong Polytechnic University, HONG KONG; ²Department of Clinical Oncology, Prince of Wales Hospital, HONG KONG.

One of the common side effects of radiation therapy for patients with malignancies of the head and neck is the post-irradiation fibrosis of the neck tissues. The process of tissue fibrosis is related to the filling in of muscle tissue space with stiffer connective tissue fibres and this will lead to an increase in the tissue elasticity. Hand palpation is the most popularly used methods for the objective documentation and scoring of neck tissue fibrosis. However, the information obtained by manual palpation is only semi-quantitative in nature and can be expressed only in ordinal rather than absolute units. Recently, we have successfully used an ultrasound palpation approach to quantitatively assess neck tissue fibrosis using the extracted effective Young’s modulus [1, 2]. There were good correlations between the effective Young’s modulus and the range of neck rotations, hand palpation grades (0 to 3) of three raters, clinical symptoms, and radiotherapy doses. In the present study, we investigated the nonlinear properties of the Young’s modulus by introducing an initial Young’s modulus together with a nonlinear factor.

The pen-size ultrasound palpation probe included an ultrasound probe at the tip and an in-series load cell. By pressing the probe against the soft tissue surface, the probe sensed the tissue deformation and applied load using the ultrasound and the load sensors, respectively. An indentation model was used to analyze the load-indentation relationship. The Young’s modulus of the tissue is represented by $E = E_0(1 + \alpha(w/h))$, where E_0 is the initial Young’s modulus, α is the nonlinear factor of Young’s modulus, w is the tissue deformation, and h is the original thickness of the tissue. A total of 77 patients were tested and the results were analyzed for both sides of the neck. Three raters were involved in the hand palpation to assign grades for the severity of the tissue fibrosis.

ANOVA test showed that there was no significant difference for the initial Young’s modulus ($p=0.13$) and the nonlinear factor ($p=0.80$) for each grade among the three raters. The averaged initial Young’s modulus was 17.8 ± 8.1 , 19.7 ± 7.7 , 26.4 ± 14.0 and 57.4 ± 42.9 kPa (mean \pm SD) for the palpation scores of 0 to 3, respectively (Figure 1). The increasing trend of the initial modulus with the increase of the palpation score was statistically significant (t-test, $p < 0.05$). This result also agreed with the effective Young’s modulus reported previously [1]. The nonlinear factor was 315 ± 228 , 426 ± 288 , 724 ± 586 and 2430 ± 2089 for the palpation scores of 0 to 3, respectively. Its increasing trend with the increase of the palpation scores was also statistically significant (t-test, $p < 0.05$). The results demonstrated that not only the initial Young’s modulus but also the nonlinear factor increased with the severity of the tissue fibrosis. The hand palpation raters appeared to combine the information of the tissue stiffness and the nonlinearity to give grades for the severity of the tissue fibrosis. Similar to the Effective Young’s modulus, the initial Young’s modulus and the nonlinear factor showed strong correlations with other symptoms of the patients like rotation range. It was noted that the nonlinear factor was more sensitive to the change of the grade and it also varied more among subjects. These two parameters combined with others, may be potentially used for the quantitative and subjective assessment of tissue fibrosis.

Acknowledgements: This project was partially supported by the Research Grant Council of Hong Kong (PolyU 5245/03E) and The Hong Kong Polytechnic University.

References: [1] Zheng et al. *Med Biol Eng Comp* 38: 1-, 2000. [2] Leung et al. *Cancer* 95: 656-, 2002.

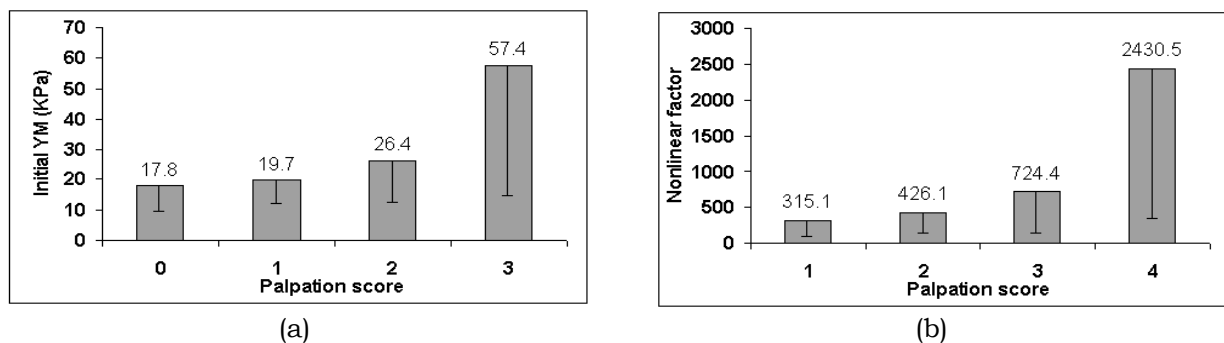


Figure 1. The relationship between the hand palpation grade and (a) initial Young’s modulus and (b) nonlinear factor of the fibrotic tissues induced by radiotherapy.

35 **MECHANICAL PROPERTY OF THE ACHILLES TENDON *IN VIVO*.**

M-C Lee¹, Y-W Shau¹, C-L Wang², T-Y Hsiao³.

¹Institute of Applied Mechanics, National Taiwan University, Taipei, TAIWAN; ²Department of Orthopedics, National Taiwan University Hospital, Taipei, TAIWAN; ³Department of Otolaryngology, National Taiwan University Hospital, Taipei, TAIWAN.

Introduction: We estimate the mechanical property of the Achilles tendon *in vivo* via resonant frequency using clinical ultrasound and an accelerometer system. A three-string physical model is introduced and solved analytically and is used to quantify the vibration modes of the Achilles tendon.

Materials and Methods: Modal testing was used to find the resonant frequency of the Achilles tendon *in vivo* (N = 10, male, age = 24.9±1.5 y, height = 174.2±4.69 cm) using both the ultrasound system and the accelerometer. A schematic is shown in Figure 1. We recorded the vibration velocities of the Achilles tendon using Doppler ultrasound, the vibration frequency of the vibrator and the strength of the force exerted by the vibrator on the Achilles tendon. The input-output transfer function of the forced vibration was calculated, and the resonant frequency was found to occur at the maximal vibration amplitude.

Results: Our results indicated that a significant resonant frequency that related to the physical status of the Achilles tendon in normal young subjects was located at about 23.0 ~ 34.7 Hz. It was found to increase with the Achilles tendon’s stiffness or tension force (Figure 2).

Concluding Remarks:

Anatomically, the Achilles tendon that connects the calcaneus to the gastrocnemius and soleus muscles behaves more like a “three-string system” than a single fixed-ended string. Thus, the physical model of strings with three branches of variable masses and lengths is more suitable for evaluating the vibration modes of the Achilles tendon *in vivo*. Analytical solution of the three-string model gave a better understanding of the frequency response of the Achilles tendon to force-vibration.

The physical status and mechanical property of the Achilles tendon can be quantified *in vivo* using ultrasound via the resonant frequency index with reasonable accuracy.

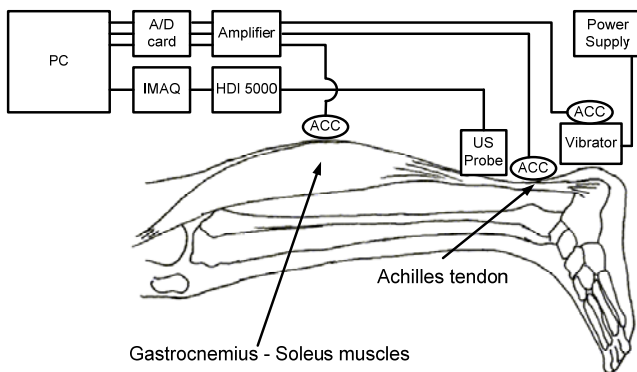


Figure1: Experimental Setup *in vivo*

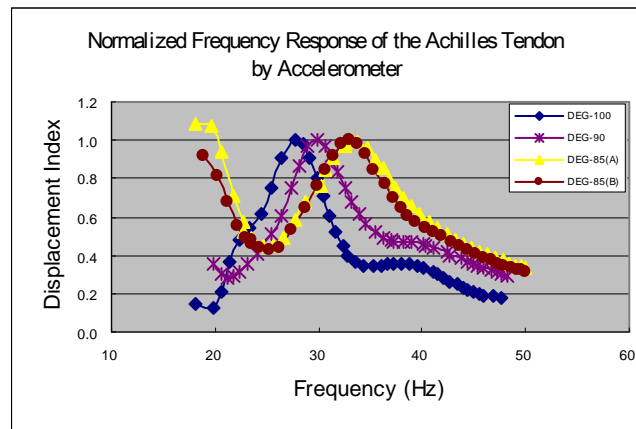


Figure2: Resonant Frequency of Achilles Tendon *in vivo*

61 **A PRELIMINARY COMPARISON OF FREEHAND ELASTOGRAPHY AND REFLEX TRANSMISSION (ATTENUATION) IMAGING FOR VISUALIZING THERMALLY ABLATED TISSUE.**

Lucy Baker¹, Alex Kolen¹, Jeffrey Bamber¹.

¹Joint Department of Physics, Institute of Cancer Research and Royal Marsden NHS Trust, Downs Road, Sutton, Surrey, SM2 5PT, UK.

A method to visualize thermally coagulated tissue would help to improve the clinical effectiveness of ablation treatments but none of the methods that have been employed clinically can yet be described as both adequately effective and convenient. Sonography is effective for imaging gas bubbles associated with cavitation or boiling but may not provide a reliable indication of the extent of necrosis and the image contrast may be unstable, tending to fade when gas bubbles disappear.

The ability of elastography to visualize thermally coagulated tissue is well established but stiffness is not the only tissue property that offers promise for this purpose; thermal coagulation causes the ultrasonic attenuation coefficient of liver to approximately double. We have been investigating reflex transmission imaging (RTI) which, in its optimum form, employs a wide aperture transducer scanned in two dimensions to create relative attenuation images in the plane of the focus by incoherently averaging echoes from the broad-beam region distal to the focus. Although not ideal for this purpose, existing clinical ultrasound scanners may easily be adapted for the generation of RT images. Using novel phantoms we have shown previously that a conventional linear array is capable of generating RT images with a performance that should be useful for monitoring thermal ablations. We have also previously described a freehand elastographic method that holds promise for visualizing thermal lesions.

In this preliminary study we have begun to assess the relative ability of elastography and RTI to visualize individual thermal ablation lesions by comparison with the blanched optical appearance of the tissue cut surface. RF ablation of *ex vivo* bovine liver embedded in gelatine enabled single lesions to be created and imaged in the same plane by sonography, elastography, RTI and C-scan imaging. Three experiments were conducted, each with a thermal exposure of about 90°C for 6 min, producing a pseudo-spherical lesion of about 15 mm in diameter.

Lesion contrast was found to be similar for the two methods (about -70%). Elastography possessed a higher lesion contrast-to-noise ratio in all three cases, with a mean of -4.2 for elastography and -3.1 for RTI. Both methods overestimated lesion size in all cases but RTI always less so than elastography (+48% elastography, compared with +18% RTI). Correspondence of displayed lesion shape to actual shape tended to be better for RTI than for elastography although this in part appeared to be due to the fact that elastography was very sensitive to damage caused to the embedding gel during treatment. Gas bubbles created during the treatment were easily visible on C-mode scans, but it was not possible to reliably localize the lesions using backscatter contrast, which in turn did not appear to fully account for lesion contrast on RTI.

Further work is required to determine whether elasticity or attenuation imaging has particular advantages in specific situations but since each method has different sources of noise and artefact, it is already clear that there is likely to be benefit in employing them simultaneously for treatment monitoring.

Acknowledgements: Thanks to Gail ter Haar for making available the RF ablation hardware. This work was supported by a grant from the EPSRC.

Alex Kolen¹, Jeffrey Bamber¹.

¹Joint Department of Physics, Institute of Cancer Research and Royal Marsden NHS Trust, Downs Road, Sutton, Surrey, SM2 5PT, UK.

The lack of an imaging method to provide feedback for monitoring the progress of thermal ablations has been recognized as an impediment to improving the clinical effectiveness of these treatment methods. For high intensity focused ultrasound surgery (HIFU) this is particularly important because (a) many factors can influence the dosimetry, causing lesions of unpredictable size, shape or position to form, and (b) to ablate entire tumours a conformal array of smaller ablations, or lesions, must be created and an accurate method of monitoring may be able to guide and confirm satisfactory placement of each lesion.

It is already known that elastography can visualize thermally coagulated tissue with high contrast; the aim of the present study was to assess the likely potential for using freehand elastography (described previously) to guide the placement of individual HIFU lesions to build up an array. Experiments were carried out both to determine the minimum size of lesion array that can be visualized and to assess the degree to which elastography could correctly visualize lesion arrays of different dimensions.

Three degassed bovine liver specimens were embedded in gelatine prior to HIFU ablation using patterns of short, 2 s, exposures from a 1.7 MHz therapy transducer that generated a spatial peak intensity of 1690 Wcm^{-2} , which results in small ellipsoidal lesions each about 2 mm diameter by 15 mm in length. Time was allowed between each exposure for the tissue temperature to return to base line (22°C) before exposing for the next lesion in an array, placed with its center 2 mm from the center of its neighbour. This provided good control over the size and shape of each lesion and a reasonable basis for assuming that arrays of lesions of different size would have similar elastic contrast. In each liver a series of arrays was created, the smallest was produced by a single exposure and the largest was an array of 5×5 exposures, 100 mm^2 in cross-section, causing each liver to become, in effect, a resolution test object at constant elastic contrast.

Due to a lack of cavitation bubbles these lesion arrays were generally not visible sonographically. Freehand elastography, however, visualized the majority of arrays created, with a threshold of visibility lying somewhere between array sizes 1×1 and 2×2 HIFU exposures, corresponding to a linear dimension in the region of 3 to 6 mm. For those arrays that were visible, elastography overestimated their size (worst case 75% overestimation, but more typically 15%) and the rectangular cross-section of the arrays was generally not apparent in the shape of the low strain area.

We conclude that freehand elastography at its present stage of development is capable of detecting HIFU lesion arrays of small size but that at least several lesions may need to be added to an array before a change in size is detectable.

Acknowledgements: Thanks to Gail ter Haar for use of the HIFU hardware and Ian Rivens for instruction in its use. This work was supported by a grant from the EPSRC.

Session D-1: Methods for Imaging Elastic Tissue Properties I

Monday, October 13 1:15P – 2:45P

04 ESTIMATION OF STRAIN TENSOR COMPONENTS FROM ANGULAR STRAIN IN ELASTOGRAPHY.

U. Techavipoo^{1,2}, T. Varghese^{1,3}, Q. Chen¹, J. A. Zagzebski¹, E. L. Madsen¹.

¹Department of Medical Physics, University of Wisconsin-Madison, Madison, WI, 53706, USA;

²Department of Electrical and Computer Engineering, University of Wisconsin-Madison, Madison, WI, 53706, USA; ³Department of Biomedical Engineering, University of Wisconsin-Madison, Madison, WI, 53706, USA.

Ultrasound elastography has developed into an imaging modality suitable for detection and diagnosis of cancers in the breast, prostate, and thyroid and for monitoring ablative therapies in the liver, kidneys and other sites. We are exploring potential benefits of elastograms obtained using spatially compounded echo data acquisition. A mechanically translated, sector scanning transducer is used to acquire compound echo data following unidirectional compressions of the sample. Strain estimated along angular insonification directions can be separated into strain tensor components along the axial (direction of compression) and lateral directions. Estimation of the axial and lateral strain tensors allows computation of the Poisson's ratio and shear strains in the object. In addition, strain tensor components separated from the angular strain estimates can be compounded to improve the signal-to-noise (SNR_e) and contrast-to-noise (CNR_e) ratio in the elastograms.

Angular weighted compounding of the local strains estimated from echo signals scanned at different insonification angles is also used. However, the mechanical stimulus is applied only along the axial direction. Experimental results using a uniformly elastic and contrast tissue-mimicking phantoms, and *in-vitro* thermal lesions demonstrate the improvement in the SNR_e and CNR_e obtained with angular weighted compounding. Variation in the SNR_e and CNR_e obtained using different angular increments is also investigated.

*This work is supported in part by start-up funds provided to Dr. Varghese by the Department of Medical Physics, Medical School and Graduate School at the University of Wisconsin-Madison and the Wisconsin Alumni Research Foundation (WARF).

06 **BRACHYTHERAPY SEEDS DETECTION USING VIBRO-ACOUSTOGRAPHY: A PILOT STUDY.**

Farid Mitri¹, Philippe Trompette¹, Jean-Yves Chapelon¹.

¹National Institute of Health and Medical Research INSERM U556, 151 Cours Albert Thomas, Lyon, FRANCE.

Brachytherapy which is used to treat prostate cancer consists of inserting radioactive cylinders into the prostate under echographic guidance. In this technique, it is desirable to insert an optimal distribution of the cylinders (seeds), which requires precise information about the seed locations. However, at the present time, echography alone cannot yield this information, because ultrasound beams are reflected specularly from the metallic seeds and the backscattered waves cannot reach the probe except at normal incidence.

In this work, vibro-acoustography imaging technique based on the radiation force of ultrasounds was used to detect metal seeds. The method was tested on an agar gel phantom block (10x6x4 cm³) in which two brass seeds of the same diameter (1 mm) with different length (10 mm and 7.5 mm, respectively) were implanted and located about 5 mm deep from its flat surface. It was essential to consider two seeds of different lengths in order to point out the resonance phenomenon on images since the resonance frequencies values depend on the seed's length. Images with pixel dimensions of 0.2 mm by 0.2 mm were produced for right (perpendicular) and parallel angle incidences. As was expected, the excitation at the resonance frequency(ies) would yield a better contrast-to-noise ratio, and hence, providing a better way for seed detection. A modal analysis was performed using the finite element method to have *a priori* information on the vibration characteristics (resonance frequencies and mode shapes) of the seeds. In the experiments, it was found that the best excitation vibration frequencies were determined either by the calculated fundamental resonance frequency of each of the seeds (i.e. 33.960 and 59.065 kHz respectively), or by the experimental optimal resonance frequency of the gel within the chosen bandwidth. As expected, the resulting vibro-acoustography images have shown significant contrast in comparison to images obtained at non-resonance frequencies, and a remarkable way to detect the metal seeds independently of their orientations relatively to the incident ultrasound beams. Results indicate that the application of this technique for controlling brachytherapy treatment is both promising and challenging. Future work must concentrate on the development of faster scanning to improve the performances of this method for clinical application.

16 **THE FEASIBILITY OF USING ELASTOGRAPHY FOR IMAGING THE LOCAL LATERAL-TO-AXIAL STRAIN RATIOS IN HOMOGENEOUSLY POROUS MEDIA.**

Raffaella Righetti^{1,2}, Jonathan Ophir^{1,2}, Seshadri Srinivasan^{1,2}, Thomas A. Krouskop^{1,3}.

¹The University of Texas Medical School, Department of Radiology, Ultrasonics Laboratory, Houston, Texas, USA; ²University of Houston, Electrical and Computer Engineering Department, Houston, Texas, USA; ³Baylor College of Medicine, Department of Physical Medicine and Rehabilitation, Houston, Texas, USA.

The feasibility of using elastography for experimentally estimating and imaging the temporal evolution of the local lateral-to-axial strain ratios in homogeneously porous media subjected to sustained axial load was investigated. The porous media were modeled as a combination of two mechanically interacting phases, a porous-permeable solid phase composed of a solid matrix, and a liquid phase composed by interstitial fluid (water), in accordance with biphasic theories originally proposed for cartilage. Using concurrent local and axial and lateral strain estimations, static and time-sequenced strain-ratio images (poroelastograms) of cylindrical gelatin and porous material samples were generated under sustained axial loading. The exudation of the internal fluid contained in the samples due to the applied load was depicted by imaging the time-dependent changes of the mechanical properties of the solid matrix, which represented the source of the elastographic signal information. In order to evaluate the agreement of the experimental findings with classical theoretical models proposed for biphasic materials, mechanical measurements of the aggregate modulus and the permeability of some of the porous material samples were performed. Finite-elements simulations were carried out in order to correctly anticipate and interpret the experimental results. The experimental data (Figure 1) show similar trends to those that were calculated from finite-elements simulations and from classical theoretical models, suggesting that poroelastography may have significant potential for quantitatively mapping the time-dependent mechanical behavior of poroelastic media, which is related to the dynamics of fluid flow and to the elasticity and permeability parameters of the media.

Supported by National Cancer Institute Program Project Grant P01-CA64597 to the University of Texas Medical School at Houston.

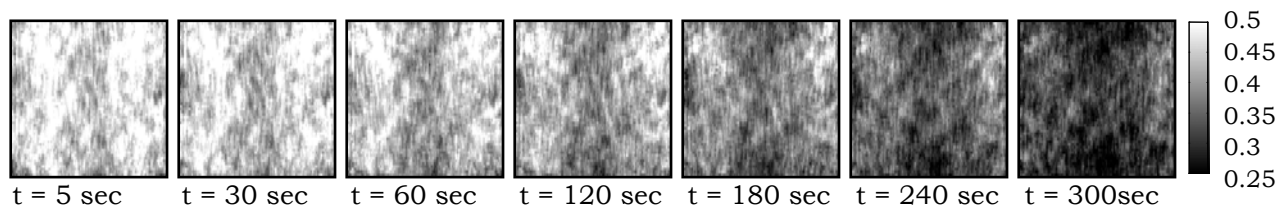


Figure 1. Time-sequenced poroelastograms (images of the local ratio of lateral-to-axial strains) obtained from cylindrical porous samples subjected to sustained axial compression.

17 **FEASIBILITY OF MODULUS IMAGING USING NANO-INDENTATION: COMPARISON OF MODULUS IMAGES WITH STRAIN ELASTOGRAMS USING PHANTOMS, PROSTATES, KIDNEYS AND CANCERS.**[†]

S. Srinivasan^{1,2}, J. Ophir^{1,2}, T.A. Krouskop^{1,3}, R.E. Price⁴.

¹The University of Texas Medical School, Department of Radiology, Ultrasonics Laboratory, Houston, TX, USA; ²University of Houston, Electrical and Computer Engineering Department, Houston, TX, USA; ³Baylor College of Medicine, Department of Physical Medicine and Rehabilitation, Houston, TX, USA; ⁴The University of Texas M. D. Anderson Cancer Center, Department of Imaging Physics, Houston, TX, USA.

Conventional elastography involves quasi-static mechanical compression (external or internal) of the tissue under ultrasonic insonification to obtain RF A-lines before and after compression. Cross-correlation of the pre- and post-compression A-lines results in displacement images whose axial gradients produce the strain images (strain elastograms). Though the strain elastograms show structural similarities to the modulus images (Figure 1), they are not related in a simple way to the modulus images since the strains depend on both modulus and geometry of the materials being deformed. Therefore a quantification of the similarities between the strain and modulus images may enhance the interpretation confidence of strain elastograms in depicting tissue structure.

To demonstrate similarities between modulus images and strain elastograms, first a feasibility study of using nano-indentation to obtain modulus images of thin slices of tissue mimicking phantoms (agar-gelatin mixtures) and tissues like canine prostates, bovine kidneys, HT29 human colon carcinoma and beef slices was performed with encouraging results. This was followed by a comparison of modulus images and strain elastograms obtained from the same sample slices. The experimental results indicated that under certain experimental conditions it is feasible to perform quantitative comparisons between strain images (using elastography) and modulus images. A good visual as well as quantitative correspondence between structures in the modulus and strain images could be obtained at scales equal to or larger than 3 mm.

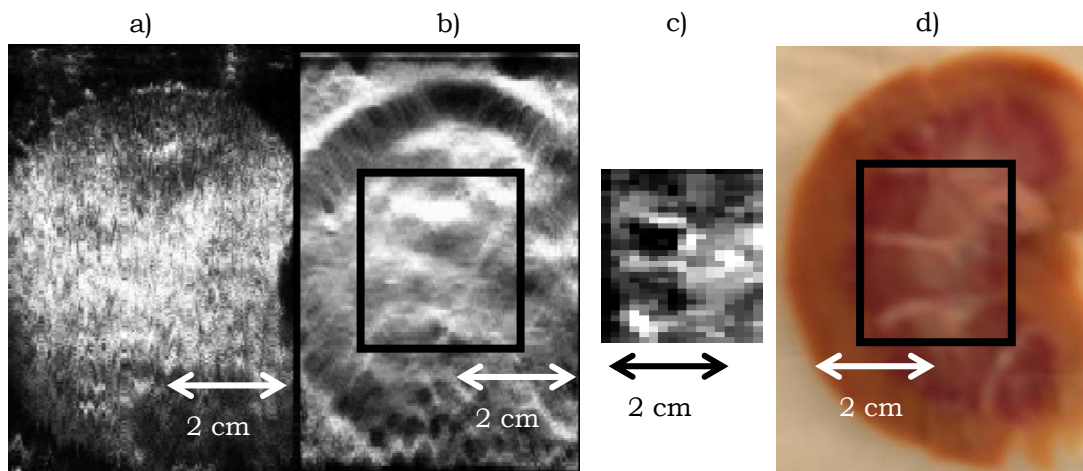


Figure 1: a) Sonogram, b) elastogram, c) modulus image and d) optical image of an ovine kidney. The boxes in the elastogram and the optical image indicate the region whose modulus image was obtained using the nano-indenter and shown in the figure. (2cm-markers indicate scale only.)

[†]Supported by National Cancer Institute Program Project Grant P01-CA64597 to the University of Texas Medical School-Houston

Walaa Khaled¹, Stefan Reichling², Otto T. Bruhns², Gareth J. Monkman⁴, Stefan Egersdrofer⁴, Mario Baumann⁵, Holger Boese⁵, Herbert Freimuth⁶, Abdi Tunayar⁶, Andreas Lorenz⁷, Andreas Pesavento⁷, Katharina Kuehne³, Theodor Senge³, Ulrich Scheipers¹, Helmut Ermert¹.

¹Institute of High Frequency Engineering, Ruhr-University, Bochum, GERMANY; ²Institute of Mechanics, Ruhr-University, Bochum, GERMANY; ³Urology University Hospital, Ruhr-University Bochum, Herne, GERMANY; ⁴Fachhochschule Regensburg, special field electrical engineering, GERMANY; ⁵Fraunhofer-Institut fuer Silicatforschung ISC, Wuerzburg, GERMANY; ⁶Institut fuer Mikrotechnik, Mainz GmbH, Mainz, GERMANY; ⁷LP-IT Innovative Technologies GmbH, Bochum, GERMANY.

Tumors can have a higher mechanical hardness than the surrounding tissue. Ultrasound strain imaging is able to measure and visualize the elastic properties of tissue regions. We developed a real time strain imaging system for tumor diagnosis. It allows biopsies simultaneously to B-mode and strain imaging investigation. Additionally, we expanded our strain imaging system towards haptic sensor actuator systems for virtual reality applications in medicine.

The strain imaging system uses the fast phase root algorithm for strain estimation with up to 40 Hz. Strain images are frame-to-frame filtered by an adaptive temporal filter which enables the use of an up to 50% smaller compression of the organ achieving the same image noise as with the conventional frame-to-frame filters. In a clinical trial with 260 prostate patients strain imaging reached a sensitivity of 76% and a specificity of 84%. Using only the B-mode image, only 34% of all carcinoma were detected.

The haptic sensor actuator system has been designed for visualization and mechanical tissue property reconstruction using ultrasonic strain imaging in combination with a haptic display based on electrorheological fluids. Goals of this development are (1) to develop an accurate imaging technique which leads to absolute or a useful relative of tissue elasticity parameters, (2) to improve the visualization of mechanical properties by reduction of artifacts, and (3) to reconstruct tissue properties on a controllable haptic display.

In order to develop inverse elastography reconstruction approaches, finite element simulations were performed for a number of soft biological tissue models. The results obtained from finite element analysis were confirmed in the ultrasonic experiments on a set of tissue-mimicking phantoms with known acoustical and mechanical properties. Finally, using numerical solution models and solving the inverse problem we can deduce relative mechanical properties.

These properties are transferred to the actuator system which consists of a 2D piston-array of elements filled with an electrorheological fluid. The array, which is electrically controlled, reconstructs the corresponding resistance forces due to the viscosity increase of the electrorheological fluid in real time.

Various modifications on the haptic sensor actuator system have been investigated. The spatial resolution of receptors on the finger tip is improved to 1 mm x 3 mm, which is useful for medical diagnosis. For the most convenient electrorheological fluid a force of nearly 10 N on the pistons of about 1 cm² area could be achieved at a field strength of 2 kV/mm. Using a novel optocoupler design we control individual high voltages for each actuator element. The final results show good agreement of analytical predictions and visual results with experimental data on the haptic display.

This system is of interest as a haptic supplement of elasticity visualization and for virtual reality applications like remote palpation, simultaneous multiple actuator palpation, teaching and telemedicine.

A project of the Ruhr Center of Competence for Medical Engineering (KMR). Supported by the Federal Ministry of Education and Research, No. 13N8079 and No. 01 IR A 14 B.

Ultrasound (US) elastography has drawn much attention as a low cost and low risk imaging modality to derive information about the biomechanical properties of soft tissues, and to understand how changes in these properties correlate with pathological developments. Accurate estimation of temporal displacement and strain tensor components is an integral part of elastography. So far, the commonly used strain estimation techniques compute the deformation mainly in the axial direction by tracking changes within the RF signals induced by an applied stress.

In this paper, we present a new approach to estimate axial displacement and strain fields. One original aspect of the method is that it does not perform the strain estimation on windows of study like classical elastographic techniques. It processes signals formed by the samples, localized at the same position, under step-wise increasing compression of tissues. Thus, for each sampling position in an image is attributed a signal, whose length is the number of compressions. At a given depth, the displacement of tissue is proportional to phase shift between these signals. As for velocity estimation, the technique is based on the spectral analysis of samples obtained at a particular depth and corresponding to several consecutive mechanical compressions of the medium. The displacement and strain can then be estimated in the spectral domain from the frequency corresponding to the phase shift induced by different levels of compression. Direct spectral estimation with FFT or Auto-Regressive methods yields to a large variance. So we present an approach based on regularized Auto-Regressive analysis for strain estimation. This estimation is regularized using a non quadratic smoothing algorithm previously developed by our group [IEEE trans. UFFC, 2002, vol. 89, no.12, pp. 1704-1919].

The performance of the developed method has been tested on simulated data. The Field II software specifically dedicated to simulate RF US data was used to compute RF signals of a 3-layer medium. The mechanical characteristics of the simulated medium are that the upper and lower layers are of the same stiffness and twice harder than the middle layer. RF image sequences of 16, 32, 64 and 128 steps of linear increasing compression were respectively used to discuss the parameters that affect the spectral estimation, such as the total number of compressions applied to the medium, the amplitude of each deformation, and the medium depth.

The displacement and strain images, the mean of displacement and strain, and the standard error profile of displacement and strain are given in this paper. From these figures, we can see the edge of every layer clearly and that the strain of the middle layer is twice than the upper and lower layers. The performance of this method is also compared with the theoretical profile in terms of distribution of error as a function of depth. Results show that this strain estimation method based on regularized Auto-Regressive analysis leads to reliable strain estimation at each given depth and allows a drastic reduction of the variance of the spectral estimation.

Preliminary experimental work will also be performed on agar and gelatin phantom.

Session E: Clinical and Animal Applications and Results

Monday, October 13 3:15P – 5:30P

33 SONOELASTIC DETECTION OF CANCER IN RADICAL PROSTATECTOMY SPECIMENS.

Kevin J. Parker¹, Brian C. Porter¹, Lawrence S. Taylor¹, Gyongyi Nadasdy², Zhe Wu¹, David Pasternack¹, P. Anthony di'Santagnes¹, Priya Nigwekar¹, Raymond B. Baggs¹, Deborah J. Rubens¹.

¹University of Rochester, Rochester, NY, USA; ²Ohio State University Medical Center, Columbus OH, USA.

We report the statistical outcomes from an *in-vitro* study of whole prostate specimens scanned immediately following radical prostatectomy. The whole prostates were embedded in an agar medium and were scanned in a 3D protocol using conventional B-scan and sonoelastography with externally applied vibrations above 100Hz.

Multiple, step-sectioned histology slides were obtained and examined by a pathologist, and these sections were utilized to recreate a 3D model of the whole gland and any tumors. B-scan information and sonoelastic "voids" representing a hard region, were also recreated in 3D.

There are 19 cases included in the study. These are broken into two groups as follows: G1) all cases with confirmed tumor size from pathology of 1.0 cm³ or greater. G2) all cases with confirmed tumor size from pathology of less than 1.0 cm³. The reason for this division by size is that, in theory and in practice, the sonoelastic imaging contrast of a lesion will increase with the size of a lesion, and as a practical matter very small tumors are not typically palpable. With this division we have 8 cases in G1 and 11 cases in G2.

Each case was read for histology and for sonoelastography by separate experts and in a blinded fashion (with no knowledge of the other read), and was then scored as either a True Positive (sonoelastography and histo both positive with significant 3D overlap), or False Positive (sonoelastography positive but histo negative or non-overlapping), or True Negative / False Negative categories.

The results are:

G1 (tumors 1.0 cm³ or greater): N=8

Accuracy of 7/8, or 87%, Sensitivity of 7/7 or 100%

The average tumor size in this group, from histology, was 3.1 cm³ +/- 2.1 cm³. The average tumor size in this group, from sonoelastography, was 2.8-cm³ +/- 1.6 cm³. Thus the average sonoelastic voids in this group were 91% of the histology confirmed tumor volume.

For G2 (tumors smaller than 1.0 cm³): N=11

Accuracy of 50%, Sensitivity of 27%

Many of the tumors in this group are physically too small to be visualized by sonoelastography at the frequencies we are currently using. And we do not know what inherent elastic contrast, if any, very small tumors have. Future work will expand the upper frequency range of applied vibrations, and the lower range of tumor dimensions, with *in-vivo* applications.

27 **SHEAR MODULUS IMAGING ON INTERSTITIAL ELECTROMAGNETIC WAVE COAGULATION TREATMENT OF HUMAN *IN VIVO* LIVER CARCINOMA.**

C. Sumi¹, M. Kubota², G. Wakabayashi³, M. Tanabe³.

¹Sophia University, Tokyo, JAPAN; ²Yamachika Memorial Hospital Kanagawa, JAPAN;

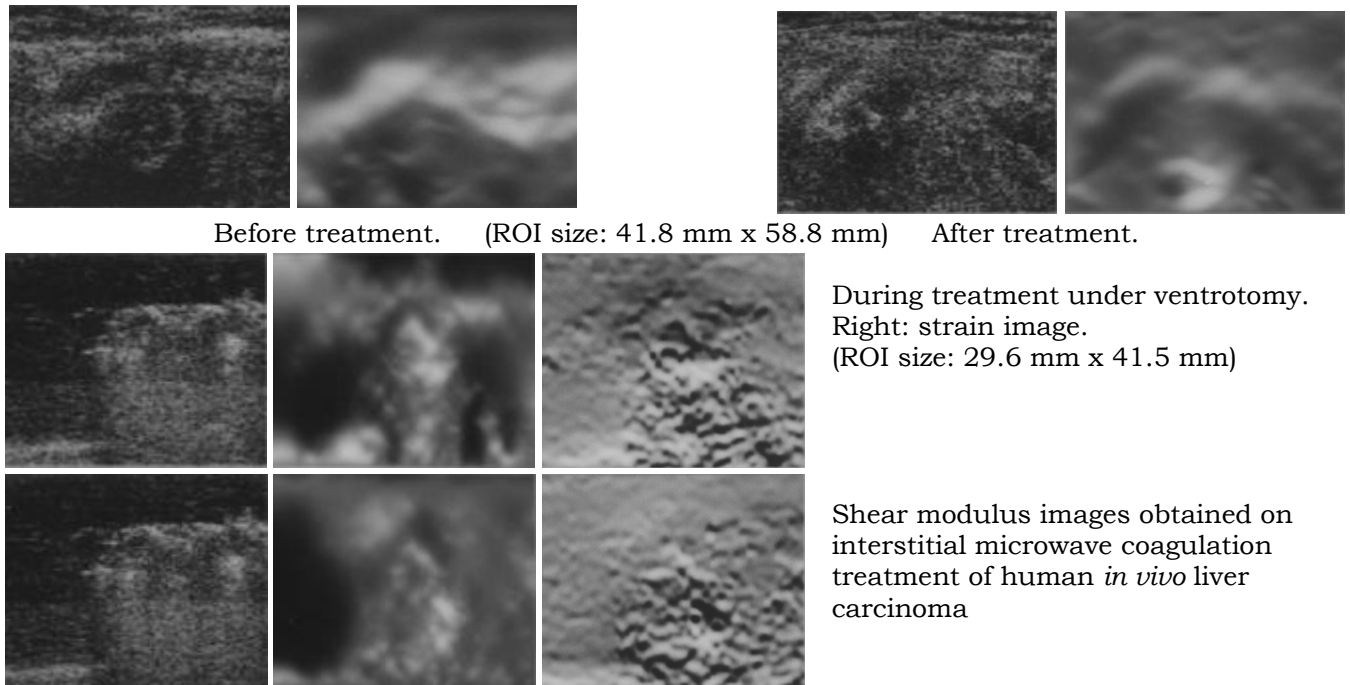
³Keio University Medical School, Tokyo, JAPAN.

For various human soft tissues (e.g., liver, breast, etc.), we are developing the ultrasonic strain measurement-based mechanical properties reconstruction/imaging technique (shear modulus, visco shear modulus, Poisson's ratio, etc.). Now, we are collecting the *in vivo* clinical reconstruction image data. Particularly, here we show shear modulus images obtained on interstitial electromagnetic coagulation therapy. As soft tissues are deformed in 3-D space, multidimensional signal processing improves strain measurement accuracy, and consequently modulus reconstruction accuracy¹. If reference values are provided, we can numerically reconstruct the Lamé's constants (shear modulus and Poisson's ratio) and the density in 3D space, i.e.,

$$\rho\alpha_i = \{\varepsilon_{\alpha\alpha}\delta_{ij}\}\lambda_{,j} + \{\varepsilon_{\alpha\alpha}\delta_{ij}\}_{,j}\lambda + 2\varepsilon_{ij}\mu_{,j} + 2\varepsilon_{ij,j}\mu,$$

where $\lambda = \frac{2\nu}{1-2\nu}\mu$, λ, μ : Lamé's constants, μ : shear modulus, ν : Poisson's ratio, ρ : density.

However, here we show quasi-real time *in vivo* human 1D shear modulus reconstruction (freehand). For instance, on monopole microwave treatment of *in vivo* liver carcinoma [segment 6], the carcinoma (dia. = 18 mm) and the safety margin was able to be favorably monitored though it is difficult through conventional B-mode imaging. During the treatment under ventrotomy the carcinoma became fragile and the margin of several millimeters became stiff, while before the treatment the tumor was stiff (dynamic range of the reconstructed images before versus after the treatment: 18.7 dB versus 27.8 dB).



On human *in vivo* liver tissues we were able to exhibit the superiority of our quasi-real time imaging to conventional B-mode imaging. Our technique is available as a clinical visualization technique both for diagnosis and treatment. Furthermore, monitored shear modulus data can be effectively utilized as the measure for controlling the therapies. Combination of the low invasive interstitial therapies with our imaging will allow combined diagnosis and the subsequently immediate treatment. This must contribute to substantial reduction of the total medical expenses.

This research was in part supported by JSPS and NEDO.

[1] C. Sumi *et al.*, "Realization of combined diagnosis/treatment style by ultrasonic strain measurement-based mechanical properties imaging technique," Proc. of the First International Conference on the Ultrasonic Measurement and Imaging of Tissue Elasticity, p. 23, [2002](#).

42 **LESION SIZE RATIO FOR DIFFERENTIATING AMONG BREAST LESIONS.**

Timothy J. Hall¹, William E. Svensson², Pat Von Behren³, Yanning Zhu², Joe Malin³, Candace Spalding⁴, Alissa Connors², Dupinder Chopra², Carol Lowery³.

¹University of Wisconsin-Madison, 1530 MSC, 1300 University Avenue, Madison, WI, 53706 USA; ²Charing Cross Hospital NHS Trust, London, UK; ³Siemens Medical Solutions Ultrasound Group, Issaquah, WA, USA; ⁴University of Kansas Medical Center, Kansas City, KS, 66160 USA.

We are testing a system for real-time freehand acquisition and display of tissue elasticity implemented on a commercial clinical sonography system. Initial clinical trials have demonstrated that sequences of high quality strain images can be obtained with this system and that real-time feedback is essential for controlling the boundary conditions for the mechanics experiment that is elasticity imaging. Initial clinical trials included only 56 patients and not all benign lesions were biopsy proven. However, that data and previous publications suggested that a single criterion, the ratio of lesion size in a strain image to that in the corresponding B-mode image, was useful in differentiating malignant from benign breast lesions. This study updates those preliminary results with additional data that increases the total number of biopsy-proven lesions to over 200.

The Siemens Elegra was programmed to compute and display streaming B-mode and mechanical strain images in real-time (strain images update at 7fps). The patient scanning technique is nearly identical to standard clinical breast sonography with compression; the patient is supine and the linear array transducer is pressed toward the chest wall over a compression range of about 15-20% while B-mode and strain images are displayed to verify acquisition of high-quality data. A sequence of phase-sensitive data is stored and processed off-line at higher spatial resolution than displayed on-line.

An ROC analysis of the preliminary data was performed to estimate the performance of lesion width ratio compared to lesion area ratio. The diagnostic performance results are overly optimistic ($A_z = 0.98$) but suggest that lesion width ratio performance is nearly equivalent to that of lesion area ratio and those results suggest a threshold area ratio of 1.29 for differentiating malignant from benign breast lesions. Increasing the number of patients has also increased the variety of benign and malignant conditions examined. Preliminary analysis of the increased data set suggests that lesion size ratio continues to be a sensitive criterion for breast lesion differentiation.

46 **OPTIMIZATION OF PRECOMPRESSION AND COMPRESSION FOR CLINICAL BREAST ELASTOGRAPHY: UPDATED RESULTS.**

BS Garra¹, E Jannicky¹, LM Mobbs¹, S Felker¹, L Weiss¹, S Srinivasan^{2,3}, J Ophir^{2,3}.

¹University of Vermont College of Medicine-Fletcher Allen Health Care, Burlington, VT, 05401, USA; ²The University of Texas Medical School, Department of Radiology, Ultrasonics Laboratory, Houston, TX, 77030, USA; ³University of Houston, Electrical and Computer Engineering Department, Houston, TX, USA.

Quantitative testing of tissues has shown significant changes in tissue hardness depending on the amount of precompression and compression applied during elastography. Recent reports have indicated that elastographic contrast changes markedly depended on the amount of precompression. Our mechanical frame elastographic system allows us to preset the amount of precompression used and a study was undertaken to quantify the amount of precompression and compression required to optimally display various breast masses using elastography.

Three human observers, two experienced in ultrasound, evaluated elastograms obtained at 9 different precompression settings ranging from 1% to 20% and at 7 compression settings ranging from 0.5% to 4.0%. The elastograms were single compression elastograms obtained on 38 Lesions including 8 carcinomas, 12 fibroadenomas and a variety of less common masses. The elastograms were graded for lesion conspicuity and “noise” (texture tending to obscure the lesion) on a five point scale where 1 signified a highly conspicuous lesion or low noise and 5 signifying that the lesion could not be seen or that the image was composed entirely of noise.

The images having lower noise and increased lesion conspicuity fell mostly between precompression values of 1% through 6% with a smaller cluster at about 15%. This smaller group was not composed of cancers or fibroadenomas, but was composed of less commonly seen lesions. The images having noise and lesion conspicuity scores of less than 3 were all grouped between .5% and 3.5% compression with the majority being obtained with <2% compression. No difference in the optimal values was noted between fibroadenomas and cancers.

We conclude that for breast mass elastography the optimal range of precompression is 1% - 7% and the optimal compression range is 0.5% to 1.5%. The precompression range may be wide enough to use change in lesion contrast vs. precompression as a feature to help distinguish benign from malignant masses.

48 **INITIAL DEMONSTRATION OF STAGING DEEP VENOUS THROMBOSIS USING ULTRASOUND ELASTICITY IMAGING.**

Jonathan M. Rubin¹, Hua Xie², Kang Kim², William F. Weitzel³, Xunchang Chen², Matt O'Donnell², Salavat R. Aglyamov⁴, Stanislav Y. Emelianov⁴, Shirley K. Wroblewski⁵, Daniel D. Myers⁵, Thomas W. Wakefield⁵.

¹Departments of Radiology, ²Biomedical Engineering, ³Internal Medicine and ⁵Surgery, University of Michigan, Ann Arbor, MI 48109, USA; ⁴Biomedical Engineering Department, University of Texas at Austin, Austin, TX 78712, USA.

Introduction: In our previous study, we demonstrated the potential of ultrasound elasticity imaging to detect and age deep venous thrombosis (DVT) using a rat-based model. To monitor DVT elasticity changes over time, we repeated our original imaging experiment with more temporal samples over DVT's maturing process and compared two independent groups of animals to test the ability of elasticity imaging to classify clot maturity.

Methods: A total of 14 Sprague-Dawley rats were studied, four of which were considered test subjects and ten were used to define a staging classifier. On the first day of all experiments, the rat inferior vena cava (IVC) and associated back branches were ligated to initiate thrombosis formation. Then, each rat was imaged on day 3, 4, 5, 6, 7, 8 and 10, corresponding to developing thrombus from acute/subacute to chronic stages. We used a Siemens Sonoline "Elegra" ultrasound scanner to capture ultrasound data while compressing rat's abdominal wall and underlying tissue with a 12.0 MHz linear array transducer. The transducer was driven by a mechanical device which allowed for continuous deformation. For each deformation, typically 174 frames of ultrasound in-phase and quadrature (IQ) data were processed off-line using a 2-D correlation-based phase-sensitive speckle tracking algorithm to derive the strain image of the thrombus and surrounding material. Strain images were normalized individually by the magnitude of the average strain estimated by tracking the displacement of the spine during each deformation.

Results: In both groups of animals, the normalized strain magnitude of thrombi consistently decreased with maturity. Strain profiles through thrombi indicate that a 10-day old clot is on average 6-times harder than a 3-day old clot. Strain inversion between blood clots and IVC walls was also observed, and the transition point occurred around day 7 or day 8. Another interesting observation is that strain profiles clearly fall into three groups for the days imaged, which might correlate to the three diagnostic stages in clinical application: acute, subacute and chronic. Using the average normalized strain in combination with strain profiles, a classifier to identify three classes was built based on the statistics derived from the second group of animals and it was consequently tested on the first group. The results showed that the training and testing accuracies are 90% and 95% respectively.

Conclusions: Our studies strongly suggest that ultrasound elasticity imaging can be applied as a useful technique for clinical assessment of DVT. Rat thrombus age may not directly compare to that for humans, but the classification of three stages may be applied similarly to patients as to rats. To further evaluate our findings, on-going research includes reconstruction of Young's modulus from strain images and direct mechanical measurement of blood clots.

This study was supported by NIH grant HL 068658.

51 **ELASTOGRAPHIC CHARACTERISTICS OF BENIGN BREAST LESIONS THAT SONOGRAPHICALLY MAY MIMIC CANCER.**

BS Garra¹, LM Mobbs¹, E Jannicky¹, S Felker¹, L Weiss¹, S Srinivasan^{2,3}, J Ophir^{2,3}.

¹University of Vermont College of Medicine-Fletcher Allen Health Care, Burlington, VT, 05401, USA; ²The University of Texas Medical School, Department of Radiology, Ultrasonics Laboratory, Houston, TX, USA; ³University of Houston, Electrical and Computer Engineering Department, Houston, TX, USA.

Clinical breast elastography studies have so far focused on the elastographic appearance of cancer and the features that allow cancers to be distinguished from benign masses such as fibroadenomas. However, since many benign lesions may occasionally mimic cancer, the elastographic features of these lesions are also important.

Elastograms of 47 breast lesions thought to be suspicious for cancer either mammographically or sonographically were studied by three different observers. Of the 47 lesions, ten were malignant and the remainders were benign by either biopsy or clinical follow-up. The benign lesions included fibroadenomas, fibrosis, fibrocystic change, adenosis, and less common lesions including adenomyoepithelioma, papilloma, and hematoma. Thirty eight of the lesions were studied using single compression elastograms and nine were studied using multicompression elastography. The elastographic characteristics of the lesions were recorded and compared to the sonographic characteristics. Characteristics recorded were: hardness (strain), lesion shape, internal texture, lesion border sharpness and irregularity. Measurements of lesion width and thickness on the elastograms were also compared with corresponding measurements on the sonograms.

The benign lesions varied widely in strain characteristics, some being barely visible against the background of normal breast tissue whereas others had much lower strain values than the surrounding breast. Margin regularity and definition also varied widely. Frequently, angular borders were seen – possibly due to signal processing artifacts in the strain images. The majority of benign lesions were smaller in transverse measurement on the elastogram compared to the sonogram consistent with results previously reported. However, the fibroadenomas were mixed in size some being larger than on the sonogram and some being smaller. Several lesions that were highly suspicious sonographically were clearly smaller on the elastogram. Thickness measurements on the other hand, were always smaller on the sonogram suggesting possible distortion or strain artifacts due to signal processing.

Conclusions:

The elastographic appearance of benign lesions is widely variable and examples of this will be shown. Features such as border regularity used to evaluate lesions sonographically may not be as useful for elastogram evaluation. Transverse lesion size still may be a useful feature, but we found an apparent bias in thickness measurements that may preclude its use as a diagnostic feature for separating benign from cancerous lesions.

53 **VIBRATIONAL DOPPLER IMAGING IN DIFFERENTIATION OF BENIGN VERSUS MALIGNANT BREAST MASSES BY VDI:B-SCAN LESION AREA RATIO.**

Brian S. Garra¹, Louise M. Mobbs¹, G. Sharat Lin².

¹University of Vermont College of Medicine-Fletcher Allen Health Care, Burlington, VT, USA;

²Advanced Imaging Associates, Fremont, California, USA.

Objective: To investigate the potential clinical usefulness of vibrational Doppler imaging (VDI) in differentiating between benign versus malignant breast masses by VDI:B-scan lesion area ratio and VDI lesion boundary characteristics.

Methods: VDI is a real-time method of imaging the soft tissue vibrational response to externally-applied vibration. Audio-frequency vibrations were applied to the skin using an audio transducer driven by a 2-watt audio amplifier fed by a variable-frequency musical tone generator. The audio transducer was attached to the ultrasound transducer through a vibration-dampening rubber pad, and acoustically coupled to the skin using ultrasound scanning gel. Vibrations at 69–298 Hz were applied to the breasts of 21 patients after written informed consent presenting with 22 histologically-confirmed masses. Induced tissue resonance vibrations were visualized by power color Doppler imaging at 6 MHz with color gain at 10–15 dB below typical blood flow settings and pulse repetition frequency (PRF) at 500–1400. Lesion boundaries in VDI and B-scan as determined by blinded readers were superimposed for comparison.

Results: The breast masses studied included 15 benign lesions (11 fibroadenomas, 2 fibrocystic masses, and one phyllodes tumor) and 7 malignancies (6 infiltrating ductal carcinomas and one invasive lobular carcinoma). Among benign lesions, VDI lesion area was smaller than B-scan lesion area in 10 cases, the VDI lesion boundary precisely followed the B-scan lesion boundary in 4 cases, and the VDI lesion boundary was incomplete at adjacent fat in one retrospective case. However, in 6 of 7 malignancies, the VDI lesion boundary was irregular (spiculated or deeply lobulated), indistinct or graduated, and larger than the lesion seen in B-scan. One retrospective case was misread during blinded readings because more subtle hypo-vibrational regions outside of the B-scan lesion boundary were not initially recognized at the color gain and PRF settings used. (This trial was still a learning process!) Sensitivity in this small sample was 86% and specificity was 94%.

Conclusions: VDI:B-scan lesion area ratios greater than 1.1 and markedly irregular and indistinct VDI boundaries are consistent with invasive neoplastic changes extending beyond the main body of malignant tumors. VDI may provide a better estimate of the minimum extent of a primary malignant lesion than B-scan. Although more data are needed, there are preliminary indications that the VDI:B-scan area ratio varies quantitatively with malignant tumor grade. VDI lesion boundaries provide visual criteria in addition to those of B-scan for differentiating benign versus malignant masses in the breast, thus potentially improving diagnostic confidence.

Lesion histology	Lesion area ratio: VDI / B-scan				Inc
	< 0.95	0.95 – 1.1	1.1 – 1.3	> 1.3	
Fibrocystic change	3				
Fibroadenoma	7	3			1
Phyllodes tumor		1			
Infiltrating ductal Ca, low grade		1	1		
Infiltrating ductal Ca, mod & hi grade				4	
Invasive lobular Ca, mod & hi grade				1	

INTRAVASCULAR ULTRASOUND STRAIN IMAGING WITH ROTATING SINGLE ELEMENT TRANSDUCERS: INITIAL *IN VIVO* EXPERIMENTS.

Christian Perrey¹, Waldemar Bojara², Stephan Holt², Michael Lindstaedt², Helmut Ermert¹.

¹Institute of High Frequency Engineering, Ruhr University, Bochum, GERMANY; ²Department of Cardiology Bergmannsheil, Ruhr University, Bochum, GERMANY.

Acute coronary syndromes are often caused by unstable coronary plaques. These lesions cannot be reliably identified with conventional intravascular ultrasound (IVUS). Strain imaging with IVUS can potentially be used for plaque discrimination by visualizing the mechanical properties of vessel walls.

In this study strain imaging is performed with rotating single element IVUS transducers. Tissue strain is estimated from 40 MHz IVUS RF data acquired *in vivo* during interventional procedures.

A Galaxy IVUS scanner (Boston Scientific, CA) with a 40 MHz single element transducer is used for data acquisition. Analog RF data are sampled at 100 MHz with an A/D converter board (Gage Applied, QC). Custom made hardware is used for triggering and signal amplification. To avoid aliasing, an analog band pass filter is used prior to digitization, which does not constrain the transducer bandwidth.

Rotating single element transducers are prone to non uniform rotational distortion (NURD), which leads to image artifacts due to misaligned A-lines and can severely degrade correlation based strain imaging. This effect is often catheter specific. To estimate this interference, additional phantom images are acquired directly after the interventional procedure. These reference measurements are used to evaluate and partly compensate catheter specific artifacts, especially in the presence of catheter angulation. The normalized correlation coefficient of corresponding A-Line pair segments is evaluated as an indicator for decorrelation due to NURD. In addition, images used for strain calculations are visually inspected.

In vivo imaging is performed with informed patient's consent during IVUS examinations. Full frame RF data are recorded for a period of three seconds along with an intra-coronary pressure signal. Only data from late end-diastole is used for strain calculations. Lateral motion was estimated and corrected using block matching algorithms. The applied strain imaging algorithm determines radial time shift from RF base band data at different compression levels by finding the phase root of complex cross-correlation functions. Strain is calculated as the derivative of the shift estimations.

Initial results show that image correlation is influenced by NURD in some cases. Phantom results indicate that NURD is not always catheter specific, but can depend on the actual catheter position. In those cases, image quality can sometimes be improved by repositioning the catheter. In the absence of severe NURD strain imaging is feasible with data acquired in late diastole. Different values of strain can be found along the circumference of the vessel wall. Regions of elevated strain can be related to areas where plaques are morphologically visible in the B-mode image.

A project of the Ruhr Center of Competence for Medical Engineering (KMR), funded by the German Federal Ministry of Education and Research (bmb+f grant No. 13N8079).

69 **MONITORING THE EFFECT OF ACUPUNCTURE NEEDLING ON HUMAN CONNECTIVE TISSUE *IN VIVO*.**

H. M. Langevin¹, E. E. Konofagou², B. S. Garra³.

Departments of ¹Neurology and ³Radiology, University of Vermont, Burlington, VT, USA;
²Department of Radiology, Brigham and Women's Hospital – Harvard Medical School, Boston, MA, USA.

Introduction:

Acupuncture has been practiced for thousands of years, but its therapeutic mechanism remains unknown. Mechanical signaling through connective tissue, with effects on cellular elements (fibroblasts, blood vessels, sensory nerves) present within this tissue recently has been identified as a potentially important consequence of needle manipulation that may be linked to acupuncture's therapeutic effect. This study investigates the hypothesis that during needle rotation in humans increased mechanical coupling between needle and tissue causes modification of this tissue's biomechanical behavior during subsequent needle manipulation.

Methods:

To test this hypothesis, *in vivo* ultrasonic imaging using a System Five (Vingmed) ultrasound scanner at 6.7 MHz was performed on the left and right thigh (subcutaneous tissue and muscle) of human subjects at different stages of needle motion, which included 1) varying amounts of needle rotation (0, 4, 8, and 16 revolutions) and 2) downward and upward axial needle movements both before and after rotation using a computer-controlled acupuncture needling instrument. Disposable stainless steel needles (0.25 mm in diameter) were used. Displacements were estimated using the RF data, and crosscorrelation techniques were utilized as previously described in Elastography with a 2 mm window and a window overlap of 60%. Seventy RF scans were acquired continuously during each experiment at the rate of 12.9 frames/s. Ciné-loop displacement images were generated off-line during the needle motion.

Results:

At the time of abstract submission, two subjects were tested. We expect to have tested an additional ten subjects by the fall of 2003. In the subjects tested so far, tissue displacement could be estimated using merely the stimulus caused by the movement of the needle. Tissue displacement during rotation increased in amplitude by up to two-fold, and spatial extent by up to four-fold, compared with no rotation. Furthermore, needle rotation appeared to stiffen the tissue, as suggested by an absence of tissue re-organization (rebound) following downward displacement post-rotation (compared with downward displacement pre-rotation). There also appeared to be a non-uniform 'footprint' of lower displacement induced by the needle into the tissue during downward movement post rotation, thus creating a signature image. This effect was less evident during upward movement of the needle.

Discussion:

Imaging of tissue displacement during controlled acupuncture needle movement allowed for quantitative analysis of the extent of the tissue affected by the needle when it is rotated, as occurs in clinical acupuncture practice. Needle rotation also modified the biomechanical behavior of soft tissue during post-rotation downward needle movement. Mechanical stimulation of tissue during acupuncture needle manipulation during and following rotation may be an important component of acupuncture therapy, and the above-described imaging technique may be key to monitoring these effects.

This study was supported by NIH grant 5 R21 AT000300.

30 **NONCONTACT ULTRASOUND INDENTATION USING A WATER BEAM.**

Minhua Lu¹, Yongping Zheng¹.

¹The Hong Kong Polytechnic University, HONG KONG.

Changes in tissue stiffness may be related to an abnormal pathological process. Hand palpation is commonly used for the assessment of soft tissues. We have previously developed an ultrasound indentation technique for measuring the stiffness of tissue specimens as well as body tissues *in vivo* [1]. An ultrasound transducer (5 to 15 MHz) was used to compress the tissue by direct contact, while the force applied to the tissue was sensed using an in-series load sensor. This ultrasound indentation approach has been applied for the assessment of many tissues. However, this contact ultrasound indentation was difficult to use with a focused ultrasound beam for high resolutions or with fast scanning for elasticity imaging.

This study was aimed to develop a non-contact ultrasound indentation system by using water beam compression. The water beam also served as a medium for ultrasound propagation. The pressure applied to the tissue was changed by adjusting the water flow and was calculated based on the water pressure within the water pipe and the force under the specimen platform. Tissue deformation was estimated from the ultrasound echoes reflected from the tissue using a cross-correlation algorithm. A prototype system for water beam compression was constructed using a focused 15 MHz ultrasound transducer. The water beam was 2 mm in diameter.

Experiments were conducted on phantoms with different stiffnesses made from silicones. The relationship between the force and the deformation for each phantom was obtained (Figure 1, 2). It was found that the force-deformation curve was approximately linear when the force ranged from 0 to 0.5 N. The ratio of the force and the deformation was higher when the phantom was harder while the ratio was lower when the phantom was softer. The use of water beam also allowed the system to perform fast scanning for tissues with various dimensions and surface conditions as well as to use high frequency ultrasound without any additional attenuation. On the other hand, to clearly understand the interaction between the soft tissue and the water beam, a finite element model was established. The linear relationship of the pressure and the deformation derived from the simulation agreed somewhat with the experimental results. The elasticity image obtained by using this non-contact loading mechanism will also be reported.

Acknowledgements: This project was partially supported by the Research Grant Council of Hong Kong (PolyU 5245/03E) and The Hong Kong Polytechnic University.

References: [1] Zheng and Mak. IEEE Trans Biomed Eng 43: 912-918, 1996.

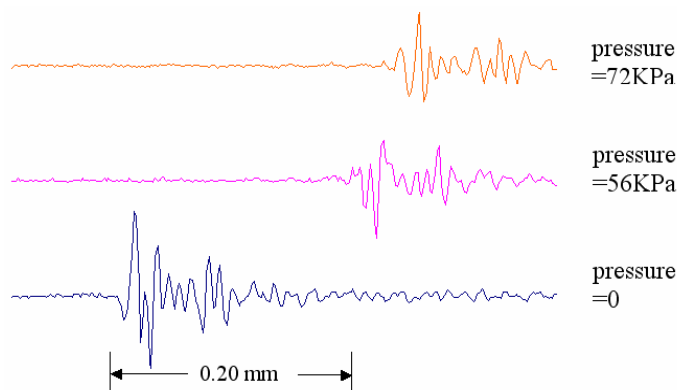


Figure 1. Ultrasound RF signals of the echoes from the phantom surface under different pressure.

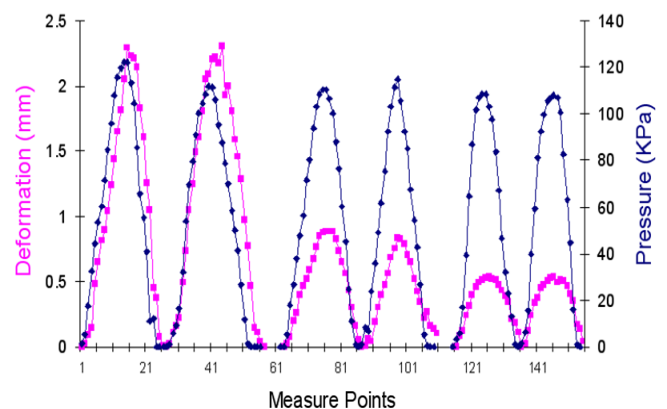


Figure 2. Measured pressures and deformation under cyclic loading. Different marks represent the results from two specimens.

Ralph Sinkus¹, Mickael Tanter², Thomas Nisius³, Christiane Kuhl⁴.

¹Philips Research, Hamburg, GERMANY; ²Laboratoire Ondes et Acoustique, ESPCI, FRANCE; ³RheinAhr campus, Remagen, GERMANY; ⁴Dept. of Radiology, University Hospital, Bonn, GERMANY.

MRE allows the assessment of the visco-elastic parameters of tissue. It is expected, that this novel information might help in tumor differentiation. Monochromatic steady-state MRE allows extending the assessable parameters from isotropic to the anisotropic elastic properties of tissue. A cubic model of anisotropy is used for reconstruction utilizing the assumption. Rotations of the coordinate system are fully taken into account. Initial *in-vivo* data indicate the presence of large anisotropic properties within malignant breast tumors.

Recent applications of MR-Elastography aim at providing additional information for lesion characterization. Motivated by the relevance of palpation in the diagnosis of breast and prostate cancer, it is expected that the visco-elastic properties provide valuable information for tumor differentiation. Top illumination microscopy suggests a very heterogeneous and irregular architecture of malignant lesions at the millimeter scale. This makes it very likely, that tumors exhibit anisotropic elastic properties, which could be of diagnostic value

Monochromatic steady-state MRE allows obtaining the solution of the wave propagation problem at each location within the object under study [1,2]. Due to the complex-valued nature of the process (caused by viscosity) there are 6 parameters available per voxel (3 amplitudes and 3 phases). The stress-strain relation for a cubic material involves 3 material parameters (Eq.1), expressed here in terms of the Lamé coefficients λ , μ and the anisotropy λ^* .

$$\begin{pmatrix} \sigma_{xx} \\ \sigma_{yy} \\ \sigma_{zz} \\ \sigma_{xy} \\ \sigma_{xz} \\ \sigma_{yz} \end{pmatrix} = \begin{pmatrix} \lambda + 2\mu & \lambda + \lambda^* & \lambda + \lambda^* & & & \\ \lambda + \lambda^* & \lambda + 2\mu & \lambda + \lambda^* & & & \\ \lambda + \lambda^* & \lambda + \lambda^* & \lambda + 2\mu & & & \\ & & & \mu & & \\ & & & & \mu & \\ & & & & & \mu \end{pmatrix} \begin{pmatrix} u_{xx} \\ u_{yy} \\ u_{zz} \\ 2u_{xy} \\ 2u_{xz} \\ 2u_{yz} \end{pmatrix}$$

Eq.1: Stress-strain relation for cubic anisotropy in so-called reduced form.

Simulations from 2D Finite Elements Methods (not shown here) demonstrate the feasibility of the method to properly recuperate Young's modulus E , anisotropy λ^* , attenuation ζ (in terms of the so-called Voigt model) as well as the angle of rotation. Aiming for the retrieval of anisotropy necessitates the utilization of a reasonable value for Poisson's ratio (σ). Via the so-called Helmholtz-Hodge decomposition it can be shown, that the large magnitude of the bulk modulus λ is compensated by the smallness of $\text{div}(\vec{u})$, with \vec{u} the displacement vector. This knowledge allows regularizing specific 2nd order spatial derivatives. It can be shown, that the method yields results for E , λ^* and ζ , which are independent on the exact value of σ . *In-vivo* results from invasive ductal carcinoma (Figure 1) indicate that the anisotropy is significantly increased at the location of the tumor.

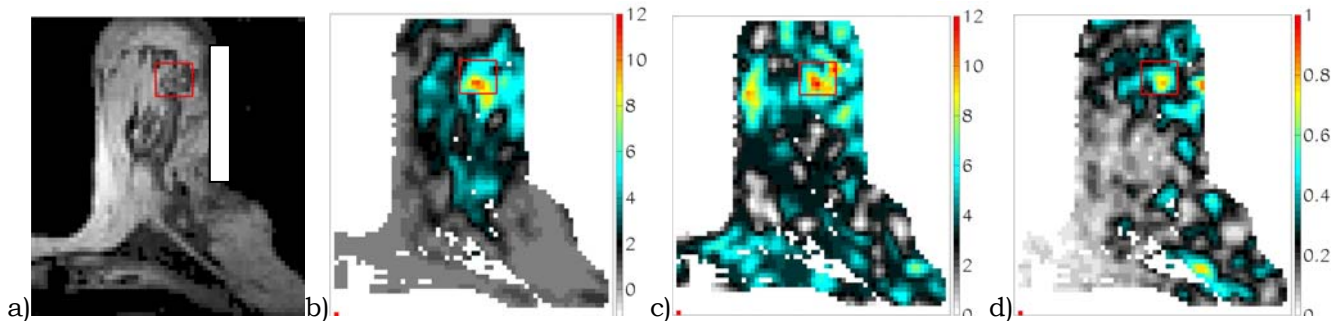


Figure 1: a): Transversely oriented MR-magnitude image depicting the location of an invasive ductal breast cancer (red rectangle). The mechanical transducer is pressed laterally against the breast (white filled rectangle). b): Reconstructed Young's modulus E [kPa], c) anisotropy λ^* [kPa] and d) attenuation ζ [kg/dm/s].

[1] R. Muthupillai et al, Science 26 (29), 1854 (Sep. 1995)
 [2] R. Sinkus et al, Phys. Med, Biol. 45 (2), 1649-1664 (June 2000)

08 **PROSTATE ELASTOGRAPHY *IN VITRO*§**

Rémi Souchon¹, Olivier Rouvière², Albert Gelet², Jonathan Ophir³, Jean-Yves Chapelon¹.

¹INSERM U556, Lyon, FRANCE; ²Hopital Edouard Herriot, Lyon, FRANCE; ³The University of Texas Medial School, Department of Radiology, Ultrasonics Laboratory, 6431 Fannin St., Houston, TX, 77030, USA.

Prostate elastography was performed *in vitro* and compared with anatomic and pathological results in order (1) to identify prostate structures that are visible in elastograms, and (2) to assess the capabilities of elastography for prostate cancer detection.

Fresh human prostates were obtained from 15 patients undergoing radical prostatectomy. They were embedded in a cylindrical gel equipped with a cylindrical cavity designed to insert a transrectal US probe covered by a balloon, so that organ orientation would be similar to conditions *in vivo*. The balloon was inflated to compress the prostate. Transverse elastograms were acquired every 2 mm in a multi-compression sequence. A standard cross-correlation technique was used to calculate the elastograms. The distance between each plane and the prostatic apex served as a reference for registration between elastograms and pathology.

As shown in Figure 1, high strain contrast was observed between the peripheral zone and the transitional zone. The peripheral zone was seen as a high strain area in the elastograms, whereas the transitional zone was seen as a stiff region. Anatomical zones shown by the elastograms corresponded well in shape and size to the corresponding pathology slices. In most cases they were not visible in the sonograms. Near the prostatic apex, the verumontanum was seen as a stiff V-shaped structure. Fibrous hyperplasia (benign excess cell replication) nodules were seen as stiff areas that had poor strain contrast with surrounding tissues, but they were easily identifiable by their high strain contour. Glandular hyperplasia was visible as stiff ellipsoidal nodules with sharp edges (Figure 2). Four of ten malignant tumors were identified from blind reading of the elastograms in the peripheral zone, and 1/6 in the transitional zone. They appeared as stiff areas with smooth edges and were visible in multiple consecutive planes. Glandular hyperplasia was usually stiffer than cancer.

Only small pre-compression (<2%) was used in this study. It is expected that a higher percentage of tumors will be detectable *in vivo* using a wider range of pre-compressions to exploit nonlinear changes in tissue stiffness for contrast enhancement. The stiffness contrast might also have been altered by the low temperature within the gel (~10°C).

In conclusion, elastography was capable of showing the prostate anatomy, including the peripheral and the transitional zones, the verumontanum, glandular and fibrous hyperplasia, and malignant tumors.

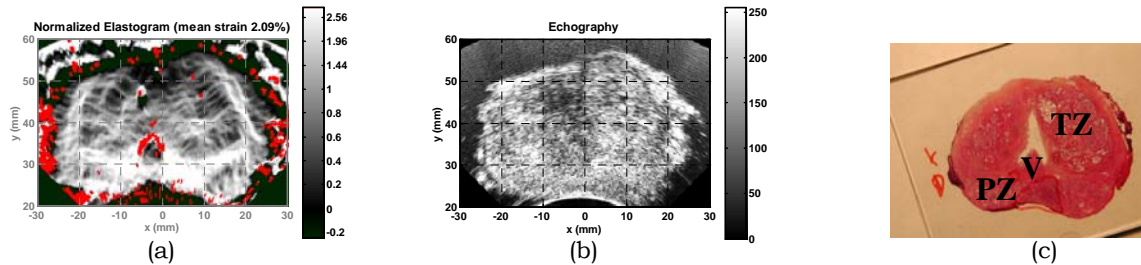


Figure 1: (a) Elastogram, (b) corresponding sonogram and (c) pathology. The peripheral zone (PZ), the two lobes of the transitional zone (TZ) and the verumontanum (V) are visible.

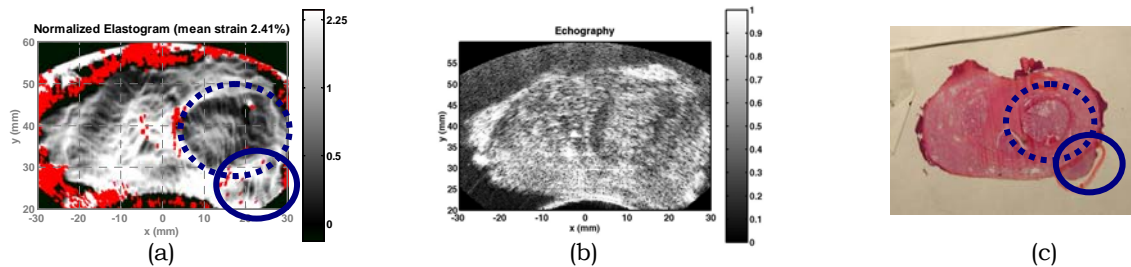


Figure 2: (a) Elastogram, (b) corresponding sonogram and (c) pathology showing glandular hyperplasia (dotted line) and cancer (solid line).

§This work was supported in part by National Cancer Institute (USA) Program Project Grant P01-CA64597

Both focused (HIFU) and unfocused ultrasound thermal therapy have been shown to be effective for the treatment of different types of tumors (1): the absorption of short high-intensity ultrasonic bursts in biological tissues induces a thermal lesion due to the local increase in temperature. In “passive” elastography, apparent strain is imaged using backscattered (RF) ultrasonic signals without any external applied compression: the deformation between consecutive RF signals is induced by temperature-dependent changes in the speed of sound and by thermal expansion during the formation of a thermal lesion. The apparent (measured) strain s is given by:

$$s = \varepsilon - \frac{\delta c}{c_0}$$

Here ε is the mechanical strain due to thermal expansion, δc is the variation in speed of sound, and c_0 the initial speed of sound. This technique was used for ultrasonic temperature estimation during RF ablation, assuming thermal expansion was negligible (2). *In vitro* experiments were carried out to determine if the apparent strain induced by high temperatures and by tissue coagulation was able to depict the formation of a HIFU lesion.

HIFU lesions of 8x15 mm² (depth 2-10 mm) were generated in bovine and porcine liver *in vitro* using a 25s 15 W/cm² burst. Consecutive RF frames (5 MHz center frequency) were digitized at 8 fps during HIFU application using an imaging probe facing the HIFU probe. Apparent strain images (elastograms) were calculated using the gradient of the time delays between consecutive RF frames and were cumulated.

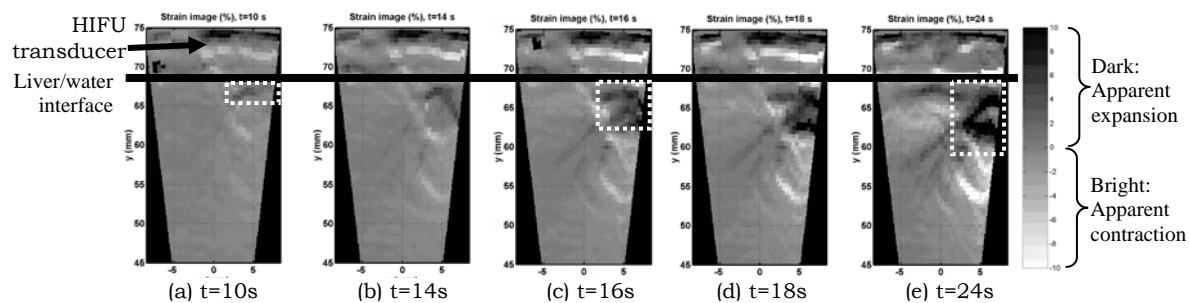


Figure 1: Cumulated apparent strain at times (a) $t=10s$, (b) $14s$, (c) $16s$, (d) $18s$, and (e) $24s$ during HIFU emission. The lesion measured from gross pathology is outlined (white) in (a), (c) and (e).

Figure 1 shows the cumulated apparent strain at different times during the formation of the lesion. The lesion was generated on the right side of the image. The lesion position and size measured from gross pathology at $t=10s$ (2-3 mm deep), $t=16s$ (5-7 mm) and $t=24s$ (8-10 mm) are shown (white outline). Small (<2%) apparent contraction (bright) was observed between 0 and 10 s, then a significant (>10%) apparent expansion zone (dark) appeared near the transducer and expanded between 14 and 18 s, while the contraction zone shifted away from the transducer. Similar results were observed in porcine and in bovine liver. It is likely that significant tissue expansion occurred with coagulation and dominated the apparent contraction (increased speed of sound) expected from *in vitro* measurements in canine tissues (3).

In conclusion, good correspondence was observed between the HIFU lesion measured from gross pathology and the expansion zone in apparent strain images acquired by “passive” elastography during the formation of the lesion *in vitro*.

- (1) Chapelon JY et al. *In vivo* effects of high-intensity ultrasound on prostatic adenocarcinoma Dunning R3327. *Cancer Research* 52(22), 6353-6357 (1992).
- (2) Varghese T et al. Ultrasound monitoring of temperature change during radiofrequency ablation - Preliminary *in-vivo* results. *Ultrasound in Med and Biol* 28(3), 321-329 (2002).
- (3) Techavipoo U et al. Temperature dependence of ultrasonic propagation speed and attenuation in canine tissue. *Ultrasonic Imaging*, 24, 246-260 (2002).

This work was supported in part by grant 01-2-93-0314 of the RNTS Project of the French Ministry of Economy, Finances and Industry, and by National Cancer Institute (USA) Program Project Grant P01-CA64597.

47 **INTERFERENCE PATTERN APPROACHES TO MEASURE THE SHEAR MODULUS OF HOMOGENEOUS BIO-MATERIALS.**

Z Wu¹, LS Taylor², DJ Rubens³, KJ Parker¹.

¹University of Rochester, ECE Dept; ²University of Rochester, BME Dept, ³Strong Memorial Hospital, University of Rochester, Rochester, NY 14627, USA.

The mechanical properties of bio-tissues have been studied by many researchers and doctors because the changes of the mechanical properties often imply the occurrences of certain diseases. Among many of the mechanical properties, the shear modulus [stiffness] is usually one of the most important parameters to help diagnoses. In this paper, two noninvasive methods are proposed to measure the shear modulus by inspecting the shear waves interference patterns using the vibration Sonoelastography. Sonoelastography visualizes the absolute value of the peak particle velocity distribution in the medium by analyzing the Doppler vibration signals.

To measure the shear modulus, two shear wave sources are placed on the opposing two sides of a sample. The wave sources are driven by the same signal. The shear waves from the two sources interfere with each other to create standing wave (stripe) patterns. The patterns are visualized by the Sonoelastography technique.

The spacing between the stripes equals half of the shear wavelength.

Since the signal frequency is known, the shear velocity can be obtained by taking the product of the wavelength and the frequency. Then the shear modulus is $V_{\text{shear}}^2 \rho$, where V_{shear} is the shear velocity and ρ is the density of the testing sample. This approach is referred to as the static pattern approach.

An alternate approach is to drive the two vibration sources at slightly different frequencies, f and $f+\Delta f$, respectively. In this case, the interference patterns no longer remain stationary. If Δf is much smaller than f , it can be proven that the apparent velocity of the moving patterns is $(\Delta f/2f) \cdot V_{\text{shear}}$, where V_{shear} is the shear velocity in the medium. Since the apparent velocity of the moving patterns can be readily measured by analyzing the video sequence, the shear velocity and the shear modulus can be obtained thereafter. This approach is referred to as the moving pattern approach.

These two approaches are validated by the shear wave time-of-flight approach. In the shear wave time-of-flight experiment, two bimorphs are placed against the two sides of the sample, functioning as transmitter and the receiver respectively. The receiver picks up the transmitted disturbance at a certain time delay, from which the shear wave speed can be calculated.

A 5% gelatin phantom, 6*8*12cm in size approximately, is used as the testing sample. Two bimorph piezo applicators [1cm*2.5cm chips] are used as the vibration sources. Two "static pattern" experiments at 180Hz and 200Hz yield shear wave speeds of 1.399m/s and 1.404m/s respectively. One "moving pattern" experiment at 200Hz yields the shear wave speed of 1.44m/s. The time-of-flight approach measures the shear wave speed to be 1.398m/s. The shear modulus of the sample is calculated thereafter to be 1.96kPa, approximately, based on the shear wave speed measurements. Thus, the interference pattern approaches are validated in tissue-mimicking material, enabling near real time measurements of material properties.

50 **A HIGH FREQUENCY (20 MHZ) ULTRASOUND BASED ELASTOGRAPHY SYSTEM FOR *IN VIVO* SKIN ELASTICITY IMAGING.**

Michael Vogt¹, Sven Scharenberg², Ruediger Scharenberg², Klaus Hoffmann³, Peter Altmeyer³, Helmut Ermert¹.

¹Institute of High Frequency Engineering, Ruhr-University, Bochum, GERMANY; ²Taberna Pro Medicum GmbH, Lueneburg, GERMANY; ³Dermatologic University Hospital, Ruhr-University, Bochum, GERMANY.

It is a common practice to assess skin elasticity tactually during dermatological examinations, because this reflects the overall constitution. Diseases like psoriasis and scleroderma, skin ageing, sun exposure as well as changes of the epidermal hydration cause elasticity changes. However, tactile investigations strongly depend on the individual sense of the physician. In dermatological research, techniques for skin elasticity assessment have been introduced. Skin deformations are caused by suction, traction or torsion, and the displacement of the skin surface is measured with optical or mechanical sensors. But the value of these techniques is limited, because only the overall skin surface displacement is measured. On the other hand, high frequency ultrasound is a powerful tool for non invasive and high resolution skin imaging. We have developed an *in vivo* skin elasticity imaging system, which is based on 20 MHz range ultrasound.

In our setup, suction is applied to cause an external skin deformation and high frequency ultrasound echo signal frames are acquired during stepwise changed negative pressure. We have equipped a high frequency ultrasound scanner (Taberna Pro Medicum GmbH, Lueneburg, Germany) with a computer controlled vacuum pump system for reproducible measurements. Mechanical scans are performed with a focused single element ultrasound transducer (20 MHz center frequency, 12 MHz bandwidth, 2.4 f-number, 47 μm / 160 μm axial / lateral resolution) inside a vacuum chamber. Negative pressures up to 12 mbar are applied while scanning over a maximum depth of 8.2 mm along a lateral dimension of 12 mm. High frequency echo signals are digitized with 100 MHz sampling frequency and 8 bit amplitude resolution.

In each echo signal frame the skin surface is segmented, utilizing an adaptive threshold technique and the skin surface displacements along the lateral coordinate are quantified. In a next step, high frequency echo signals are aligned to the segmented skin surface, which is as a premise to measure relative deformations and, thus, strains in the skin over depth. The phase root seeking algorithm is applied to estimate the axial strains from axially windowed baseband signals in consecutive echo signal frames. We calculate the correlation coefficient of the time shifted signals and we use these data to verify the reliability of the strain estimates. Only reliable strain estimates corresponding to correlation coefficients larger than 90% are displayed.

Measurements on agar and gelatin speckle phantoms were performed to test and to establish the implemented system. Results will be presented and the system performance will be analyzed. It will be shown with results from *in vivo* measurements that in healthy skin strains in the subcutaneous fat are significantly larger than strains in the corium. Results from measurements on skin burnings and skin lesions, which have been performed in a clinical study, show the potential of the developed system to image changing mechanical properties in the skin non invasively *in vivo* with high resolution.

A project of the Ruhr Center of Competence for Medical Engineering (KMR). Supported by the Federal Ministry of Education and Research, No. 13N8079.

Session F: Biomechanical Tissue Modeling

Tuesday, October 14 10:00A – 10:45A

11 **A GENERALIZED KELVIN-VOIGT VISCOELASTIC CONSTITUTIVE MODEL FOR SOFT TISSUE.**

L. S. Taylor¹, D. J. Rubens¹, K. J. Parker¹.

¹University of Rochester, Rochester, NY, USA.

Ultrasonic attenuation in the very soft tissues is known to follow an empirical equation with power law frequency dependence not explained by spring and dashpot viscoelastic models. In a recent paper by Szabo and Wu (JASA 2000) a generalized Kelvin-Voigt three parameter viscoelastic model was derived which explains this power law when frequency is raised to a non-integer power, $1 < \gamma < 2$. A modified constitutive equation of their model is presented and the stress relaxation, creep compliance, impulse response and complex modulus functions are derived. These time-domain and frequency-domain relations are found to follow power laws with non-integer exponents equal to $\gamma - 1$.

In order to validate the applicability of this model, viscoelastic testing was performed on bovine liver specimens. The derived theoretical responses for creep, stress relaxation and complex modulus are compared to experimental data. Model parameters are extracted from the tests and the linear correlation coefficient is calculated to derive the goodness-of-fit. For the complex modulus the best fits were $R^2 = 0.992$ and 0.995 for thermally ablated and normal samples respectively. Model parameters for the power law exponent, $(\gamma - 1)$, were in the range 0.17 to 0.29, which corresponds to the reported range of γ for liver tissue in the ultrasonic literature.

It is believed that this model will be useful in various dynamic elasticity techniques when viscoelastic parameters need to be extracted and when estimates of material properties need to be extended to a range outside that which can be easily tested. Tests run on the same tissue will be needed to determine if the correspondence between the value of γ for MHz range attenuation, low frequency (0.1 – 25 Hz) cyclic testing and stress relaxation (time domain) tests are merely coincidental.

Eunyoung Park¹, Antoinette M. Maniatty¹.

¹Rensselaer Polytechnic Institute, Department of Mechanical, Aerospace, and Nuclear Engineering, 110 8th Street, Troy, NY, 12180, USA.

The elastic properties of tissue are directly related to the underlying structure of the tissue and are therefore strongly affected by pathological changes in the tissue. To be precise, it is the elastic property of shear stiffness, i.e. the property that characterizes resistance to shape change, that is most affected by pathological changes. Furthermore, the bulk stiffness, i.e. the property that characterizes resistance to volume change, is typically six orders of magnitude higher than shear stiffness making tissue nearly incompressible in a relative sense. The bulk stiffness is also less affected by pathological changes. Because the shear wave speed is directly related to the shear stiffness, observing the propagation of transient shear waves in tissue could lead to new diagnostic tools. In this work, we examine, using numerical simulation, the behavior of a pulse-induced elastic wave traveling through a nearly incompressible, heterogeneous body. The longer term goal is to use this information to reconstruct the shear stiffness distribution to a known resolution given ultrasonic measurements of interior displacements over time, such as that reported in Tanter et al. [1].

Issues that will be discussed include: (a) efficient forward modeling approach using the finite element method for modeling transient elastic waves in the context of near incompressibility, (b) studies investigating the response of tissue to a pulse-induced elastic wave, especially considering the effect of near incompressibility, (c) use of the near incompressibility to reconstruct one component of the displacement field given noisy measurements of the other component(s) (1 in 2-d and 2 in 3-d), and (d) sensitivity analysis to investigate the effect of the variations in the shear modulus on the resulting displacement field and the potential effect of noisy data on shear stiffness reconstruction.

[1] M. Tanter, J. Bercoff, L. Sandrin, M. Fink, Ultrafast compound imaging for 2-D motion vector estimation: application to transient elastography, *IEEE Transactions on Ultrasonics, Ferroelectrics, and Frequency Control*, vol. 49, no. 10, 1363-1374, 2002.

T-C Hsu¹, Y-W Shau², C-L Wang³.

¹Department of Physical Medicine and Rehabilitation, Chang Gung Memorial Hospital, Taoyuan TAIWAN; ²Institute of Applied Mechanics, National Taiwan University, Taipei, TAIWAN;

³Department of Orthopedics, National Taiwan University Hospital, Taipei, TAIWAN.

We investigated the shock absorbing properties of plantar soft tissue under the metatarsus that was subjected to various strain rates to simulate the conditions of different walking velocities. A new *in vivo* method was developed that combines ultrasonography and a pressure gauge to measure directly the local soft tissue mechanical properties under each metatarsus at loading velocities of 2 cm/s, 5 cm/s, and 9 cm/s respectively (Figure 1). Based on the repeated loading-unloading stress-strain cycles, a simple three-parameter viscoelastic mathematical model that accounted for the effects of strain rate was proposed.

Metatarsus for eight healthy young adults with the age of 24 ± 1.8 y (mean \pm standard error of mean) and nine healthy elderly with the age of 54.6 ± 3.3 y were measured. The unloaded plantar soft tissue thickness under the metatarsus decreased progressively from the first to the fifth metatarsus in all subjects. The thickness was similar in the young and elderly groups. The compressibility index (CI) and elastic modulus (E_p) increased significantly from 30-40% to 50-60% and 300-500 kPa to 400-500 kPa respectively from the lowest to the highest loading velocities in young adults. However, the elderly did not show the same trend.

The elderly typically had a greater CI and E_p in the metatarsus than the young. Energy dissipation ratio (EDR) in the young and elderly groups increased significantly from 30-40% to 50-60% and from 40-50% to 60-65% respectively from the lowest to the highest loading velocities. The elderly had a greater EDR than the young. Moreover, the mechanical properties of the plantar soft tissue under the metatarsus are time-dependent in young adults. Changes in the mechanical properties of the metatarsus in the aged group, including the increase in tissue stiffness and a higher energy dissipated in the soft tissue, may be responsible for the geriatric podiatric conditions. The cyclic biomechanical behavior of the metatarsus soft tissue at various loading rates and aging can be quantified satisfactorily using the optimum mathematical model presented (Figure 2).

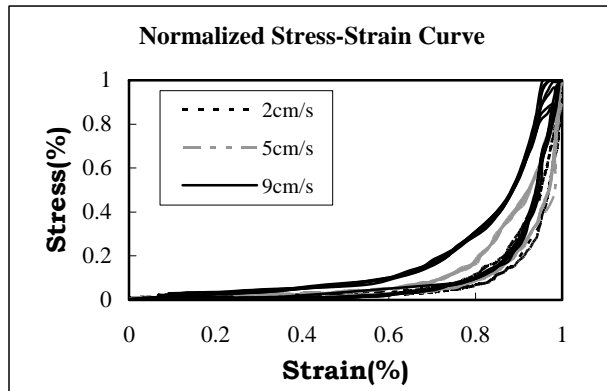


Figure 1: Stress-strain curve at various loading rate

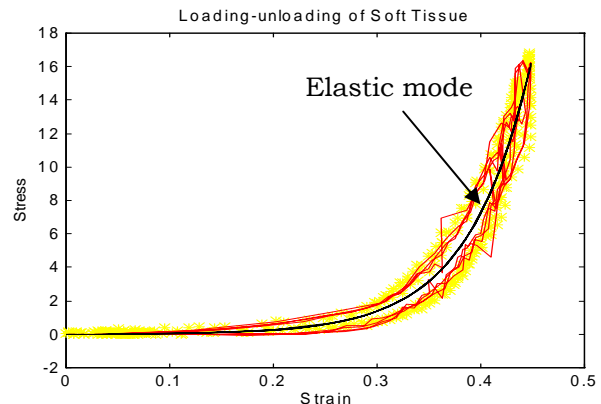


Figure 2: Viscoelastic modeling of metatarsus

37 **BREAST AND PROSTATE CANCER DIAGNOSIS BY REAL-TIME TISSUE ELASTICITY IMAGING SYSTEM -A FEASIBILITY STUDY.**

T Shiina¹, M Yamakawa¹, N Nitta¹, E Ueno², T Matsumura³, S Tamano³, R Shinomura³, T Mitake³.

¹Institute of Information Sciences & Electronics, University of Tsukuba, Tsukuba, JAPAN;

²Institute of Clinical Medicine, University of Tsukuba, Tsukuba, JAPAN; ³Research & Development Center, Hitachi Medical Corporation, Kashiwa, JAPAN.

Many diseased tissues such as breast and prostate cancer become hard with disease progression. Then, various techniques for tissue elasticity imaging have been proposed as a new modality for cancer diagnosis based on characteristics of tissues. In clinical application, a high-speed processing is required for real-time diagnosis and freehand manipulation of ultrasonic probe like the usual ultrasonic diagnosis is desirable for simple operation. We have therefore previously developed a method for tissue elasticity imaging with freehand tissue compression based on the extended Combined Autocorrelation Method (CAM). The method enables us to obtain an elasticity image with high-speed processing and accuracy, and achieve a wide dynamic range for strain estimation by combining envelope correlation and phase shift while avoiding errors due to the aliasing and lateral probe slip caused by freehand compression.

Our group realized a real-time imaging system by adopting its algorithm and using a commercial ultrasound scanner. The details will be reported in another work submitted to this conference. Here, we show results of preliminary clinical evaluation of the system in breast and prostate cancer diagnosis.

In breast examinations, elasticity images of breast cancer were obtained from more than 90 subjects using 7.5MHz linear probe. The echo signals are captured in real time while the probe compressed or relaxed the body in freehand operation. The frame rate for the strain image at present can attain 20 fps, which depends on the measurement area and CPU performance. Strain images are superimposed on B-mode images with a translucent color scale. Some results showed the high availability of the elasticity image, that is, visualization of the expansion area of a tumor and detection of a small size (<5mm) of non-invasive ductal carcinoma. Benign and most of invasive ductal carcinomas can be significantly differentiated based on elasticity (strain) image.

In prostate examination, we use a 7.5MHz transrectal ultrasonic probe (convex type) with a diameter of 22 mm. As a demonstration, we measured some prostate glands suspected of being cancerous. Although cancer detection is difficult using a conventional B-mode image, the strain image clearly shows the cancerous area to be hard. A comparison of strain images with needle biopsy results revealed a 94% agreement (15 out of 16) in detection of non-treated cancer. We therefore concluded that the real-time elasticity imaging system is useful as a prostate needle biopsy support technology.

These results validate that the real-time elasticity imaging system can provide the high-quality and stable elasticity image in the clinical measurement. Consequently, it is confirmed that the system is applicable to the breast and prostate examination *in vivo*.

Acknowledgement: This research is partly supported by grants of research promotion from the Ministry of Education, Culture, Sports, Science and Technology (MEXT).

AGAR/GELATIN LOW CONTRAST SPHERICAL LESION PHANTOMS FOR ASSESSING MR AND ULTRASOUND ELASTOGRAPHY PERFORMANCE.

E Madsen¹, G Frank¹, T Krouskop^{2,3}, M Hobson¹, H Shi¹, MM Doyley⁴, T Varghese¹, J Ophir².

¹University of Wisconsin-Madison, Madison, WI, USA; ²The University of Texas Medical School, Department of Radiology, Ultrasonics Laboratory, Houston, Texas, USA; ³ Baylor College of Medicine, Department of Physical Medicine and Rehabilitation, Houston, Texas, USA; ⁴Dartmouth College, Hanover NH, USA.

Agar/gelatin materials have been developed allowing elastic contrasts (ratio of Young's moduli) from 1 to 7. The materials exhibit NMR relaxation times, T1 and T2, which are in the human soft tissue ranges and can be produced to mimic simultaneously the ultrasonic properties of soft tissues. As the dry-weight agar concentration increases, the Young's modulus (E) increases and T2 decreases. Formaldehyde cross-linking of the gelatin component produces a minimum melting point of 60 degrees C, thimerosal prevents bacterial invasion, and T1 is controlled with Cu⁺⁺/EDTA.

Four heterogeneous phantoms have been produced from these materials where the dry-weight gelatin concentration is uniform throughout, but the dry-weight agar concentration varies. Geometric and elastic stability were tested. The phantoms contain 1-cm diameter cylinders in direct contact with surrounding material having lower agar concentration. Elastic contrasts, E, measured quasi-statically on small samples via Instron®, varied by only about 10% over 10 months, and elastic strain contrasts, derived from elastograms over a 2-month period, changed by +7%, -3%, -1% and +4%, probably within experimental error. Also, using elastic strain profiles from elastograms, no significant changes in cylinder diameters occurred. Thus, these materials are promising for production of "contrast-detail" or anthropomorphic type phantoms for use in both MR and ultrasound elastography.

To develop an understanding for the ranges of sphere diameters and elastic contrasts required to allow discrimination between systems based on detectability, a preliminary spherical lesion test phantom was produced. (As the sphere diameter decreases and the elastic contrast approaches 1, the spheres should become undetectable on elastograms.) Preliminary values of elastic contrast (sphere E/background E) measured quasi-statically via Instron® are 1.2, 1.5, 1.8 and 2.5. Values at 1 Hz using a newly acquired ELF 3200 system were 1.2, 1.4, 2.3 and 3.5 with phase lags for each material being less than 6 degrees; at 100 Hz the absolute values of the complex Young's moduli increased by about 10% as the frequency increased from 1 Hz to 100 Hz. The 100 Hz phase lags were about 16 degrees. The 10cmx10cmx10cm phantom has 7 vertical sets of five spheres, each set having the same diameter and elastic contrast. Four 2-mm diameter sets have all four elastic contrasts represented while three 1.6-mm diameter sets have the three lowest elastic contrasts. Sets of five spheres are located at depths of 2.0, 3.5, 5.0, 6.5 and 8.0 cm.

At this writing, only ultrasound elastograms have been acquired using an Aloka SSD 2000 scanner and 5 MHz linear array focused at 3 cm. Preliminary results are that there is not a significant dependence on the sphere size. Regarding elastic contrast dependence, spheres were detected at 2.0, 3.5 and 5.0 cm depths for spheres with the two highest elastic contrasts, 3.5 and 5.0 cm for the next highest contrast, and 3.5 cm for the lowest contrast.

Results for phantoms with higher (more statistically significant) numbers of spheres at each diameter, elastic contrast and depth will be presented. Sphere diameters will include 1.0 through 4 mm.

43 **ELASTICITY RESEARCH PLATFORM.**

WG Scott¹, RM Schmitt¹, RD Irving¹.

¹WinProbe Corporation, 11662 Lakeshore Place, North Palm Beach, FL, 33408, USA.

Many of today's studies of elasticity appear to be hampered by the lack of a suitable research platform. Elasticity studies require a special set of functions that can be met with a specifically designed research platform. This platform should be able to:

- ◆ Transmit, receive and digitize multiple ultrasound channels,
- ◆ Perform correlations in parallel at RF speed,
- ◆ Interconnect RF data paths together under a high-level program language,
- ◆ Scan convert the data for display in real-time.

Today's large Field Programmable Gate Arrays (FPGAs) can accomplish beamforming, correlation, interconnection and scan-conversion in one chip.

An ultrasound channel should consist of a transmit pulser, switch, preamplifier, time gain correction amplifier and an analog-to-digital converter (ADC). Channel parameters such as focal points, apertures, sequences, etc. should be programmable on a PC using simple graphical user interface menus. Tables could then be generated by the PC and downloaded to memories in the research platform, which could execute the functions in parallel at RF speeds.

Today the ADC can be 12-14 bits deep and can convert at 40-105 MHz. A suitable quantum of channels today is 32 per module, or grouping on a printed circuit board, because even on a 1500 pin FPGA the FPGA's I/O resources are rapidly consumed. An optional memory bank between the ADC and the FPGA would permit ultra-fast image acquisition. The use of gigabyte PC memory modules will allow recording of many seconds of ultra-fast data.

A research platform should consist of from one to sixteen modules for 32 to 512 acoustic channels operating in unison.

Suitable FPGAs are available which have 3 to 10 million programmable gates per chip. The FPGAs also contain up to 500 hardware multiplier accumulators (MACs) as well as memory buffers. The FPGA MACs can be programmed to perform hundreds of cross correlation functions operating at over 100 MHz simultaneously. This is sufficient to perform phase aberration correction and multiple cross correlations for displacement in three axes and companding with results computed at every clock of the ADCs.

The challenge for the design and development of the research platform is not in developing the hardware, as that has been conveniently supplied in powerful components by the semiconductor industry. The challenge today instead is in the development of software and algorithms to run the platform. Fortunately, there is a convenient path to the design of the algorithms. Programs in Matlab, familiar to many researchers, can be converted through Simulink and System Generator into the FPGA programming language, VHDL.

Functions for the movement and storage of data need to be provided with the platform operating system. The basic tools of beam forming, such as color flow Doppler, correlation and scan conversion, need also be provided as library functions that researchers can use to develop their own algorithms and protocols.

Such a system will be available to the research community in 2004.

40 **ULTRASONIC TEMPERATURE IMAGING FOR GUIDING FOCUSED ULTRASOUND SURGERY: EFFECT OF ANGLE BETWEEN IMAGING BEAM AND THERAPY BEAM.**

Naomi Miller¹, Konstantin Bograchev¹, Jeffrey Bamber¹.

¹Joint Department of Physics, Royal Marsden NHS Trust/Institute of Cancer Research, Downs Road, Sutton, Surrey, SM2 5PT, UK.

Ultrasonic estimation of heat-induced echo strain has been suggested as a noninvasive technique for the guidance of focused ultrasound surgery (FUS). The proposed strategy is to run the FUS system at an initial, non-ablative intensity and to use a diagnostic transducer to produce an image of the heat-induced echo strain, which is proportional to the temperature rise. Thus, the strain image can be used to predict the location and spatial extent of the thermal lesion.

In a preliminary *in vitro* study of this technique, we demonstrated that temperature rises as low as 3-5°C (starting from room temperature) can be visualised with excellent spatial and contrast resolution. However, these investigations were carried out with the imaging beam perpendicular to the treatment beam, whereas the most convenient system design for *in vivo* use would be to mount the imaging probe within the housing of the therapy transducer such that the two transducers are co-axial. In addition to the fact that such a design would only require one acoustic window to the tumour site, it would provide automatic registration between the therapy plane and the imaging plane.

The aim of the current *in vitro* study, therefore, was to compare the quality of temperature images obtained using a perpendicular and a co-axial transducer arrangement. A non-ablative temperature rise was induced in 4 *ex vivo* animal livers using an FUS system and the apparent axial displacements (i.e., along the axis of propagation of the imaging beam) were measured by applying a one-dimensional cross-correlation search to the pre- and post-heated radiofrequency (RF) ultrasound image. Axial strains were calculated using least squares strain estimation.

The strain (temperature) images were found to be substantially noisier for the co-axial configuration than for the perpendicular arrangement. For example, for spatial and temporal peak temperature rises of approximately 4°C, the mean contrast-to-noise ratio (CNR) between the hot spot and background tissue for each of these transducer arrangements was 0.37 and 2.00, respectively. Furthermore, the decorrelation noise observed for the co-axial configuration obscured one of the axial borders of the hot spot. Nevertheless, this decorrelation noise resulted in high visibility of the heated region, and after processing the strain image to produce a parametric image of a first order texture feature, the average CNR increased to 2.10. Simulation results showed that for the co-axial configuration, the maximum decorrelation between the pre- and post-heated RF image occurs at sharp lateral gradients in axial displacement, presumably due to RF signal decorrelation within the beamwidth of the imaging transducer. Consequently, the magnitude of the strain noise, which was the parameter portrayed in the texture image, is not likely to be directly related to temperature rise.

We conclude that the co-axial configuration is likely to be useful for localising the hot spot in the lateral direction, but it is unlikely that it will be able to depict the axial extent of the hot spot or to portray a parameter that is directly related to temperature rise.

Timothy J. Hall¹, Larry T. Cook², Yanning Zhu².

¹University of Wisconsin-Madison, 1530 MSC, 1300 University Avenue, Madison, WI, 53706 USA;

²University of Kansas Medical Center, 3901 Rainbow Boulevard, Kansas City, KS, 66160 USA.

We have developed a modified 2-D block matching algorithm that significantly reduces the computational load of high-resolution motion tracking with ultrasound. We implemented that algorithm on a clinical sonography system for real-time elasticity imaging and have begun initial clinical trials. We have now acquired adequate radio-frequency (rf) echo data from *in vivo* elasticity imaging experiments to begin optimizing our motion tracking techniques.

Previous studies comparing the performance of various 2-D motion tracking (or time-delay) estimators often used pure translations of the data fields and introduced additive noise to simulate echo signal decorrelation. However, the rate of echo signal decorrelation varies with the type of deformation, and the performance of various motion tracking estimators for data with combinations of axial strain and axial, or lateral, shear have not been reported.

In this study, thirty pairs of pre- and post-deformation 2-D rf echo data were simulated with parameters (center frequency, 2-D PSF, beam spacing, etc.) similar to that of the Siemens Elegra. Deformations included uniaxial strain ranging from 1-4% and combinations of axial strain and lateral and axial shear. Three 2-D motion estimators (normalized cross correlation (NCC), sum-squared difference (SSD) and sum absolute difference (SAD)) were tested with varying 2-D kernel sizes. The results were also compared to 1-D NCC with 2-D search. Sub-sample displacement estimation was obtained with parabolic interpolation. Simulated data allow measures of estimator bias and variance.

The best-performing 2-D kernel (with all three estimators) generally provided a 2-D displacement estimate error variance that was a factor of ten lower than the best-performing 1-D NCC (without window overlap). In the absence of significant shear, the optimum kernel length depends on the applied strain, and the minimum variance was obtained with the widest kernel tested. However, relatively low (1%) axial strain and small (1°) axial shear significantly increased displacement estimate variance.

Significant reduction in the displacement estimate variance is available over that currently implemented in our system. These results also clearly demonstrate the advantage in motion tracking with 2-D versus 1-D kernels. Very wide kernels are not optimal because of the high computational cost and the presence of local axial shear with some *in vivo* data. However, 2-D kernels always outperformed 1-D kernels of equal length, and the reduction in variance in using 5 correlated A-lines, compared to a single A-line, was typically more than a factor of 5.

Naotaka Nitta¹, Yuka Aoki¹, Makoto Yamakawa¹, Tsuyoshi Shiina¹.

¹Institute of Information Sciences and Electronics, University of Tsukuba, 1-1-1 Tennoudai, Tsukuba, Ibaraki 305-8573, JAPAN.

The abnormal myocardial motion caused by the stiffness change often appears in the early stage of ischemic heart disease. Since the myocardium exhibits complex 3-D motion, 3-D assessment of the stiffness distribution is required for accurate diagnosis. However, conventional tissue Doppler and strain rate imaging techniques cannot meet the above requirement completely because these are angle-dependent and in-plane (2-D) processing. In addition, these techniques have other limitations such as aliasing for large motion of myocardium.

In order to overcome these problems, we propose novel methods to track the 3-D motion by using a 2-D phased array with a small aperture and to assess myocardial malfunction based on a full strain tensor obtained by 3-D motion analysis. For a new method of 3-D myocardial motion tracking, our phase gradient method, which is capable of real-time 3-D displacement vector measurement based on the phase shifts obtained at each element on a 2-D phased array, and our combined autocorrelation method that measures large phase shifts at each element accurately with no aliasing are incorporated. For a new method to assess the myocardial stiffness, the invariants of full strain tensor obtained by the measured 3-D vectors are visualized as the strain invariant imaging. Since the invariants of strain tensor are independent of the coordinate system, visual axis and beam direction, valid myocardial stiffness can be assessed.

We evaluated the feasibilities of the proposed methods by numerically simulating the left ventricle short-axis imaging of a 3-D elliptic myocardial model with a wall thickness of 15mm, including a hard area between 1 and 3 o'clock, whose modulus is tenfold larger than that of the surrounding area. A circular 2-D array aperture with a diameter of 20mm, and the pulse sequences with a center frequency of 3.75MHz and a fractional bandwidth of 31% were used. Simulated successive echoes at each array element on the receiving aperture were digitized at a rate of 20MHz through volumetric sector scanning (91 lines/frame x 11 frames). Typical translation velocity of 50mm/s and strain rates of 0.66 were applied to the model. These two values at a volume rate of 100Hz correspond to the displacements of 0.5 mm and 0.1 mm per volume, respectively. These values were appropriately assigned as 3-D vectors of the wall, based on the incompressibility condition. All components of 3-D vectors were accurately measured by the proposed 3-D motion tracking method, and mean errors for lateral, axial and elevational components could be suppressed up to 4.6%, 2.0% and 3.9%, respectively. Subsequently, the invariants of the full strain tensor were visualized. Although conventional methods as typified by tissue Doppler imaging and strain rate imaging could not discriminate the hard part due to angle dependency and aliasing, the invariant imaging based on the full strain tensor faithfully reconstructed the original shape of hard part at high contrast.

Acknowledgement:

This research is supported by Grants-in-Aid for Scientific Research of Japan Society for the Promotion of Science and grants from the Japan Society of Ultrasonics in Medicine.

Daniel Renzi¹, Joyce McLaughlin¹.

¹Department of Mathematics, Rensselaer Polytechnic Institute, Troy, NY, USA.

We present and test an algorithm to create a stiffness image based on changes in shear wave speed. This algorithm is based on transient elastography experiments performed by Sandrin et al. [1]. These experiments are of particular interest because they obtain accurate time dependent displacement fields in the interior of the body resulting from a short duration impulse. During the experiments, a shear wave propagates through the medium. We use the interior displacements to find the first arrival times of this wave with a cross correlation technique. We establish that Lipschitz continuous arrival times satisfy the Eikonal equation, and present an algorithm to find the shear wave speed based on the level set method, simulation results, and a reconstruction example using a phantom experiment developed and performed by Mathias Fink's group (the Laboratoire Ondes et Acoustique, ESPCI, Université Paris VII).

References:

- [1] Sandrin L, Tanter M, Catheline S, Fink M. Shear modulus imaging with 2-D transient elastography. IEEE Transactions on Ultrasonics, Ferroelectrics and Frequency control, 2002;49(4):426-35.
-
-

Session I: Forward and Inverse Problems

Tuesday, October 14 2:30P – 3:15P

22 **A VARIATIONAL FORMULATION LEADING TO DIRECT ELASTIC MODULUS RECONSTRUCTION.**

*Paul E. Barbone*¹.

¹College of Engineering, Boston University, 110 Cummington St., Boston, MA 02214, USA.

We present an advanced algorithm for reconstructing the elastic modulus distribution from measured displacement fields. Our goal in developing this method was the design of a method that is: robust to small noise levels, is guaranteed to give an estimate of the correct (unique) modulus distribution, requires only data that is realistically measurable in practice, and can be implemented efficiently. In this technique, we have accomplished all of these goals.

Our method is based on a variational formulation of the inverse problem. We show that though the inverse problem is not itself mathematically well-posed, the solution of our variational problem is. Furthermore, the reconstruction based on the variational problem depends continuously on the measured data. One practical implication of this is that noise in the reconstruction (i.e. error) scales linearly with noise in the data.

The data required for our reconstruction is realistically measurable *in vivo*. In particular, we require two the measurement of two distinct displacement fields, and knowledge of the modulus distribution in a small "calibration" region in the image. Apart from this, no boundary data whatsoever is required. Furthermore, we make no assumptions regarding the value of the modulus on the boundaries of the images, nor do we need to measure contact forces.

The method is an example of a "direct" inversion technique, in the sense that no iteration is required. The matrix that results from the discretization of the variational method has the properties that it is symmetric, banded, sparse and positive semi-definite. Two different implementations of the method are possible. In one, computing the solution requires finding the inverse of a large matrix. In the other, computing the solution requires finding the smallest eigenvectors of a large matrix. Either problem can be solved efficiently.

The presentation shall include the results of theoretical analysis and computational experiments to demonstrate the behavior of the method. Our current implementation of this technique is based on the assumption that the modulus distribution is a continuous function. When this assumption is satisfied, the results are remarkably accurate. When this assumption is violated, however, our technique gives poor results. Finally, the mathematical structure of the inverse problem allows for the possibility of correcting for small errors in the data when computing the reconstruction. This possibility will be discussed.

Lin Ji¹, Joyce McLaughlin¹, Daniel Renzi¹, Jeong-Rock Yoon¹.

¹Department of Mathematical Sciences, Rensselaer Polytechnic Institute, Troy, NY 12180, USA.

Transient Elastography is the focus of our work. In the experiment, the tissue is initially at rest when a broad band pulse, with central frequency 50-200 Hz, is applied on the boundary. An elastic wave, with propagating front, propagates into the body and the downward component is measured using an extension of Doppler ultrasound, see Tanter, et al. The goal of our work is to extract rich data subsets from these displacement measurements, to develop reconstruction algorithms utilizing these data sets, and to create accurate, informative images of shear wavespeed to use as a medical diagnostic tool. This talk is an (abbreviated) overview of our joint work on this problem.

The amplitude of the wave is on the order of microns and the shear stiffness is an elastic property. For this reason our mathematical model is the linear equations of elasticity. When the measured data is a single downward component, we also use the wave equation with a variable stiffness parameter and a variable density. Soft tissue is mostly composed of water, so the compression wavespeed is approximately 1500 m/sec and varies by approximately 5%. The shear wavespeed is approximately 3 m/sec in normal tissue and 2-4 times that amount in abnormal tissue. For that reason we focus on recovering the shear wavespeed in our algorithms.

For our uniqueness and continuous dependence results we establish: (1) that there is at most one stiffness/density pair corresponding to a time and space dependent solution of the scalar wave equation or the linear equations of elasticity when the boundary traction force is given and when, in the case of the linear elastic equations, the Lamé parameter, λ , is given; (2) that there is at most one shear wavespeed corresponding to a given time and space dependent propagating front of a solution of the wave equation; and (3) that the wavespeed depends continuously on the gradient of the propagating front locations.

In our algorithms we use the wave equation model for the measured downward component of the propagating wave. In one algorithm we assume the density is constant and use the central frequency content of the propagating wave and a geometric optics approximation to the displacement. In a second algorithm we extract the arrival times of the wave from the front of the propagating wave. We show that the arrival time satisfies the eikonal equation. This exact equation is the basis for two recovery procedures that yield images of the shear wavespeed and are implemented with both simulated data and data provided by Mathias Fink's group at Laboratoire Ondes et Acoustique, ESPCI, Université Paris VII.

References:

- [1] Tanter M, Bercoff J, Sandrin L, and Fink M (2002): Shear modulus imaging with 2-D transient elastography IEEE Trans. Ultrason., Ferroelect., Freq. Contr. 49 1363-74.
 - [2] Ji L, McLaughlin J, Renzi D, and Yoon J (2003): Interior elastodynamics inverse problems: shear wave speed reconstruction in transient elastography, submitted for publication.
-

Elasticity imaging, or the process of generating images of the elastic modulus of tissue, involves three basic steps:

- 1) Generating ultrasound images of the region of interest as it is deformed.
- 2) Registering these images to determine an estimate of the displacement field in this region.
- 3) Solving an inverse problem to determine the elastic modulus from the displacement field.

Often step 3 above is replaced by simple numerical differentiation to generate strain images, which are then interpreted as the reciprocal of modulus images.

We have recently proposed an efficient elasticity imaging methodology based on reconstructing elastic modulus images directly from ultrasound images. This involves combining the registration and reconstruction problems (steps 2 and 3 above, respectively) into a single inverse problem. We expect the proposed methodology (the new inverse problem and its solution) to be efficient, as it combines the registration and reconstruction steps into one, and to be accurate, as the converged displacement and elastic modulus distributions satisfy the physical constraint of linear elasticity.

In this talk we describe the proposed inverse problem, its attributes, and its relation to other formulations. We also describe an efficient adjoint equations-based algorithm for solving it. We analyze the performance of the proposed algorithm by testing it on synthetically generated, and experimentally measured ultrasound images.

Session J: Cardiovascular Elasticity

Tuesday, October 14 3:45P – 5:30P

01 MYOCARDIAL REGIONAL ELASTIC PROPERTIES MAPPING BASED ON ECHOCARDIOGRAPHIC 3-D RECONSTRUCTION OF THE LEFT VENTRICLE.

Svetlana G. Kolchanova¹, Sergey S. Ustuzganin¹, Sergey Yu. Sokolov¹, Ekaterina S. Saveljeva¹, Elena V. Marchenko², Vasily V. Chestukhin², Boris L. Mironkov², Felix A. Blyakhman¹.

¹Ural State University, 51 Lenin Ave., Ekaterinburg, RUSSIA; ² Institute of Transplantology and Artificial Organs, Moscow, RUSSIA.

As is well known, myocardial contractility is closely related to the passive properties of cardiac muscle. To assess intact left ventricle (LV) performance, indirect indices of diastolic myocardium stiffness (e.g., end-diastolic pressure) were widely introduced in clinical investigations. However, in the case of regional heart diseases (e.g., ischemic heart disease (IHD)), it is extremely important to know the functional status of both the damaged myocardium segments and of the adjacent ones.

The present study evaluates the human LV myocardial regional elastic properties on the basis of relative change in heart wall thickness ($\delta H = (H_1 - H_2) / H_1$) during the diastolic filling phase. Two-dimensional LV long-axis images were obtained with a "Powervision-380" ("Toshiba") transesophageal echocardiographic imager. The LV endocardial and epicardial borders for all sections were manually outlined frame-by-frame using "DICOR"® software ("Ruspatent" #2002610607). Three-dimensional reconstruction of the LV was carried out by rotation of the plane of each cross-section in 15 degree calibrated steps. Endocardial and epicardial surfaces were approximated to the shape of the heart wall by means of spherical functions of the fourth order.

At the beginning of the diastolic filling phase, the LV endocardial surface was divided into equal angular segments of about 4x4 mm size by angles θ and φ in a spherical coordinate system. To define the displacement direction of the heart wall surface fragments at every moment (frame) of diastolic filling, a new algorithm was developed (Patent #2002104521/14 RU). The nodes' motion direction for every surface point was calculated for each frame as a normal to this point. As a result of the frame-by-frame normals building, a location of each node point was calculated. The wall thickness at the beginning (H_1) and at the end (H_2) of LV filling phase was calculated as the length of normal vector building from node points at the inner LV surface to the outer one. The elastic properties of LV wall regions were represented as regional δH map.

A qualitative test of the method was carried out by means of the heart wall δH mapping for nine IHD patients before and one day after angioplasty. The maps agreed with data that were obtained in parallel by clinical and instrumental (coronary angiography and ventriculography) inspections of patients. Possible error sources were considered to evaluate the method quantitatively. The root-mean-square error of the method was about 5.2%, including errors of initial data, approximation and roundoff.

Supported by Russian Foundation for Basic Research.

05 **CORRECTION FOR SIMULTANEOUS CATHETER ECCENTRICITY AND TILT ON STRAIN ESTIMATION IN INTRAVASCULAR ELASTOGRAPHY.**

H. Shi¹, T. Varghese^{1,2}, G. Gimelli³, J.A. Zagzebski¹, M. Wolff³, E.L. Madsen¹.

¹Department of Medical Physics, University of Wisconsin-Madison, Madison, WI, 53706, USA;

²Department of Biomedical Engineering, University of Wisconsin-Madison, Madison, WI, 53706, USA; ³Section of Cardiovascular Medicine, Department of Medicine, University of Wisconsin-Madison, Madison, WI, 53792, USA.

Intravascular elastography with an intravascular ultrasound (IVUS) scanner can provide significant new information about the elastic properties of vascular tissue and coronary atherosclerotic plaque. Knowledge of plaque composition, vulnerability and its elastic properties may assist the clinician in selecting appropriate interventional techniques. However, several noise sources have to be addressed to obtain quality intravascular elastograms. Misalignment of the vessel and the ultrasound beam can produce erroneous strain estimates in elastography. Errors in the strain estimate are introduced due to the eccentricity and tilt of the intravascular transducer within the vessel lumen. Previous work in this area has provided theoretical expressions for the correction of eccentricity and tilt errors when they occur independent of each other. However, under most imaging conditions both eccentricity and tilt errors are simultaneously present. In this paper we extend the theoretical correction factor by accounting for the influence of both of these errors occurring in the positioning of the catheter within the vessel lumen.

The theoretical expression for the correction factor is evaluated experimentally using elastographic phantoms with straight lumens and eccentric lumens pressured using an oil-column system. IVUS elastography is performed with the Clear View Ultra System (CVIS) (SciMed/ Boston Scientific Corp. Boston, MA) using a 2.6F 30 MHz catheter (Discovery, Boston Scientific Corp.). This intravascular catheter consists of a mechanical motor driven rotating transducer mounted on a flexible drive shaft. The ultrasound RF signals are digitized at 8-bits and a sampling rate of 250 MHz using a GAGE board. Each RF frame from the CVIS system consists of 256 RF vectors over a 360° rotation of the mechanical ultrasound probe. Offline filtering of the echo data is also used to reduce noise artifacts in the RF signal. Data acquired from the phantoms show the validity of the theoretical expressions.

*The work was supported in part from a grant to the University of Wisconsin Medical School under the Howard Hughes Medical Institute Research Resources Program for Medical Schools, and start-up funds provided to Dr. Varghese by the Department of Medical Physics, Medical School and Graduate School at the University of Wisconsin-Madison.

09 **NON-INVASIVE VASCULAR ELASTOGRAPHY: THEORETICAL INVESTIGATION.**

Roch L. Maurice¹, Jacques Ohayon², Gérard Finet³, Gilles Soulez⁴, Guy Cloutier¹.

¹Laboratory of Biorheology and Medical Ultrasonics, Research Center, University of Montreal Hospital, Montreal, CANADA; ²Laboratory TIMC-IMAG, UMR CNRS 5525, Institut A. Bonniot, 38706 La Tronche, FRANCE; ³Department of Hemodynamics, Cardiovascular Hospital, Claude Bernard University, Lyon, FRANCE; ⁴Department of Radiology, University of Montreal Hospital, Montreal, CANADA.

Changes in vessel wall elasticity may be indicative of vessel pathologies. It is known, for example, that the presence of plaque stiffens the vascular wall, and that the heterogeneity of its composition may lead to plaque rupture and thrombosis. This gave rise to vascular elastography, which aims to outline the elastic properties of vessel walls using ultrasound. So far, vascular elastography is invasive; its clinical application is thus restricted to a complementary tool to assist IVUS echograms in pre-operative lesion assessments and to plan endovascular therapy. In this study, this technology is introduced as an approach to non-invasively characterize superficial arteries. In such a case, a linear array ultrasound transducer is applied on the skin over the region of interest, and the arterial tissue is dilated by the normal cardiac pulsation. The elastograms, the equivalent elasticity images, are computed from the assessment of the vascular tissue motion. Investigating the forward problem, it was shown that motion parameters might be difficult to interpret; that is because tissue motion occurs radially within the vessel wall while the ultrasound beam propagates axially. As a consequence of that, the elastograms are subjected to hardening and softening artifacts, which are to be counteracted. To circumvent such mechanical artifacts and then to appropriately characterize the vessel wall, the Von Mises coefficient (VM) was proposed. Regarding the motion assessment, the Lagrangian estimator was used; that is because it provides the full 2D-strain tensor necessary to compute the VM parameter. The theoretical model was validated with biomechanical simulations of different atherosclerotic plaque configurations. In each case, the computational structural analysis was performed on a typical *in vivo* IVUS image of a plaque. To emulate the vessel wall kinematics, finite-element computations were performed using the ANSYS 5.7® software (Ansys, Inc., Cannonsburg, PA). RF data, simulating the vessel wall motion, were then generated with the assumption of a 10 MHz transducer with a 60% bandwidth at -3dB. The results showed the potential of the method to distinguish different tissue structures such as dense and cellular fibroses, calcified plaques, and lipid pools from the healthy vascular tissue. Potential *in vivo* implementation of non-invasive vascular elastography to characterize superficial arteries such as the femoral and the carotid is discussed.

32 **IMAGING OF VULNERABLE PLAQUE IN CORONARY ARTERY BY PARAMETRIC IVUS AND ACOUSTIC MICROSCOPY.**

Y. Saijo¹, A. Tanaka², H. Sasaki¹, N. Owada¹, Y. Akino³, M. Tanaka¹.

¹Department of Medical Engineering and Cardiology, Institute of Development, Aging and Cancer, Tohoku University, Sendai, JAPAN; ²Department of Electrical, Communication, Electronic and Information Engineering, Graduate School of Engineering, Tohoku University, Sendai, JAPAN;

³Division of Cardiology, Miyagi Social Insurance Hospital, Sendai, JAPAN.

Acoustic microscopy with 100-200 MHz ultrasound visualizes more precise tissue structure than those obtained by clinical intravascular ultrasound (IVUS) imaging with 20-40 MHz ultrasound. However, if the central frequency of IVUS is merely increased, the scatter of blood cells would interfere with the ultrasonic imaging of coronary artery. Our goal is to achieve the precise quantitative imaging of tissue elasticity in clinical settings. In the present study, we observed vulnerable coronary arteries by parametric IVUS and acoustic microscopy and compared both images.

Radio-frequency (RF) signal from a clinically used IVUS apparatus was digitized at 500MSa/sec and stored in a workstation. First, the correlation coefficient between two consecutive frames was calculated in the rotational direction and the rotational non-uniformity was corrected to obtain the maximum correlation coefficient. Then, the polar coordinate images were converted into rectangular coordinate images and the images were divided into 64 by 64 square regions of interest (ROIs). The correlation and displacement of the ROIs between the consecutive two frames were calculated by template-matching method. Two-dimensional tissue velocity was defined as the vectors of displacement of ROI with 0.7 and more correlation.

The tissues for acoustic microscopy were formalin fixed, embedded in paraffin, and cut in sections 10- μ m thick with a microtome. The specimens were mounted onto glass slides and the paraffin was removed by the graded alcohol method, just before the ultrasonic measurement. Acoustic microscopy operating in the frequency range of 100-200 MHz was employed, and the lens focuses the ultrasonic beam to 5- μ m at 200MHz. As the square of sound speed is proportional to the elasticity, sound speed image of acoustic microscopy can be considered as elasticity imaging at microscopic level.

Ten cases (including two no re-flow cases and one perforation case) were intra-operatively observed by parametric IVUS and the coronary arteries were obtained with directional coronary atherectomy (DCA) procedure. Figure 1 is the correlation image and Figure 2 is the 2D velocity image in one of no-reflow case. Figure 3 is the acoustic microscopy imaging of DCA specimen. The parametric IVUS visualized a lesion with complex vectors and acoustic microscopy revealed that the lesion contained foam cells and degenerated collagen fibers, which indicated that the plaque was vulnerable.

Parametric IVUS can provide precise tissue elasticity information as those provided by higher frequency acoustic microscopy.

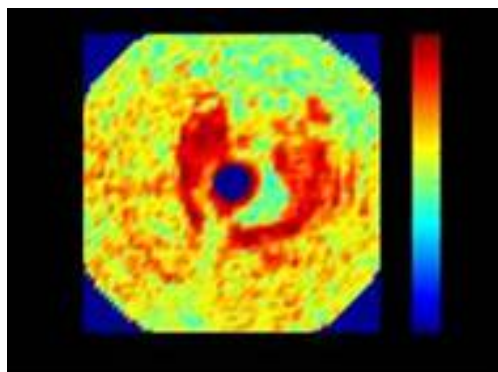


Figure 1

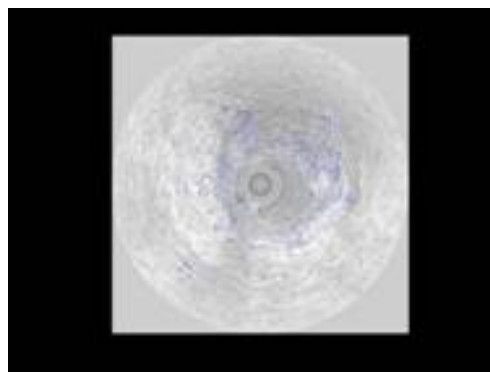


Figure 2

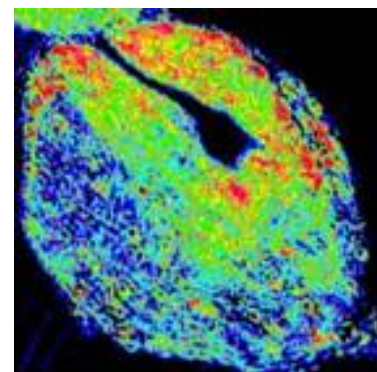


Figure 3

12 **PERIPHERAL ARTERIAL STRAIN IMAGING USING EXTERNAL PRESSURE EQUALIZATION.**

W.F. Weitzel¹, K. Kim², J.M. Rubin³, H. Xie², X. Chen², M. O'Donnell².

Departments of ¹Internal Medicine, ²Biomedical Engineering, and ³Radiology, University of Michigan, Ann Arbor, MI 48109, USA.

Non-invasive peripheral arterial ultrasound strain imaging was performed while applying external pressure to induce changes in the baseline pressure difference across the arterial wall. By equalizing the baseline internal and external arterial pressure during the ultrasound measurement, increased arterial strains are induced by the relatively stable pulse pressure (pulse pressure = systolic pressure – diastolic pressure) during the cardiac cycle. We imaged the brachial and radial arteries of a 43 year old man with a 7.2 MHz linear ultrasound transducer while external deformations were continually increased over several cardiac cycles. External pressure was increased until the arteries collapsed during diastole but distended during systole when the applied force exceeded the internal reference pressure of 80 mmHg (subject's diastolic pressure). Correlation-based, phase-sensitive, 2-dimensional speckle-tracking algorithm was employed to calculate strain and strain rate from the internal displacement of the artery wall.

Imaging of the arteries without external deformation resulted in measured strains up to 2% over the cardiac cycle. When applied pressure matched the internal baseline diastolic pressure of 80 mmHg, the strains increased by a factor of 10 with peak strains of 20% over the cardiac cycle. In addition, the peak strain rate under physiological conditions ranged from 0.1 sec⁻¹ during diastole to -0.2 sec⁻¹ during systole. After arterial pressure equalization, the peak strain rate increased to 1.0 sec⁻¹ during diastole and -2.5 sec⁻¹ during systole, similar to the increase in peak strains. By applying external pressure, the pressure difference across the arterial wall at baseline (diastole) is reduced, while the pressure change from diastole to systole remains stable. As a result, the preload on the arterial wall can be decreased to near zero, leading to maximal strain during the cardiac cycle. By varying the external pressure the range of measured strains vary over a cardiac cycle, and the non-linear properties of the arterial wall may be better characterized. Methods such as this that elicit the non-linear properties of the arterial wall could be used to better characterize vascular pathologies such as vessel hardening, neointimal hyperplasia, and vulnerable plaques.

Work supported in part by NIH grants DK-47324, HL-47401, HL-67647, and HL-68658 and a grant from the Renal Research Institute.

20 **IVUS MODULOGRAPHY OF VULNERABLE PLAQUES USING A PARAMETRIC FINITE ELEMENT MODEL: VALIDATION ON A PHANTOM AND HUMAN CORONARY ARTERY.**

Radj A. Baldewsing¹, Johannes A. Schaar^{1,2}, Frits Mastik¹, Cees W. J. Oomens³, Antonius F. W. van der Steen^{1,2}.

¹Biomedical Engineering, Thoraxcenter, Erasmus Medical Center Rotterdam, Rotterdam, The NETHERLANDS; ²Interuniversity Cardiology Institute of the Netherlands (ICIN), Utrecht, The NETHERLANDS; ³Material Technology, Biomedical Engineering, Eindhoven University of Technology, Eindhoven, The NETHERLANDS.

Background: Tissue characterization using the Young's modulus distribution of an atherosclerotic artery allows for monitoring of atherosclerosis and choosing interventional procedures.

Currently, IntraVascular UltraSound (IVUS) elastography generates IVUS elastograms, i.e. arterial radial strain images. This paper describes the reconstruction of the Young's modulus distribution of vulnerable plaques. Hereby, an IVUS elastogram is used as input in a parameter reconstruction algorithm that utilizes a newly developed Parametric Finite Element Model (PFEM).

Materials: A vessel phantom containing a soft eccentric plaque and an excised human coronary artery containing a lipid pool covered by a fibrous cap were used for this study.

Methods: IVUS elastograms were measured *in vitro* with a 20 MHz IVUS catheter. Furthermore, simulated IVUS elastograms were computed using a FEM; tissue was modeled as linear elastic, isotropic, incompressible plane strain material. Young's moduli of lipid, media, and cap areas in the artery FEM were set to 25, 1000, and 1500 kPa respectively; for the phantom FEM, measured Young's moduli were used.

A vulnerable plaque was modeled by a PFEM as a lipid pool covered by a fibrous cap. The PFEM has 4 circles, i.e. lumen, lipid, cap, and media circles, defining the geometry of a vulnerable plaque and its areas, i.e. lipid, cap, and media area. Since the lumen and media contour are known from the IVUS echogram, only the parameters describing lipid circle, cap circle and Young's moduli of lipid, cap, and media areas were reconstructed.

Parameter reconstruction consisted of a sequential-quadratic-programming algorithm that minimizes the difference between measured/simulated IVUS elastogram and PFEM elastogram, by iteratively updating the PFEM parameters.

For both phantom and artery two reconstructions were done: one using the measured IVUS elastogram and the other using the simulated IVUS elastograms as input.

Results: Measured phantom Young's moduli are 4.2 kPa for plaque and 16.8 kPa for wall. For the phantom, plaque location, size, and Young's moduli of plaque (E_p) and wall (E_w) are successfully reconstructed using both the measured IVUS elastogram and the simulated IVUS elastogram as input. Reconstructed E_p and E_w are 3.5 and 17.6 kPa respectively using the measured IVUS elastogram and 4.1 and 15.6 kPa respectively using the simulated IVUS elastogram.

For the artery, plaque location, size, and Young's moduli of lipid (E_L), media (E_m), and cap (E_c) are successfully reconstructed using both the measured IVUS elastogram and the simulated IVUS elastogram as input. Reconstructed E_L , E_m , and E_c are 30, 650, and 1780 kPa respectively using the measured IVUS elastogram and 1, 1150, and 1490 kPa respectively using the simulated IVUS elastogram.

Discussion: The PFEM is capable of reconstructing the Young's modulus distribution of vulnerable plaques using an IVUS elastogram as input. It can be used to study the influence of noise, catheter position, initial parameter estimate, and used objective-function upon a unique and fast reconstruction. A future application may be the monitoring of lipid reduction of vulnerable plaques, in patients undergoing lipid-lowering drug treatment.

Acknowledgement: Supported by the Dutch Technology Foundation (STW) and the Netherlands Organization for Scientific Research (NWO).

10 **NON-INVASIVE ELASTICITY IMAGING IN SMALL VESSELS: EXPERIMENTS ON TISSUE-MIMICKING PHANTOMS.**

Roch L. Maurice¹, Michel Daronat¹, Zhao Qin¹, F. Stuart Foster², Guy Cloutier¹.

¹Laboratory of Biorheology and Medical Ultrasonics, Research Center, University of Montreal Hospital, Montreal, CANADA; ²Department of Medical Biophysics, Sunnybrook and Women's College Health Sciences Centre, University of Toronto, CANADA.

Non-invasive ultrasound elastography (NIVE) was recently introduced to characterize mechanical properties of superficial arteries. In NIVE, the ultrasound transducer is applied on the skin over the region of interest, and the arterial tissue is dilated by the normal cardiac pulsation. In this approach, tissue motion occurs radially within the vessel wall while the ultrasound beam propagates axially. Regarding the forward problem, it was shown that motion parameters might be difficult to interpret. For instance, the elastograms are subjected to hardening and softening artifacts, which are to be counteracted. Owing to that, the Von Mises (VM) coefficient was proposed as a new parameter to circumvent such mechanical artifacts and then to appropriately characterize the vessel wall. The Lagrangian estimator was used, because it provides the full 2D-strain tensor required to compute the VM coefficient. In this study, the feasibility of NIVE for the purpose of studying small vessels in humans and small animals is investigated. Experiments were performed *in vitro* on vessel-mimicking phantoms with wall thickness on the order of one mm. Polyvinyl alcohol cryogel (PVA-C) was used to create double-layer vessel walls; in each case, the stiffness of the inner wall was made softer. Indeed, PVA-C is a biogel that solidifies and acquires its mechanical rigidity by increasing the number of freeze/thaw cycles. In this study, several double-layer vessel configurations were investigated, setting the numbers of cycles from 2 to 8. The phantoms were insonified with an ultrasound biomicroscanning system (Visualsonics, Toronto, Canada) providing access to the radio-frequency (RF) raw data. The measurements were performed with a single-element oscillating transducer with a central frequency of 32 MHz, and a bandwidth at -6 dB of 100%. Sequences of RF images were collected while incrementally adjusting the intraluminal static pressure steps with a column of water-glycerol. Regarding the VM elastograms, the potential of NIVE to distinguish different tissue structures in small vessels was demonstrated *in vitro*. The results also suggested that there may exist a range of intraluminal pressures, for which contrast between different tissue structures detected in the elastograms is optimal. While the lateral resolution of current ultrasound systems remains a potential limitation, the feasibility of NIVE for small vessel elasticity imaging was demonstrated *in vitro*. *In vivo* application is also discussed.

07 **TISSUE REGION DELIMINATION THROUGH STATISTICALLY BASED PARAMETER CONSOLIDATION.**

Elijah E.W. Van Houten¹, Kai P. Mecke², John B. Weaver³, Keith D. Paulsen⁴.

¹University of Canterbury, Christchurch, NEW ZEALAND; ²Technische Universität Darmstadt, Hessen, GERMANY; ³Dartmouth-Hitchcock Medical Center, Lebanon, NH, USA; ⁴Thayer School of Engineering, Dartmouth College, Hanover, NH, USA.

The high resolution of MR generated displacement data used in elasticity imaging is a benefit in terms of the detail and accuracy with which motion patterns within the tissue can be determined. The completeness and quality of these data sets allows a variety of elastic property reconstruction schemes to be used for the generation of elasticity images. These high resolution levels can also be a drawback to the elasticity imaging process however, as large numbers of degrees of freedom (DOF) may be required to specify the mechanical properties of a single tissue type over a relatively large spatial area. For example, sections of fatty tissue within the breast may require large percentages of the total number of DOF within the elasticity image to describe a tissue with very little property variance.

This side effect of high resolution MR displacement data becomes particularly evident when reconstructive property imaging techniques are used, such as those previously described by the author[1]. In these cases, the computational load of the image reconstruction algorithm grows cubically with the total number of DOF in the resulting elasticity image, so that any efficiency in the number of elasticity values needed to generate the final image will go a long way towards improving the overall processing time. To this end a statistically based scheme has been implemented to combine neighboring DOF with property values that are indistinguishable to a prescribed level of certainty. This process has the combined effect of reducing the overall number of DOF necessary to accurately classify the material property distribution within the tissue as well as clearly delimiting single-tissue regions within the overall image domain.

To implement this elastic property consolidation scheme within the iterative, subzone based elastography method previously documented by the author, variance levels must be calculated for each DOF of the elasticity image [2]. Given these variance levels, statistical comparisons between two adjacent DOF can be made based on their current estimated property values and their associated confidence intervals. When the properties of two neighboring DOF are found to be statistically identical they are combined into a single DOF that thereafter encompasses the spatial domain of the two original DOF. Implementing this method within a finite element based subzone reconstruction scheme involves accounting for several differing layers of basis support, such that individual nodes of the mesh will have independent displacement DOF and yet may have a shared mechanical property value with any number of their neighboring nodes. Within this scheme, individual nodes with elasticity values independent from any of their neighbors are able to retain their singly supported property values, thus the resolution capabilities of the imaging process are left intact even with the reduction of the overall number of DOF.

Initial results have shown the method is capable of rapidly reducing the number of property values required to accurately characterize an imaging region by factors of 3 and higher. This has a dramatic effect on the runtime of the algorithm and provides several additional advantages to the overall performance of the method such as an increase in final signal-to-noise values, clearer depiction of single-tissue regions and an improved ability to delineate the boundaries between differing tissue types.

Supported by National Cancer Institute Program Project Grant P01-CA80139.

- [1] E.E.W. Van Houten, M.I. Miga, J.B. Weaver, F.E. Kennedy and K.D. Paulsen, Three-dimensional subzone-based reconstruction algorithm for MR elastography, *Mag. Res. Med.*, Vol. 45(5), pp 827-837, 2001.
 - [2] E.E.W. Van Houten, M.M. Doyley, F.E. Kennedy, J.B. Weaver and K.D. Paulsen, Initial *in vivo* experience with steady-state subzone-based MR elastography of the human breast, *J. Magn. Reson. Imaging*, Vol. 17(1), pp 72-85, 2003.
-

MM Doyley^{1,2}, EEW Van Houten³, JB Weaver^{1,2}, S Poplack^{1,2}, F Kennedy², KD Paulsen^{2,3}.

¹Department of Radiology, Dartmouth Medical School, Hanover, NH 03755, USA; ²Thayer School of Engineering, Dartmouth College, Hanover, NH 03755, USA; ³Norris Cotton Cancer Center, Lebanon NH 03766, USA.

Magnetic resonance elastography (MRE) is an emerging imaging modality that could potentially detect breast cancer earlier and reduce the benign biopsy rate by exploiting the large difference in stiffness that exists between malignant and benign breast tumors. MRE produces stiffness images using a three-step process. First, motion is induced within the tissue (in or case the breast) using a harmonic mechanical excitation. Second, the time-varying harmonic displacements are visualized using motion sensitive magnetic resonance imaging. Third, the spatial variation of shear modulus is computed from measured displacements using a model-based inversion technique. The reported preliminary clinical experiences with MRE have been very encouraging. However, the clinical efficacy of MRE is currently limited by the computationally intensive numerical methods that are employed to compute high-resolution 3D shear modulus images (i.e elastograms). Consequently, we have developed a pragmatic parallelized inverse reconstruction technique, which computes high-resolution 3D elastograms from a substantially reduced reconstruction field of view. In this paper, we report the results of experiments conducted on breast phantoms and volunteers (n=6) to validate the performance of the proposed technique. The results demonstrated that accurate high-resolution elastograms can be computed within an hour using the partial volume reconstruction approach without any significant degradation in either image quality or accuracy. It was concluded that the parallelized partial volume reconstruction approach performs sufficiently well to warrant more in-depth clinical evaluation.

45 **NUMERICAL EVALUATION OF A 1.5D 3x3 BEAMFORMER ARRAY FOR REAL TIME CROSS-CORRELATION IMAGING (CCI).**

Rainer. M. Schmitt¹, Walter. G. Scott¹, R.D. Irving¹.

¹WinProbe Corporation, 11662 Lakeshore Place, North Palm Beach, FL 33408, USA.

We are currently developing a Real Time engine for cross-correlation imaging to be utilized in various approaches to elastography and 3D-flow detection.

To overcome the problems associated with out of plane scatterer displacement, the concept of a 3x3 beamformer matrix is presented and numerically evaluated.

The basic idea is the formation of overlapping parallel beams in the azimuthal as well as in the elevation direction. While parallel receive beamforming in 1D arrays using principles like Explosive scan are well established and already utilized for lateral (azimuthal) tracking of tissue displacement, tissue movement in the elevational direction can not be detected with 1D arrays without mechanical movement.

We propose to use a 1.5D array with five rows of 64 elements of identical azimuthal spacing, a typical linear phased array for center and two rows of equal height (elevation) above and below the center row. The height of the elements is chosen according to the elevation translation of the aperture to achieve the desired beam overlap. For maximum beamforming flexibility each row is fed to an individual 64-channel beamformer of the Cross-Correlation Engine (CCE). Parallel receive beams in the azimuthal direction are then obtained by state of the art beamforming, thus a 3x3 matrix of partially (50%) overlapping beams is created. This allows computing cross-correlation in all 27 voxels surrounding a center voxel simultaneously and track the correlation in 3D for out of plane tissue displacement in real time.

Beam patterns are numerically evaluated for a 5 MHz frequency array (70 % fractional bandwidth), half wavelength spaced 1.5 arrays with 10 mm height for the center and 1 mm for all other rows. Beam modeling is performed using the Field II software package [1]. Methods are discussed to maintain constant beam overlap over depth.

[1] Field II see information @ <http://www.es.oersted.dtu.dk/staff/jaj/field/papers.html>

56 **SUPERSONIC SHEAR IMAGING: A NEW TECHNIQUE FOR TISSUE VISCOELASTICITY MAPPING: *IN VITRO* AND *IN VIVO* RESULTS.**

J. Bercoff¹, M. Muller¹, M. Tanter¹, M. Fink¹.

¹Laboratoire Ondes et Acoustique, Université Paris VII, CNRS UMR 7587, ESPCI, 10 rue Vauquelin 75231 Paris cedex 05, FRANCE.

Supersonic Shear imaging (SSI) is a new ultrasound based technique for real time visualization of soft tissues viscoelastic properties. Using ultrasound focused beams, it is possible to remotely generate, inside the body, mechanical sources radiating low frequency shear waves. SSI is based on the ultrasonic generation of a shear source moving at a supersonic speed inside the body. In a complete analogy with the “sonic boom” created by a supersonic aircraft, the resulting shear waves will constructively interfere along a Mach cone, creating two intense plane waves. These plane shear waves propagate through the medium and are progressively distorted by tissue mechanical inhomogeneities. The ultrafast scanner developed at our laboratory (5000 images/s) is able to generate this supersonic source and image, in real time, the propagation of the resulting shear waves. Using inversion algorithms, a complete elasticity map of the medium can be deduced from this shear wave propagation movie. Creating such a supersonic regime enables quantitative tissue elasticity mapping in less than 20 ms, even in strongly viscous medium like breast or liver. Moreover, SSI only requires a single ultrasonic transducer, typically the same than ones used today by physicians, linked to the ultrafast scanner.

This simplicity allows several potential medical applications: the monitoring of thermally-induced lesions, micro-calcifications detection, viscosity and elasticity mapping for breast cancer diagnosis. SSI has been studied theoretically and experimentally *in vitro* and *in vivo*. A derivation of the Green’s function in a viscous and elastic medium will be presented and used to simulate the supersonic regime. Comparison with experiments will be shown.

Based on this theoretical background, tissue mimicking phantoms viscosity will be estimated. Results validating SSI for quantitative shear elasticity mapping in heterogeneous tissue mimicking phantoms will be presented. Detection of thermally-induced lesions on fresh tissue samples will be shown. Finally, *in vivo* tests made on healthy volunteers will show the potential clinical applicability of SSI for breast cancer detection.

18 **EXPERIMENTAL CHARACTERIZATION OF SPATIAL RESOLUTION IN ELASTOGRAPHY: ANALYSIS OF THE TRADEOFFS BETWEEN SPATIAL RESOLUTION AND CONTRAST-TO-NOISE RATIO.[†]**

S. Srinivasan^{1,2}, R. Righetti^{1,2}, J. Ophir^{1,2}.

¹The University of Texas Medical School, Department of Radiology, Ultrasonics Laboratory, Houston, TX, USA; ²University of Houston, Electrical and Computer Engineering Department, Houston, TX, USA.

Theoretical and simulation studies on the spatial resolution of elastography have established lower bounds as well as practical limits on the achievable spatial resolution. In this work, we validate those theoretical and simulation results via an experimental study of the spatial resolution in elastography. Models that involved two cylindrical inclusions placed in the form of a wedge (Figure 1(b)) were used to characterize the axial and lateral resolution of the axial strain elastograms. A study of the dependence of the spatial resolution on several factors such as the algorithmic parameters, the applied strain, and the modulus contrast was performed. The axial resolution was found to show a linear dependence with respect to the algorithmic parameters, namely the window length and the window shift used for strain estimation. The lateral resolution showed a weak dependence on the algorithmic parameters. A weak dependence of the axial as well as lateral resolution on factors such as the modulus contrast and the applied strain was found.

The tradeoff between the spatial resolution and the elastographic contrast-to-noise ratio (CNR_e) was then analyzed. A non-linear tradeoff between the CNR_e and the axial resolution was shown for conventional strain estimation techniques (Figure 1(a)), with the CNR_e improving at a more than linear rate with respect to a linear degradation in the axial resolution. Similarly the CNR_e showed a non-linear tradeoff with the lateral resolution. This study provided an experimental framework for characterizing the spatial resolution in elastography and for elucidating the tradeoffs between the CNR_e and the spatial resolution.

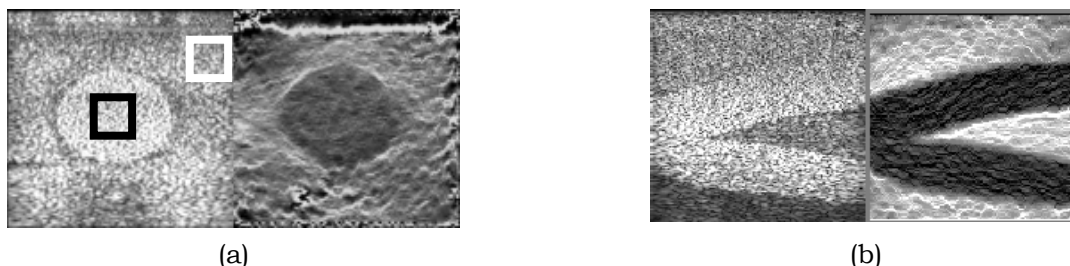


Figure 1: Sonogram-elastogram pairs of (a) a phantom with a 20mm diameter cylindrical inclusion and (b) a phantom with two 10mm diameter cylindrical inclusions arranged as a wedge. The square boxes in (a) indicate the ROI from which the CNR_e was computed.

[†]Supported by National Cancer Institute Program Project Grant P01-CA64597.

Bernhard Brendel¹, Stefan Siebers¹, Martin Scholz², Christoph Welp³, Juergen Werner³, Andreas Lorenz⁴, Andreas Pesavento⁴, Helmut Ermer¹.

¹Dept. of Electrical Engineering, Ruhr-University, Bochum, GERMANY; ²Dept. of Biomedical Engineering, Ruhr-University, Bochum, GERMANY; ³Neurosurgical University Hospital, Ruhr-University, Bochum, GERMANY; ⁴LP-IT Innovative Technologies GmbH, Bochum, GERMANY.

Intraoperative imaging for therapy monitoring and surgical navigation has become of high interest in the last years. Because of its general advantages – non-ionizing, real-time capability, cost-efficiency, ease of handling – diagnostic ultrasound is ideally suited for intraoperative usage. However, conventional B-mode imaging alone is not sufficient for many applications. Elastography can be useful, if isoechoic tissue with different elastic properties has to be differentiated.

Elastography using manual compression is difficult to apply intraoperatively, because of motional artifacts, high pressure exposure to the tissue and required experience of the user. In order to avoid these disadvantages an extended form of elastography, called vibrography, was developed. The transducer is moved axially in a low frequent vibrational mode of low amplitude, replacing manual compression. For the estimation of time shifts, we are using a fast phase root seeking algorithm, which allows to run elastography in real time on a conventional PC. Since the strain changes periodically in a sequence of frames, the periodic strain-time signals can be processed by a narrowband filter according to the frequency of vibration. Subsequent envelope detection delivers stable image sequences with good SNR, even for low compression amplitudes.

We have applied this method to neurosurgery and thermal therapy monitoring. The real-time vibrography system consisted of a Siemens Sonoline Omnia ultrasound system with a custom designed rf-interface. The rf-data was digitized using a 50 MHz, 12-bit PCI A/D converter (Gage) for real-time or offline processing.

For neurosurgery, vibrography was used to detect brain tumors in the open skull. For this purpose, a vibrography applicator with a total compression amplitude of only 0.3 mm and a vibration frequency of 5-10 Hz was developed. Ultrasound rf-data were acquired using the above described system and a 6.5 MHz endocavity curved array. First *in vivo* applications showed, that this setup produces high quality strain images. In these images, the tumor can be clearly differentiated from the surrounding brain tissue.

Minimally invasive methods for thermal treatment of pathological tissue have been improved in the past but still lack of suitable modalities for accurate real-time monitoring. During the therapeutic process tissue is heated locally up to temperatures between 60°C and 100°C. Cancerous tissue is thus destroyed by coagulation. The treated tissue volume shows a significant increase in stiffness as well as changes in spectral and textural behavior, which can be utilized to visualize the coagulated zone using vibrography and tissue characterization. The potential of these methods in discriminating coagulated from healthy tissue has been shown in experiments, where porcine liver underwent rf-ablation treatment. Ultrasound rf-data were acquired with a 9 MHz linear array. The coagulated zones could be clearly visualized in the strain images as areas of increased stiffness. Furthermore measurements on liver samples showed the potential of several parameters from spectral and spatial domain (co-occurrence and autoregressive parameters) in discriminating treated from untreated tissue.

A project of the Ruhr Center of Competence for Medical Engineering (KMR). Supported by the Federal Ministry of Education and Research, No. 13N8079.

MM Doyley^{1,2}, S Srinivasan^{3,4}, A. Mohns², J Ophir^{3,4}.

¹Department of Radiology, Dartmouth Medical School, Hanover, NH 03755, USA; ²Thayer School of Engineering, Dartmouth College, Hanover, NH 03755, USA; ³The University of Texas Medical School, Department of Radiology, Ultrasonics Laboratory, Houston, TX, USA; ⁴University of Houston, Electrical and Computer Engineering Department, Houston, TX, USA.

Elastography is an emerging imaging modality that depicts tissue stiffness by imaging externally or internally induced tissue strains. The spatial variation of internal tissue strain is related to the elastic properties of the underlying tissue. Nevertheless, it is important to realize that strain by itself represents an approximate measure of tissue elasticity. To accurately quantify shear modulus from strain elastograms requires knowledge of all components of the internal stress distribution. Currently, this represents a major limitation because at present stress cannot be measured *in vivo*. Alternately, shear modulus can be computed from the measured internal displacements using a model-based inversion technique. This approach has the advantage of not requiring quantification of the internal stress distribution because the forward model can be formulated entirely in terms of the known variables. However, inverting the measured displacements using a model-based inversion approach could prove to be problematic because of instability problems. Despite this potential limitation it is envisaged that model-based elastography will provide better images than those created using standard elastographic imaging methodology. The long-term objective of this work is to produce the evidence that will either confirm or refute this expectation.

The results of computer simulations demonstrate that there is good visual agreement between strain and modulus elastograms. It was also demonstrated that our ability to detect focal lesions in both modulus and strain elastograms improved with increasing lesions size and modulus contrast. However, modulus elastograms would appear to offer better contrast to noise ratio but lower spatial resolution. It was also apparent from the results of simulation studies the effect of elastographic imaging parameters (i.e. percentage applied strain, window length) on the quality of modulus elastograms was similar to that observed in strain elastograms. These results were corroborated by performing experiments on gelatin phantoms containing cylindrical inclusions with diameters in the range of 2-20 mm. It was also observed that in both cases, the visual appearance inclusions that were greater than 2 mm in diameter was comparable to elastograms produced using a nano-indentor machine.

#Supported in part by a National Cancer Institute Program Project Grant P01-CA64597 to The University of Texas Medical School, Houston, TX, USA.

68 **CONTINUED SCANNING ACOUSTIC MICROSCOPY AND ULTRASONIC WAVE PROPAGATION FOR IMAGING AND MEASUREMENTS OF CONNECTIVE TISSUE PROPERTIES.**

J. L. Katz^{1,2}, Y. Wang¹, H.-J. Hein³, P. Spencer¹, D. Hazony⁴.

¹School of Dentistry, University of Missouri-Kansas City, Kansas City, Missouri 64108, U.S.A.;

²School of Computing and Engineering, University of Missouri-Kansas City, Kansas City, Missouri 64110, U.S.A.; ³Martin-Luther-University Halle-Saale Medical School, Halle/Saale, GERMANY;

⁴Case School of Engineering, Case Western Reserve University, Cleveland, Ohio, 44106, U.S.A.

Our previous studies (reported at the 1st Annual Conference (2002) in Niagara Falls, Canada) of the elastic properties of mineralized tissues, e.g. human femoral cortical and trabecular bone and tissue/material interfaces, e.g. the dentin/adhesive (a/d) interface, were performed on an Olympus (Japan) UH3 Scanning Acoustic Microscopy (SAM) using the 400 and 600 MHz lenses. Recently, we have acquired at the University of Missouri-Kansas City (UMKC) for our Center for Research on Interfacial Structure and Properties (UMKC-CRISP) both the Krämer (Germany) Low Frequency Winsam 100 and High Frequency KSI SAM 2000. The latter has as its highest frequency a 2 GHz lens (nominal lateral resolution ~ 500nm). We are continuing our study of the elastic properties of the d/a interface at high resolution using the KSI 2000. Thus, in order to relate the new imaging capabilities with that obtained with the Olympus UH3, we have imaged the d/a interface with the Krämer 400 MHz and 1 GHz lenses over various areas from 60 x 60 μm to 1 x 1 mm under different focusing conditions within the same region. These variations in area and focus provide different insight into the assessment of material properties.

The Krämer KSI 2000 at Halle/Saale was used to study the effects of age on the structure of human femoral bone in both females and males; samples from pairs of both sexes in the 20s, 60s and 70s were used. Samples were cut under flowing water from each bone at every 15° from along the bone axis to that in the transverse direction. SAM images for each of the 7 samples from the each of the 3 female femora and 3 male femora were obtained with the 400, 600 and 800 MHz lenses. The alternation in gray levels of adjacent lamellae in both haversian and interstitial bone provide periodic structures allowing the use of Fourier transforms to do additional image processing. This is an important feature when analyzing the impact of bone resorption and remodeling that occurs with age. Image reconstruction using superposition of the Fourier transform images obtained from different orientations for the same sample eliminates some of the artifacts introduced in the cutting and polishing of the sample prior to the SAM measurements.

We also have developed miniaturized ultrasound transducers (mut) for incorporation in orthopaedic screws in order to measure bone elastic properties *in vivo* when using external fixators for fracture healing and distraction osteogenesis (Ilizarov) instrumentation. Changes in such properties can also be assessed externally with a novel 3 transducer technique for monitoring bone fracture healing.

03 **PROGRESS IN THE ELASTOGRAPHIC IMAGING OF RADIOFREQUENCY ABLATED THERMAL LESIONS.**

T. Varghese^{1,2}, *U. Techavipoo*^{1,3}, *J.A. Zagzebski*¹, *Q. Chen*¹, *W. Liu*¹, *F.T. Lee Jr.*⁴.

¹Department of Medical Physics, University of Wisconsin-Madison, Madison, WI, 53706, USA;

²Department of Biomedical Engineering, University of Wisconsin-Madison, Madison, WI, 53706, USA; ³Department of Electrical and Computer Engineering, University of Wisconsin-Madison, Madison, WI, 53706, USA; ⁴Department of Radiology, University of Wisconsin-Madison, Madison, WI, 53792, USA.

Elastography is a promising tool for visualizing the zone of necrosis resulting from radio-frequency ablation. Since heat-ablated tissues have increased stiffness compared to normal tissue, this modality may prove useful for following the results of radio-frequency ablation. Several studies have demonstrated that lesion volumes estimated using areas computed from multiple, planar slices through the region of interest are more accurate than volumes estimated assuming simple shapes and incorporating single or orthogonal diameter estimates. To extend this concept to thermal lesion monitoring, we have developed an automated segmentation algorithm for extraction of thermal lesion boundaries to estimate both areas and volumes of thermal lesions. The results obtained on 44 thermal lesions imaged *in vitro* using elastography were compared to manual segmentation of both elastographic and pathological images. Results obtained using automated segmentation show a close correspondence with manual segmentation results.

Attenuation artifacts from gas bubble formation during radio frequency ablation are a significant problem for ultrasonic visualization of the treated region. The progressively increasing hyper-echogenic region due to formation of gas bubbles in heated tissue does not represent the region of tissue coagulation, and generally resolves within an hour of ablation. Bubbles often obscure the visualization of the ablation probe and treated region, thereby increasing the difficulty in probe repositioning for further treatment. In contrast to conventional sonography, ultrasound elastography appears to be very effective for visualizing the zone of necrosis during RF ablation therapy. Some degradation in elastographic images was observed in regions where attenuation due to increased presence of gas bubbles reduced the signal-to-noise ratio of the echo signals. In cases observed during *in vitro* studies, the degradation occurred distal to the thermal lesions and was confined to the lower one-fifth quadrant of the thermal lesion. However, accurate estimates of the thermal lesion areas could still be made by extrapolation of the visualized boundaries of the thermal lesion. No degradation accompanying motion of bubbles or bursting of gas bubbles could be observed on the elastograms.

*This work is supported by start-up funds provided to Dr. Varghese by the Department of Medical Physics, Medical School and Graduate School at the University of Wisconsin-Madison and the Whitaker Foundation.

Joyce McLaughlin¹, Jeong-Rock Yoon¹.

¹Department of Mathematical Sciences, Rensselaer Polytechnic Institute, Troy, NY 12180, USA.

We consider the question: What can be determined about the stiffness distribution in biological tissue from the time and space dependent interior displacement measurement in the transient elastography? This leads us to consider an inverse problem for the identification of coefficients in the second-order hyperbolic system that models the propagation of elastic waves. Here we give uniqueness results that show both the richness of a time and space dependent displacement from a single experiment and the limitations of this data set in the anisotropic case.

Different from quasi-static and dynamic (time-harmonic) excitation on the surface of specimens, the transient, short time pulse excitation shows clearly observable “propagating fronts” in elastograms. These propagating fronts are also “arrival time surfaces” when the tissue remains at rest until a traction force or displacement on the boundary initiates a wave that propagates into the tissue. The existence of propagating fronts is a main feature of the transient elastography data and a fundamental idea used in our analysis for the uniqueness proofs.

Using the property that we have propagating fronts, we establish “shrink and spread argument”, which says that the solution starting out as zero in a region and satisfying both the finite propagation speed (hyperbolic property) and the unique continuation (elliptic property) at each time slice in that region must be identically zero for all time. Utilizing this property as a basic ingredient, we establish sufficient conditions for the unique identifiability of wave speeds. The application of interest is for nearly incompressible isotropic media. For this reason we also investigate the purely incompressible analogue.

Additionally, utilizing the given boundary traction force information, the “energy” of the elastic system and some additional arguments, the simultaneous unique identifiability of both density and shear modulus is obtained. For the displacement boundary condition, we show that an a priori specification of either density or one elastic parameter on the boundary is necessarily required.

In the anisotropic case, counterexamples are presented to show that the unique identification of any elastic parameters (even wave speeds) is impossible in general anisotropic media. The established structure of the set of possible shear tensors corresponding to the single measurement is highly related to the direction of propagating wave. This structure shows that we need more independent probing propagation directions to get full information of anisotropic shear tensors, and suggests how to design multiple experiments to recover such an anisotropic tensor.

References:

- [1] Joyce McLaughlin and Jeong-Rock Yoon (2003): Unique identifiability of elastic parameters from time dependent interior displacement measurement, submitted for publication.
 - [2] Lin Ji, Joyce McLaughlin, Daniel Renzi, and Jeong-Rock Yoon (2003): Interior elastodynamics inverse problems: shear wave speed reconstruction in transient elastography, submitted for publication.
-
-

Yongping Zheng¹, Jun Shi¹, Ling Qin², Sushil G. Patil¹.

¹The Hong Kong Polytechnic University, HONG KONG; ²Department of Orthopaedics and Traumatology, The Chinese University of Hong Kong, HONG KONG.

The articular cartilage (AC) is the thin layer of connective tissue that covers the articulating bony ends in diarthrodial joints. AC has many important functions and unique structural characteristics, such as multi-phasic compositions and multi-layered structures, special diffusion-based nutrition transportation, and frequent degeneration with aging. The extracellular matrix of AC contains negatively charged proteoglycans embedded in a collagenous network. In the biological condition, there is a balance between collagen tension and swelling pressure, contributed by the negative charges. This balance plays an important role in the unique biomechanical behavior of AC. It has been suggested that the quantification of the swelling effects in AC can be used to characterize the degenerative changes associated with osteoarthritis. In this project, high frequency ultrasound was used to probe the transient depth-dependent strains of AC induced by changing the concentration of the bathing saline.

Full-thickness AC specimens with bone layers were collected from fresh bovine patellae. The AC specimens were continuously monitored using a focused beam of 50 MHz ultrasound during sequential changes of the bathing solution from 0.15 M to 2 M saline, 0.15 M saline, 1 mg/ml trypsin solution, 0.15 M saline, 2 M saline, and back to 0.15 M saline. The ultrasound signals were digitized at a sampling rate of 500 MHz. The transient displacements of ultrasound echoes from the AC tissues at different depths were used to represent the tissue deformation. The trypsin solution was used to selectively digest the proteoglycans in AC. M-mode displays were used to represent the transient behavior of tissues at different depths.

It was demonstrated that high frequency ultrasound was useful for monitoring the transient osmotic swelling and the progressive degeneration of AC in real time. The normal bovine patellar AC shrank during the first several minutes and then recovered to its original state in approximately one hour when the solution was changed from 0.15 M to 2 M saline. Degenerated AC showed neither shrinkage nor recovery during the same process. In addition, a dehydrated-hydrated AC specimen showed much stronger shrinkage and it resumed to the original state when the solution was changed from 2 M back to 0.15 M saline. It was demonstrated that the swelling strains in AC induced by the osmotic loading were not uniform throughout its depth. The digestion process of proteoglycans induced by trypsin was also successfully monitored in real time.

Acknowledgements: This work was partially supported by the Research Grants Council of Hong Kong (PolyU5199/02E).

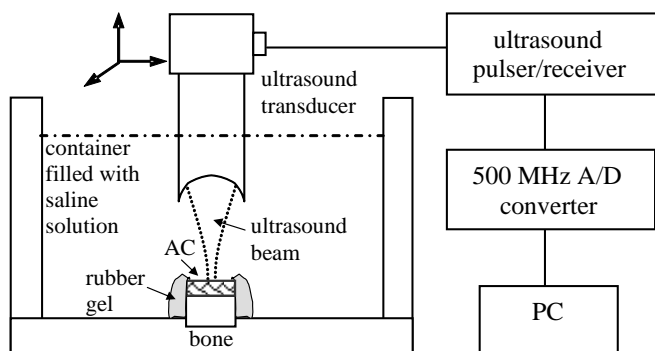


Figure 1. Schematic diagram of the ultrasound system used for monitoring the strains in AC induced by osmotic loading

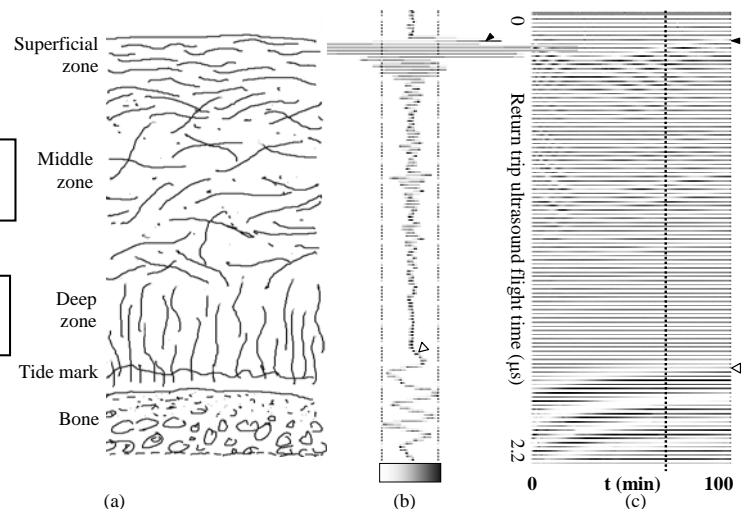


Figure 2. (a) structure of AC; (b) A-mode ultrasound signal from AC; (c) M-mode representation of ultrasound signal collected after the saline was changed from 0.15 to 2 M.

G. Sharat Lin¹, Louise M. Mobbs², Brian S. Garra².

¹Advanced Imaging Associates, Fremont, California, USA; ²University of Vermont College of Medicine-Fletcher Allen Health Care, Burlington, VT, USA.

Objective: To evaluate vibrational Doppler imaging (VDI) as a means of imaging mechanical properties of soft tissues.

Methods: VDI uses power Doppler imaging for real-time visualization of the tissue vibrational response to externally-applied audio-frequency vibration. The VDI apparatus included an audio-frequency transducer driven by a 2-watt audio amplifier and variable-frequency sinusoidal waveform generator (function generator or musical tone generator). The audio transducer was attached to the ultrasound transducer through a vibration-dampening rubber pad. Vibrations at 60–247 Hz were applied through acoustic coupling gel to several tissue-equivalent phantoms containing regions or inclusions of differing hardness. One phantom contained a 10-mm hard spherical inclusion that was isoechoic relative to the surrounding medium. VDI scanning was done on skeletal muscles of healthy human volunteers. VDI was applied to breasts of patients with palpable or histologically-demonstrated benign and malignant masses. Induced tissue vibrations were visualized by power color Doppler at 6 MHz with 500–1000 Hz pulse repetition frequency and color gain at 10–15 dB below typical blood flow settings.

Results: In phantoms, regions or inclusions of greater hardness always appeared as dark areas of lower Doppler amplitude, indicating reduced vibrational amplitude. This was particularly significant in the phantom containing an isoechoic inclusion that was essentially invisible in B-scan, but clearly visible as a dark hypo-vibrational region in VDI. *In vivo* VDI scanning of human muscle revealed bright parallel lines associated with directional muscle fascicles, which amounted to a low-resolution echogenicity image. Breast masses consistently appeared as regions of reduced vibrational amplitude relative to the surrounding normal tissues (Figure 1). However, the VDI contrast ratio between masses and normal tissues varied with vibrational frequency. The size and shape of the phantoms or organs scanned did not appreciably affect VDI image characteristics.

Conclusions: VDI may be useful as an adjunctive method of detecting and identifying isoechoic inclusions or masses of different hardness from the surrounding medium or soft tissue. However, unlike elastographic strain imaging, VDI does not provide a “pure” image of a single physical property such as elastic modulus. VDI visualizes a combination of hardness, echogenicity, and vibrational resonance. The method presented here also appears to differ from “sonoelastography” because vibrational damping limits the penetration of VDI while suppressing the vibrational eigenmodes that depend on the boundary conditions (size and shape) of the structure in which vibrations are induced.

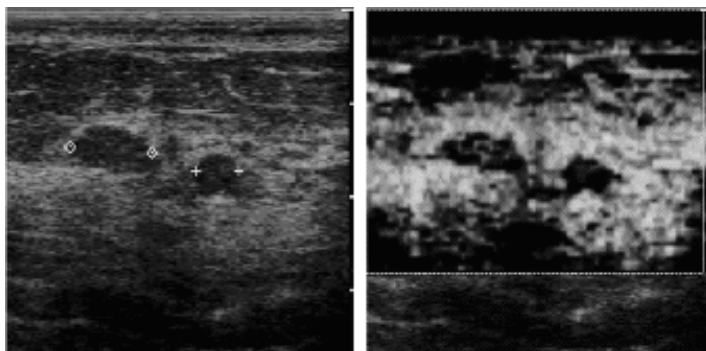


Figure 1: Two fibroadenomas in breast parenchyma.

B-scan (LEFT) shows encapsulated lesions isoechoic to fatty tissue.

VDI image (RIGHT) indicates fibroadenomas to be hypovibrational relative to both parenchyma and fat.

25 DEVELOPMENT OF REAL-TIME TISSUE ELASTOGRAPHY.

Takashi Oosaka¹, Takeshi Matsumura¹, Naoyuki Murayama¹, Tsuyoshi Mitake¹, Ei Ueno², Yongmin Kim³, Tsuyoshi Shiina⁴.

¹Hitachi Medical Corporation, JAPAN; ²Institute of Clinical Medicine, University of Tsukuba, JAPAN; ³Image Computing System Laboratory, University of Washington, USA; ⁴Institute of Information Sciences & Electronics, University of Tsukuba, JAPAN.

We previously reported on an elasticity imaging prototype system based on the algorithm called Extended Combined Autocorrelation Method (Extended CAM), which was developed by Shiina's group in Tsukuba University.

In this paper, we present the progress with the aforementioned prototype system and our new system in which Real-Time Tissue Elastography has been integrated.

The prototype system is composed of an ultrasound scanner with 7.5-MHz linear array probe and external PC with dual 2.2-GHz Pentium processors. The echo signals are captured during compression of the body by the probe in freehand. The tissue displacement is detected as a consequence of the deformation of body. The extended CAM enables us to realize the rapid, robust and precise detection of the tissue displacement based on the correlation of envelope and the carrier phase shift between pre-compression and post-compression. Then, the strain of tissue is color-coded according to its magnitude and translucently superimposed on the conventional 2D images. This simultaneous display enables us to understand anatomical correspondence between the tissue elasticity image and the traditional B-mode image. The PC-based prototype system tries to evenly distribute task to dual processors, therefore, its frame rate can reach up to 10 fps. We have found that 10 fps is sometimes not fast enough. However, this capability is useful for sonographers to visually confirm the strain images during compression, so he/she can change the compressing plane, direction and speed as needed. In addition, we have implemented several post-processing techniques such as frame-to-frame smoothing and adaptive contrast optimization in order to increase the stability of strain estimation substantially. The clinical evaluation of this prototype was performed on breast tissue from over 90 patients. Generally, ductal carcinoma was depicted as hard tissue. The prototype system requires the space for an external PC for elasticity signal processing. Furthermore, the user interface is from the PC keyboard and any combined use of CFM and Doppler measurements has been difficult.

To overcome this limitation and inconvenience, we are developing a new system where Real-Time Tissue Elastography is integrated in an ultrasound scanner. To prepare for clinical use, we are integrating it into a commercial ultrasound scanner, i.e., HITACHI EUB-8500. By (1) utilizing a significant amount of computation power available in EUB-8500 and (2) developing high-performance programs to implement the Extended CAM algorithm, we can increase the strain imaging frame rate to more than 20 fps. We plan to perform clinical evaluations with this new system.

In conclusion, with the PC-based prototype system, we were able to obtain the high quality strain images and confirmed that Real-Time Tissue Elastography is useful, especially for the detection of carcinoma.

We also demonstrated the feasibility of the Real-Time Tissue Elastography integrated into a commercial ultrasound scanner (EUB-8500) for ease to use and higher frame rates for hopefully routine clinical use in the future.

Acknowledgement – The following individuals also contributed to this research:

Dr. Nitta and Dr. Yamakawa at the Tsukuba University, JAPAN. Dr. Ravi Managuli and Ms. Unmin Bae at the University of Washington, USA.

X-ray Tomosynthesis is an imaging modality that reconstructs X-ray absorption in 3D tissue volumes from multiple planar X-ray images taken at different angles relative to the sample volume. Specifically, Tomosynthesis mammography is used for imaging 3D breast volumes to aid in the detection and diagnosis of breast cancers. Due to the nature of the Tomosynthesis mammography examination, the breast is under a controlled compression (perpendicular to the detector) while being imaged. Tomosynthesis images have a higher resolution in the planes parallel to the detector and a lower resolution in the direction perpendicular to the detector.

We present preliminary results of an initial feasibility study to evaluate elastography based on Tomosynthesis image data. For this study, gelatin breast phantoms have been created with both fine and coarse calcium particles intermixed. The fine calcium particles are thought to contribute to the average (background) attenuation, while the role of the larger particles is to simulate microcalcifications in the breast. Stiffer inclusions, relative to background, were created using gelatin of a higher concentration. Visual inspection of the Tomosynthesis images indicates that the phantom's attenuation closely matches that of breast tissue. In part because of the resolution anisotropy of the Tomosynthesis system, and in part due to our motivation to quantitatively reconstruct the elastic modulus, we investigate both compression and shear deformations of the phantom. We estimate the 3D phantom displacement field using an in-house 3D cross correlation program created for this purpose. Initial results are encouraging, with well-behaved displacement estimates at 1-2 millimeter resolution in the planes perpendicular to the imaging detector.

Eva Maciejko¹, Michel Bertrand¹, Thomas A. Krouskop².

¹Institut de génie biomédical, École Polytechnique, C.P. 6079, Succ. Centre-ville, Montréal, Québec, H3C 3A7, CANADA; ²Dept. of Physical Medicine and Rehabilitation, Baylor College of Medicine, Houston, TX, 77030, USA.

It has been shown that tumors in soft tissue can be imaged using elastography on the basis of their stiffness contrast relative to the surrounding tissue. However, the ability to differentiate between different classes of lesions, for example between benign vs. malignant lesions is still being investigated. Physical differences other than stiffness contrast exist between both types of tumors. Hence examining these differences and how they appear in the elastograms may provide a way to identify the type of lesions.

Benign lesions are typically well-circumscribed and surrounded by a capsule that makes them mobile under palpation. Malignant lesions often exhibit irregular borders and tendrils that extend in a radial fashion to invade the surrounding normal tissue. Therefore, to study their mechanical behavior, a breast malignant tumor can be modeled as a stiff elastic inclusion bound to the tissue matrix, whereas a breast benign tumor can be modeled as an inclusion that has a sliding boundary as it is not attached to the matrix.

Our study aims to determine what parameters can be extracted from elastographic data (comprising the displacement field, strain and/or modulus elastograms), that would enable characterization of the mechanical behavior of the inclusion-matrix interface. To do so, analytical and computer models are used. First, analytical solutions of a circular inclusion with bounded and sliding (frictionless) boundaries in an infinite medium are presented and their major differences outlined. For example it is shown that the axial strain within a homogeneous inclusion is constant for the attached inclusion and parabolic for the sliding inclusion. Second, finite element analyses are carried on 2D and 3D models of a discrete or continuous elastic inclusion in a homogeneous finite medium and elastograms are simulated. The mechanical behavior in the transition zone between the inclusion and matrix is inferred from a combination of parameters extracted from the elastographic data.

This characterization of the internal boundary conditions could suggest methods to identify the type of lesion (benign vs. malignant), as well as give some useful information for mesh generation with inverse problem modulus reconstruction.

Acknowledgements: Supported by the Natural Sciences and Engineering Research Council of Canada (NSERC) and the FCAR (Quebec Ministry of Education). A part of the project upon which this publication is based was performed pursuant to the University of Texas Grant CA64597-01 with the NIH, USA.

M Jeong¹, S Kwon¹, J Park¹, G Cho¹.

¹Daejin University, Pocheon, Kyeonggi, 487-711, KOREA.

A lot of research has been done into ultrasonic elastography as a method of detecting tumors in soft tissue. Elastography may be categorized into two types: one is to apply static pressure to human body and estimate the resulting displacements using correlation coefficient, and the other is to apply a mechanical vibration and image the vibration pattern using Doppler technique. Recently, we proposed a method of imaging the stiffness of tissue subject to externally applied vibration based on the temporal brightness variation of adjacent B-mode image frames at each pixel. This method is advantageous in that it can deliver a vibratory force uniformly to the region of interest compared with other methods relying on static compressive force. Because it involves a vibrator, the system is mechanically rather complex to build compared with freehand systems using static pressure.

Both methods were implemented in an ultrasound scanner (ACCUVIX-XQ, Medison, KOREA) to run on its Intel Pentium 4 processor. Images have been obtained by applying static pressure freehand as well as by delivering vibration using a mechanical vibrator. In the case of using static pressure, the displacement was obtained by first computing the phase difference followed by time difference between several adjacent image frames using baseband I and Q data. This approach requires less computation than those seeking the peak of correlation function.

We fabricated elastographic phantoms using agar and gelatin, embedded with a 10 mm diameter agar-gelatin rod which was three times harder than the surrounding medium. The vibration up to a frequency of 300 Hz was provided by an electro-mechanical vibrator with a diameter of 50 mm and thickness of 10 mm, which was constructed in house.

We obtained elastographic images at a rate of 4 to 10 frames/s. In the case of applying static pressure, the image contrast did not decrease even for the freehand case compared with the case of fixing the transducer. In the case of using mechanical vibration whose frequency ranges from 50 to 300 Hz, we could easily identify the hard inclusion, but the resolution around its boundary was not as good as for the static pressure case. In the case of freehand, the image contrast was quite dependent on hand motions. And the resolution of elastographic images varied depending on the transducer and vibration positions as well as the vibration frequency. We will present at the conference video clips of elastographic images of phantoms obtained in real time using both methods.

Rheumatoid Arthritis (RA) and Diabetes Mellitus (DM) are common disease in both developed and developing countries. For RA, symmetric polyarthritis over time leads to destruction of joint cartilage and bone, and to deformities of the joint. Most patients develop prominent impairments of joint function. For DM, distal sensorimotor polyneuropathy leads the callus and ulcer formation in high-pressure area of plantar tissue. Foot amputation or even death is the consequence of the diabetic ulcers without medical treatment. Orthotic footwear is a main conservative treatment for the RA patients and DM patients with foot problems to reduce the progress of deformities and the plantar pressure. Currently, medical providers assign suitable orthotic footwear based on their clinical experiences together with manual palpation. However, it is not easy to decide which materials should be used in orthoses and where the callus would form. Quantitative measurement of the stiffness and thickness of plantar tissues may help to choose suitable footwear materials and to determine pressure-sensitive areas. In the present study, we investigated the tissue properties of RA and DM patients using an ultrasound indentation approach that has been previously developed.

The pen-size ultrasound palpation probe included an ultrasound probe at the tip and an in-series load cell. By pressing the probe against the soft tissue surface, the probe sensed the tissue deformation and applied load using the ultrasound and the load sensors, respectively. An indentation model was used to analyze the load-indentation relationship to obtain an effective Young's modulus. Two sets of experiments were carried out. In the first study, 31 normal subjects and 30 RA patients were tested. In the second study, 20 DM patients and 10 normal subjects were tested. The test areas included the 1st and 5th metatarsal heads, heel and big toe. The thickness and stiffness of plantar tissue of normal and patients were compared and the correlation between plantar tissue thickness and stiffness were also studied.

For RA, t-tests showed that there were significant difference for the plantar tissue thickness between RA patients and normal subjects in heel ($p=0.004$) and 5th metatarsal head ($p=0.01$) and there was significant difference for the plantar tissue stiffness between RA patients and normal subjects ($p=0.02$). There was weak positive correlation ($R^2<0.3$) between the tissue stiffness and thickness for all three measuring sites (1st metatarsal head, 5th metatarsal head and heel) and for both normal and RA subjects. For DM, there was no significant difference of the plantar tissue thickness between DM patients and normal subjects (two-way mixed repeated ANOVA, $p=0.12$) and there was significant difference of the plantar tissue stiffness between DM patients and normal subjects ($p=0.008$). There was weak correlation ($R^2<0.3$) between the stiffness and thickness for both normal subjects and DM patients, for all four measurement sites (Big toe, 1st and 5th metatarsal heads, and heel). Further studies need to be followed to investigate how these results can be used for clinical application in the assessment and treatment of the RA and DM patients.

Acknowledgements: This project was partially supported by the Research Grant Council of Hong Kong (PolyU 5245/03E) and The Hong Kong Polytechnic University.

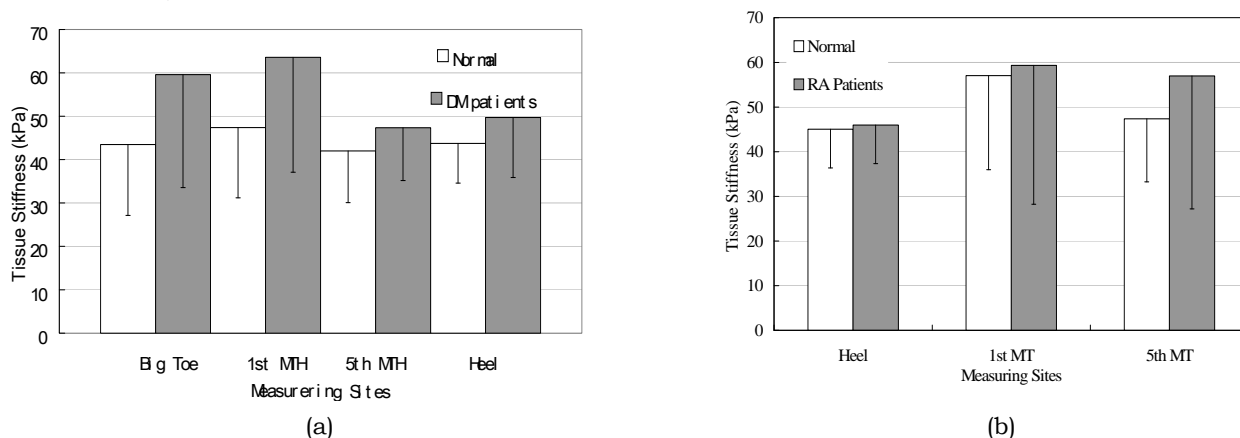


Figure 1. The plantar tissue stiffness between different subjects (a) Diabetes Mellitus patients vs. normal subjects (b) Rheumatoid Arthritis patients vs. normal subjects.

Takayuki Sato¹, Yasuaki Watanabe¹, Shigeyoshi Goka¹, Hitoshi Sekimoto¹.

¹Department of Electronics and Information Engineering, Faculty of Engineering, Tokyo Metropolitan University, Circuits and Systems Engineering Laboratory, 1-1 Minami Oosawa, Hachioji, Tokyo, 192-0397 JAPAN.

In elastography, a technique called 'Data Companding' has traditionally been performed before correlation processing, in order to compensate for the difference in data lengths between the pre- and post-compression echo signals. In the most primitive version of the Data Companding technique, the data sequence is uniformly compressed or expanded throughout one A-line signal.

In the 'Phase Root Seeking' technique, each corresponding unit of data for dataset A, i.e. A-line data for pre-compression, is sought in dataset B, i.e. A-line data for post-compression. The difference in positions between the corresponding two units of data is considered to be the time delay, defined as Δt . Subsequently, the 2-dimensional distribution of Δt is regarded as a strain image (elastogram). Using this technique, errors in size and the location of the hard region are smaller than those obtained using the traditional data companding of tissue. However, there may be a problem where Δt is the accumulated time delay.

According to the definition of Δt , this increases as the seeking process advances, thus the dimensions and location of delay are not clear. Furthermore the SNR of the tissue image decreases in deeper tissues.

In this study, we estimated the time delay with a pattern matching method based on maximum correlation seeking. Then, we defined Δt_{local} as the 'newly yielded time delay at a certain point', and compute a sequential estimate between the two datasets. According to this new definition, Δt_{local} does not increase as the seeking process progresses, and the strain distribution can be estimated precisely at all tissue depths.

Where the traditional 'Data Companding' and this method were applied to the same experimental data, the average correlation coefficient in the axial direction increased from 0.509 to 0.696. There was also a remarkable improvement in the correlation image in deeper tissue compared with images obtained with 'Phase Root Seeking'.

Jun Liu¹, Cynthia J. Roberts¹.

¹The Ohio State University, 270 Bevis Hall, 1080 Carmack Road, Columbus, OH 43210, USA.

The biomechanical properties of the cornea have been investigated to better predict refractive surgery outcome. A mechanical model of elastic wave propagation in multi-layered viscoelastic media was constructed to study the relationship between biomechanical properties of the cornea and its reflection spectra when high-frequency elastic waves are applied. Mechanically, the examined system is composed of two continuous subspaces (water bath and aqueous humor) and a thin layer of ocular tissue between the two subspaces. In our first model, tear film was incorporated into the tissue layer due to similarity in acoustical impedances. The imposed mechanical problem was solved as a boundary value problem (BVP) by enforcing the continuity of stress and displacement at the two boundaries/interfaces in the system. Brekhovskikh's method was followed to obtain the solution to the magnitudes of all the unknown waves, assuming the incident wave is known. The reflection coefficients of the thin tissue layer, which can be experimentally measured by ultrasound systems, were calculated according to literature data on corneal elasticity under different pressure loadings. The results showed that the reflection spectra varied due to the changes in corneal biomechanical properties. In combination of an ultrasound non-destructive evaluation system, the model might be used for *in vivo* measurement of corneal elasticity.

Jun Liu¹, Thomas J. Rosol¹.

¹The Ohio State University, 339 Goss Laboratory, 1925 Coffey Road, Columbus, OH 43210, USA.

Surface-modified organic or inorganic nanoparticles have attracted strong interest as molecular probes for imaging cell surface markers; nevertheless, relatively little investigation has been done on nanoparticles as ultrasound contrast agents. We hypothesize that surface-engineered nanoparticles will create characteristic acoustical enhancement through their specific physical properties (e.g., high density or elasticity), and selectively highlight tissues that over-express certain markers. In this preliminary study, we have tested tissue sections taken from mammary gland preparations. The thin sections of tissue with and without nanoparticle treatment were embedded between two pieces of flat substrates for ultrasonic measurement. A theoretical model for wave propagation in discrete media was used to reconstruct the elastic and other physical properties of the tissue sections. Nanoparticles were arbitrarily distributed in phantom samples (agarose gel) and imaged by B-mode ultrasound. Our preliminary results showed that most of the reconstructed properties of tissues with nanoparticle treatment differed from those without treatment, and the differences were greater than the measured system errors (< 1%). Ultrasonic imaging also demonstrated the contrast effect created by the nanoparticles.

AUTHOR INDEX

AUTHOR	PAGE	AUTHOR	PAGE	AUTHOR	PAGE
Aglyamov, SR	46	Khaled, W	40	Roberts, CJ	95
Akino, Y	73	Kim, K	46, 74	Rohling, R	29
Altmeyer, P	56	Kim, Y	89	Rosol, TJ	96
Aoki, Y	65	Kiss, MZ	30	Rouvière, O	53
Baggs, RB	42	Kliwer, MA	30	Royer, D	24
Baker, L	34	Kolchanova, SG	70	Rubin, JM	46, 74
Baldewising, RA	75	Kolen, A	34, 35	Saijo, Y	73
Bamber, J	34, 35, 63	Konofagou, EE	50	Salcudean, S	29
Barbone, PE	67, 69, 90	Kopans, DB	90	Sasaki, H	73
Barrière, C	24	Krouskop, TA	38, 39, 61, 91	Sato, T	94
Baumann, M	40	Kubota, M	43	Saveljeva, ES	70
Bercoff, J	80	Kuehne, K	40	Schaar, JA	75
Bertrand, M	91	Kuhl, C	52	Scharenberg, R	56
Blyakhman, FA	70	Kwon, S	92	Scharenberg, S	56
Boese, H	40	Lafon, C	54	Scheipers, U	40
Bogachev, K	63	Langevin, HM	50	Schmitt, RM	62, 79
Bojara, W	49	Lee Jr., FT	85	Scholz, M	82
Bouchoux, G	54	Lee, MC	33	Scott, WG	62, 79
Brendel, B	82	Leung, S	32	Sekimoto, H	94
Bruhns, OT	40	Lin, GS	26, 48, 88	Senge, T	40
Brusseau, E	41	Lindstaedt, M	49	Shau, YW	27, 33, 59
Catheline, S	24, 25	Liu, J	95, 96	Shi, H	61, 71
Cathignol, D	54	Liu, W	85	Shi, J	87
Chai, HM	27	Lorenz, A	40, 82	Shiina, T	60, 65, 89
Chang, YJ	27	Lowery, C	44	Shinomura, R	60
Chapelon, JY	37, 53, 54	Lu, M	28, 51	Siebers, S	82
Chen, Q	36, 85	Maciejko, E	91	Sinkus, R	52
Chen, X	46, 74	MacIntosh, S	29	Sokolov, SY	70
Chestukhin, VV	70	Madsen, EL	30, 36, 61, 71	Souchon, R	53, 54
Cho, G	92	Malin, J	44	Soulez, G	72
Choi, APC	93	Maniatty, AM	58	Spalding, C	44
Choi, CYK	32	Marchenko, EV	70	Spencer, P	84
Chopra, D	44	Mastik, F	75	Srinivasan, S	38, 39, 45, 47, 81, 83
Cloutier, G	72, 76	Matsumura, T	60, 89	Stryker, R	21
Connors, A	44	Maurice, RL	72, 76	Sumi, C	43
Cook, LT	64	Mazza, E	23	Svensson, WE	44
Cui, Y	41	McLaughlin, J	66, 68, 86	Tamano, S	60
Daronat, M	76	Mecke, KP	77	Tanabe, M	43
Delon, G	25	Meehan, GD	31	Tanaka, A	73
di'Santagnes, PA	42	Miller, N	63	Tanaka, M	73
Doyley, MM	61, 78, 83	Mironkov, BL	70	Tanter, M	24, 52, 80
Egersdrofer, S	40	Mitake, T	60, 89	Taylor, LS	42, 55, 57
Emelianov, SY	46	Mitri, F	37	Techavipoo, U	30, 36, 85
Ermert, H	40, 49, 56, 82	Mobbs, LM	26, 45, 47, 48, 88	Trompette, P	37
Felker, S	45, 47	Mohns, A	83	Tunayar, A	40
Finet, G	72	Monkman, GJ	80	Turgay, E	29
Fink, M	24, 25, 80	Moore, RH	90	Ueno, E	60, 89
Foster, FS	76	Muller, M	80	Ustuzganin, SS	70
Frank, G	61	Murayama, N	89	Valtorta, D	23
Freimuth, H	40	Myers, DD	46	van der Steen, AFW	75
Friboulet, D	41	Nadasdy, G	42	Van Houten, EEW	77, 78
Garra, BS	26, 45, 47, 48, 50, 88	Nigwekar, P	42	Varghese, T	30, 36, 61, 71, 85
Gelet, A	53	Nisius, T	52	Vogt, M	56
Gennisson, JL	24, 25	Nitta, N	60, 65	Von Behren, P	44
Gimelli, G	71	O'Donnell, M	46, 74	Vray, D	41
Goka, S	94	Oberai, A	69	Wakabayashi, G	43
Gokhale, N	69	Ohayon, J	72	Wakefield, TW	46
Hall, TJ	30, 44, 64	Oomens, CWJ	75	Wang, CL	27, 33, 59
Hamilton, MF	31	Oosaka, T	89	Wang, Y	84
Hazon, D	84	Ophir, J	38, 39, 45, 47, 53, 61, 81, 83	Watanabe, Y	94
Hein, HJ	84	Owada, N	73	Weaver, JB	77, 78
Ho, JMW	93	Park, E	58	Weiss, L	45, 47
Hobson, M	30, 61	Park, J	92	Weitzel, WF	46, 74
Hoffmann, K	56	Parker, KJ	42, 55, 57	Welp, C	82
Holt, S	49	Pasternack, D	42	Werner, J	82
Hsiao, TY	33	Patil, SG	87	Wolff, M	71
Hsu, TC	59	Paulsen, KD	77, 78	Wroblewski, SK	46
Huang, Q	28	Perrey, C	49	Wu, T	90
Huang, Y	32	Pesavento, A	40, 82	Wu, Z	42, 55
Ilinskii, YA	31	Poplack, S	78	Xie, H	46, 74
Irving, RD	62, 79	Porter, BC	42	Yamakawa, M	60, 65
Jacobs, X	24	Price, RE	39	Yoon, JR	68, 86
Jannicky, E	45, 47	Qin, L	87	Zabolotskaya, EA	31
Jeong, M	92	Qin, Z	76	Zagzebski, JA	30, 36, 71, 85
Ji, L	68	Reichling, S	40	Zheng, Y	28, 32, 51, 87, 93
Jiang, J	30	Renzi, D	66, 68	Zhu, Y	44, 64
Katz, JL	84	Richards, MS	90		
Kennedy, F	78	Righetti, R	38, 81		

